الجمهورية الجزائرية الديمقراطية الشعبية République Algérienne Démocratique et Populaire

وزارة التعليم العالى والبحث العلمى

Ministère de l'Enseignement Supérieur et de la Recherche Scientifique

Centre Universitaire Abdelhafid Boussouf - Mila

Institut des Sciences et de Technologie

Département de Génie Mécanique et Electromécanique



N°Ref :.....

Mémoire présenté en vue de l'obtention du diplôme de

MASTER

Spécialité : Mécanique Energétique.

THEME

Study of the behavior of thermal conduction in a CMT welding process

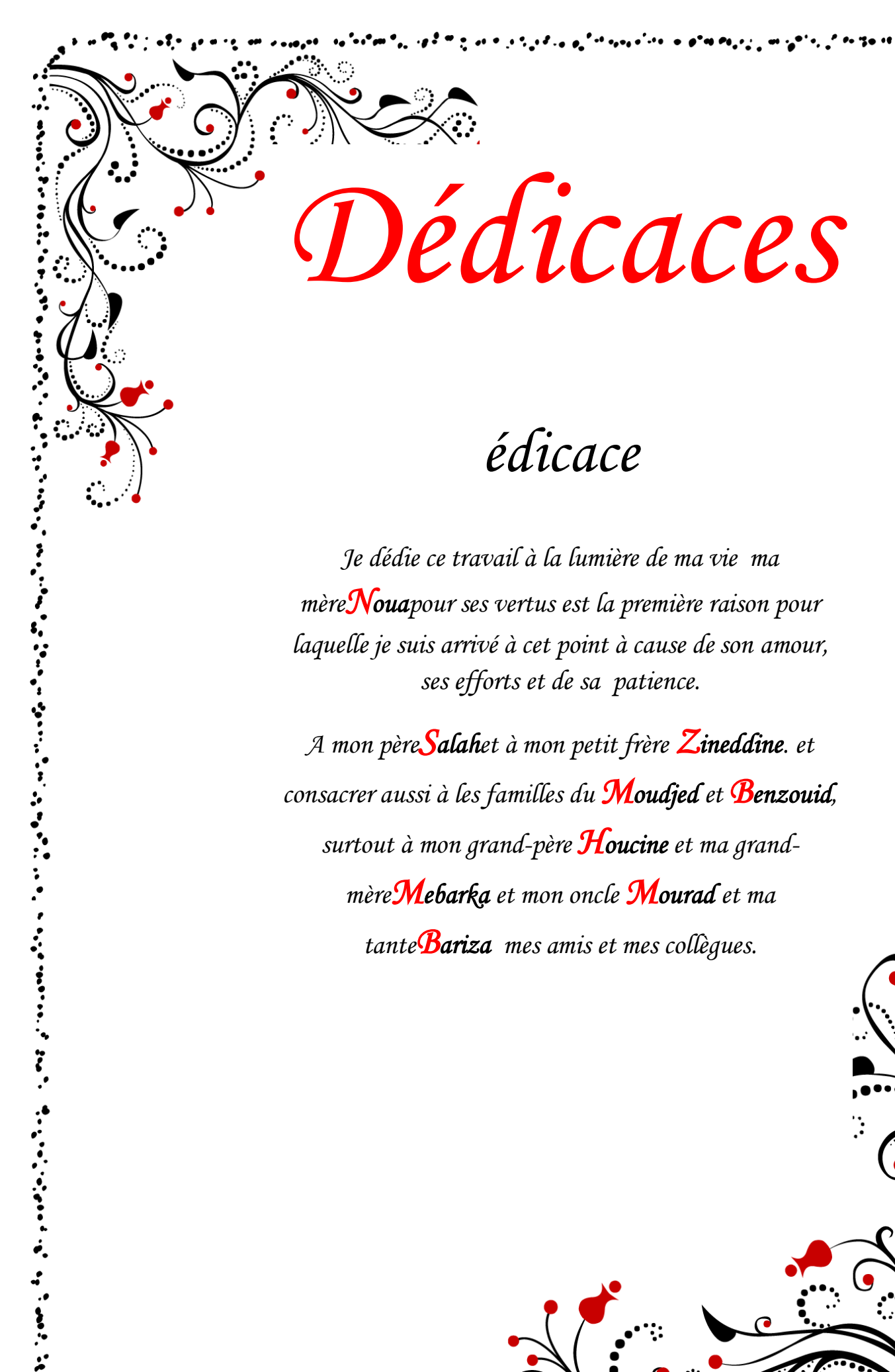
Réalisé par :

- AMRI Idris
- DJEMAOUNE Aissa

Soutenu devant le jury :

Mr. AZIZI. M	MCA	Président
Mr. HAMIDAN. A	MAA	Examinateur
Mr. DEBBAH.DJ	MCB	Rapporteur
Mr. FATMI. H	MRA	Co- encadreur

Année universitaire : 2023/2024



Ie dédie ce travail à la lumière de ma vie ma mère Noua pour ses vertus est la première raison pour laquelle je suis arrivé à cet point à cause de son amour, ses efforts et de sa patience.

A mon père Salahet à mon petit frère Zineddine. et consacrer aussi à les familles du Moudjed et Benzouid, surtout à mon grand-père **Houcine** et ma grandmère Mebarka et mon oncle Mourad et ma tante Bariza mes amis et mes collègues.

NOMENCLATUR

U Arc Tension (electric voltage) (Volt)

I Intensity of electric current (A)

Π Arc efficiency (%)

 Q_m , Q, q_s , q_n Surface heat flux(W/m²)

 Q_0, Q Net power (w or j/s)

A Surface (m^2)

B Volume (m^3)

 r_x , r_y , r_{yav} , r_{yar} Double-ellipsoïde source radius (m)

a, b, c Ellipsoid source radius (m)

V Arc speed (m/s)

t Time (s)

 q_v Volume heat flux (w/m^3)

 ρ Density (kg/m^3)

Cp Thermal mass capacity at constant pressure (J/kg.K)

S The heat source

k Thermal Conductivity (W/m.K)

 h_{∞} Convective heat transfer Coefficient ($w/m^2.K$)

 σ Boltzmann constant (5.67.10–8 w/m^2 . K^4)

 ε Thermal emissivity

 T, T_{∞} Temperature; ambient Temperature (K)

 R_S heat source destribution radius (m)

LISTE OF CONTENTS

NOMENCLATURE

FIGURES LIST	1
TABLES LIST	3
GENERAL INTRODUCTION	6
IChapter I: Cold Metal Transfer: Theory and definitions	8
I.1-The cold metal transfer-CMT process	8
I.1.1-Definition of CMT- Cold Metal Transfer	8
I.1.2-Step-by-step procedure of CMT:	9
I.1.3-CMT machine setup and working principle:	11
I.1.3.1-Setup:	12
I.1.3.2-Working principle of CMT:	13
I.1.4-Various Process Parameters and Their Influence during CMT process:	15
I.1.4.1-Electrode Polarity:	15
I.1.4.2-Wire Feed Speed (WFS) and Welding Speed:	15
I.1.4.3-Substrate and Interlayer Temperature:	16
I.1.4.4-Shielding Gas:	16
I.1.5-Applications of CMT	17
I.1.6-Advantages and benefits of CMT	18
I.1.7-Common defects encountered in CMT	20
I.1.7.1-Porosity	20
I.1.7.2-Lack of fusion	20
I.1.7.3-Cracking	21
I.1.7.4_Undercut	22
I.1.7.5-Inclusion:	22
I.2-Thermal phenomena in CMT process	23
I.2.1-Parameters linked to incident energy	23

I.2.2-Parameters linked to the convection of liquid metal	23
I.3-State of the art on the simulation and analysis of the thermal aspect of CMT	24
I.3.1-Consequences and interaction of different physical phenomena	24
I.3.2-Mathematical models of heat sources	26
I.3.2.1-Surface heat sources	27
I.3.2.2-Volume heat sources:	30
II-Chapter II: numerical modeling	32
II.1-welding of metal plate	32
II.1.1Thermal modeling	32
II.1.2-Thermal problem: equation	32
II.1.2.1-Hypotheses	32
II.1.2.2-Boundary and initial conditions	34
II.1.2.3Final equations system	34
II.1.2.4-Pulsing effect	5
II.1.3-Materials3	36
II.1.4-properties	36
II.1.5-COMSOL modeling Instructions	7
II.2-Simulation of the droplet spreading4	15
II.2.1-Flow dynamics	6
II.2.2-Advection on the interface	6
II.2.3-Heat transfer and solidification	.7
II.2.4-Boundary conditions4	9
II.2.5-Results and discussions	9
II.2.6-Spreading with and without solidification5	0
II.2.7-Materials5	50
II.2.8-properties5	51
II.2.9-COMSOL modelling Instructions	51

III-Chapter III: results and discussion	46
III.1-welding of metal plate results	46
III.1.1- meshing effect.	46
III.1.1-The influence of plate thickness on temperature distribution	47
III.1.2-The influence of welding power on temperature distribution	54
III.1.3-The influence of welded material on temperature distribution	59
GENERAL CONCLUSION.	66
REFRENCES	67

FIGURES LIST

Figure I.1: STL file format	9
Figure I.2: A piece manufactured after the machine finishes it, and as is clear in the picture, it still needs to go through sanding, heat treatment, and even chemical treatments to obtain the perfect clean final shape	1.1
Figure I.3: CMT machine basic parts	11 12
Figure I.4: High-speed images of droplet transfer	13
Figure I.5: Current and Voltage waveforms of CMT process	14
Figure I.6: Micrograph showing the holes formed during CMT process	20
Figure I.7: Energy transfer in CMT process	24
Figure I.8:: Illustration of double-ellipsoid heat source shape	29
Figure I.9: 3D double-ellipsoid heat sources	31
Figure II.1: the welding process of two thin sheets	33
Figure II.2: Ω domain and boundaries	33
Figure II.3: 3D double-ellipsoid heat sources	35
Figure III.1: different mesh types	46
Figure III.2: temperature destribution for three mesh types	46
Figure III.3: temperature distribution in a 2mm height titanium plate in different time steps with 800W welding power	47
Figure III.4 : 3D graphic representation temperature evolution along the welding path at different time steps in a 2mm height titanium plate with 800W welding power	48
Figure III.5: 2D graphic representation temperature evolution along the welding path at different time steps in a 2mm height titanium plate with 800W welding power Figure III.6: temperature distribution in a 5mm height titanium plate in different	48
time steps with 800W welding power	49
Figure III.7: 3D graphic representation temperature evolution along the welding path at different time steps in a 5mm height titanium plate with 800W welding power	50
Figure III.8 : 2D graphic representation temperature evolution along the welding path at different time steps in a 5mm height titanium plate with 800W welding power.	50
Figure III.9: temperature distribution in a 8mm height titanium plate in different time steps with 800W welding power	51
Figure III.10: 3D graphic representation temperature evolution along the welding	
path at different time steps in a 8mm height titanium plate with 800W welding power. Figure III.11: 2D graphic representation temperature evolution along the welding path	52
at different time steps in a 8mm height titanium plate with 800W welding power	52
Figure III.12: 2D graphic representation temperature evolution along the welding path	
at t=5s in the different thickness plates	53
steps with 850W	54

Figure III.14: 3D graphic representation temperature evolution along the welding path	
at different time steps in a 5mm height titanium plate with 850W welding power	55
Figure III.15: 2D graphic representation temperature evolution along the welding	
path at different time steps in a 5mm height titanium plate with 850W welding power.	55
Figure III.16: temperature distribution in a 5mm height titanium plate in different time	
steps with 900W welding power	56
Figure III.17: 3D graphic representation temperature evolution along the welding path at different time steps in a 5mm height titanium plate with 900W welding power	57
Figure III.18: 2D graphic representation temperature evolution along the welding path	
at different time steps in a 5mm height titanium plate with 900W welding power	57
Figure III.19: temperature distribution in a 5mm height aluminum plate in different time steps with 800W welding power	59
Figure III.20: 3D graphic representation temperature evolution along the welding path at different time steps in a 5mm height aluminum plate with 800W welding power	60
Figure III.21: 2D graphic representation temperature evolution along the welding path at different time steps in a 5mm height aluminum plate with 800W welding power	60
Figure III.22 : temperature distribution in a 5mm height iron plate in different time steps with 800W welding power	61
Figure III.23: 3D graphic representation temperature evolution along the welding path at different time steps in a 5mm height iron plate with 800W welding power	62
Figure III.24: 3D graphic representation temperature evolution along the welding path at different time steps in a 5mm height iron plate with 800W welding power	62
Figure III.25: volume displacement magnitude distribution in a 5mm height titanium, aluminum and iron plates in different time steps with 800W welding power	64
Figure III.26: volume displacement magnitude distribution in a 5mm height titanium, aluminum and iron plate, along the welding path in different time steps with 800W	
welding power	65

TABLES LIST

Table I.1: surface heat sources examples.	28
Table I.2: some models adapted for the simple volume heat source	30
Table I.3: simulation properties.	

GENERAL INTRODUCTION

In modern engineering applications, there is a growing demand for reducing the overall component weight without compromising strength and integrity. This has led to the combined use of multiple materials. Conventionally, various methodologies such as mechanical fastening, friction stir welding, and transition joints have been proposed to join dissimilar metals. It is worth noting that components made of dissimilar metals present several challenges when it comes to metallurgical joining. These challenges arise from the chemical and thermal properties of the metals, which result in the formation of intermetallic compounds at the interfaces and the occurrence of thermal stresses in the joints. Cold metal transfer method employs controlled short circuiting to minimize heat input, making it ideal for dissimilar metal welding. This reduced heat input effectively prevents excessive thermal stress, distortion, and the formation of brittle intermetallic compounds at the joint interfaces.

Cold Metal Transfer (CMT) is an automated welding process based on dip transfer welding. CMT operates as a controlled short-circuit transfer mode. During welding, the short-circuit is managed by synergic line parameters, along with a wire back movement. This movement allows the wire to detach during the short-circuit state. Compared to traditional short-circuit welding, CMT enables spatter-free welding, improving the weld bead quality.

CMT reduces heat input, which enhances weld quality by minimizing:

- Distortion and spatter.
- The minimal heat input preserves the metal's structure, reinforcing the weld bead.
- For thin materials, CMT prevents deformation due to excessive heat.

In summary, CMT offers versatility and efficiency across various industrial sectors. As we continue to explore innovative welding solutions, CMT plays a crucial role in advancing welding technology.

During this study, we used COMSOL Multiphysics simulations to compare several impact criteria. Here's how it unfolded:

1. Thermal Exchange Study:

- ➤ We investigated the thermal exchange resulting from welding using the CMT technique with titanium for linear welding.
- ➤ Simulations allowed us to understand the movement and deformation of the metal droplet during the welding process, shedding light on the thermal mechanisms and phenomena occurring during linear welding.

2. Impact of Process Parameters :

- We examined the effect of workpiece thickness using three values (2mm, 5mm, and 8mm).
- The influence of applied electrical power (800W, 850W, and 900W) was also analyzed.
- Additionally, we studied the impact of material type by welding with three different metals (titanium, aluminum, and Iron).

To explore the effects of the aforementioned influencing parameters, the study results are presented in terms of temperature distribution at different time intervals, 2D and 3D graphs showing temperature evolution along the welding path, and the 2D temperature profile at (t = 5s) in various plate thicknesses.

I. Chapter I: Cold Metal Transfer: Theory and definitions

I.1. The cold metal transfer-CMT process

I.1.1. Definition of CMT- Cold Metal Transfer

Cold Metal Transfer (CMT) welding is an advanced arc welding technique derived from Gas Metal Arc Welding (GMAW) [1], characterized by its intermittent regulation of the arc current. In GMAW, an electric arc which is a discharge of electricity across a gap, causing ionization of the air or gas and resulting in a bright, hot plasma [2], is established between a consumable a piece of wire called electrode, which can be of metal or alloy and carries an electric current to obtain sufficient heat for welding [3], and the work piece, where the arc serves as a controlled source of intense heat to melt or fuse the feed wire. This process results in the formation of molten metal droplets at the wire tip, which are subsequently transferred to the work piece, with a speed and a path controlled by computer use, to get the desired shape.

CMT welding distinguishes itself from other GMAW technologies by modulating the arc current intermittently, an initial high pulse of current is formed which formed an arc between the advancing electrode and the substrate that melt the electrode tip. The current is reduced following the pulse, as soon as a short circuit is indicated, the voltage reduces, the current is further reducing to a low background value and the wire is retracted, which leads to detachment of the molten droplet allowing for precise detachment of molten metal droplets from the feedstock wire [4]. This modulation enables controlled droplet detachment, significantly reducing spatter, minimizing distortion, and enhancing process stability. The ability of CMT to regulate the arc current contributes to its capacity to deliver high-quality welds, even under challenging welding conditions, thereby enhancing the overall efficacy and reliability of the welding process.

In the domain of Additive Manufacturing, particularly Wire Arc Additive Manufacturing (WAAM), CMT assumes a pivotal role as a mode of metal transfer, revolutionizing the metal deposition process. Integrating CMT into the WAAM framework enhances precision and efficiency, facilitating the fabrication of intricate geometries with exceptional accuracy. The absence of spatter in CMT welding, which can get to 16% less than other additive methods [5], is particularly advantageous in WAAM applications, ensuring superior deposition quality while minimizing distortion and enhancing process tolerance. Through seamless integration, CMT empowers manufacturers to optimize material utilization,

reduce waste, and maximize cost-effectiveness, thereby ushering in a new era of additive manufacturing characterized by unparalleled quality and performance [6].

I.1.2. Step-by-step procedure of CMT:

In the field of Cold Metal Transfer (CMT) manufacturing, the production process typically entails a series of essential steps aimed at transforming raw feed materials into the intended product. These fundamental stages are indispensable for achieving the desired final output. The manufacturing procedure can be subdivided into six major steps, each of which plays a critical role in the overall fabrication process.

✓ CAD file preparation:

Computer-aided design (CAD) models are indispensable in CMT processes, whether for prototyping or producing finished products. The process relied heavily on 3D modeling. Initially, designs are represented by rough sketches, which are then refined into detailed drawings using software like SOLIDWORKS, CATIA, or TINKERCAD. Alternatively, actual components can be digitally replicated using 3D scanning or photogrammetry tools. The digital data generated from CAD models or 3D scans is stored in formats like Standard Triangular Language (STL), pioneered by 3D Systems, which represents surfaces as small triangles. This digital representation serves as the foundation for the subsequent stages, allowing for accurate fabrication of the desired components.

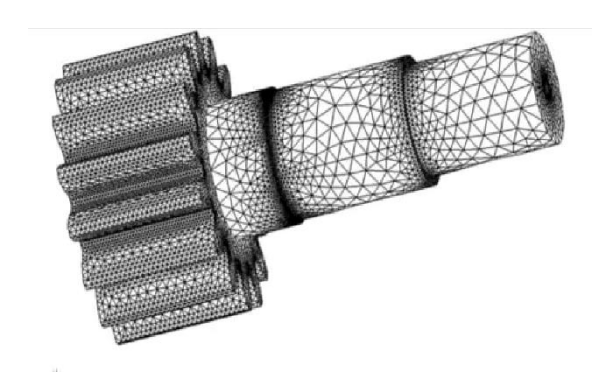


Figure I.1: STL file format [31]

✓ Pre-processing of Design:

Once the STL file is created, several preparatory steps are necessary before printing, during this stage, the digital representation of the component is positioned within the build volume. Support structures become essential, especially when the component is oriented at specific angles, as they prevent deformation due to residual stress, enhance printing capabilities

for overhangs, and ensure proper heat conduction. Despite their benefits, support structures often pose aesthetic challenges. Moreover, designers can use software to determine the optimal number of components to be produced simultaneously within the build volume. These software solutions also ensure that the part is printed as efficiently as possible, with "efficiency" referring to improved qualities, cost savings, and time optimization achieved through parameter optimization.

✓ Slicing of the Part:

After applying pre-preprocessing techniques, the software segments the component into 2D sections as per requirement. This slicing process divides the object into various levels, providing detailed instructions for the heat source's path on each layer. These instructions are generated as G-codes, which are compatible with CMT equipment. Slicing a 3D model essentially means translating the blueprint into instructions that the CMT CNC machine can interpret

✓ Machine Configuration:

After uploading the STL file to the CMT technology, additional system startup procedures are necessary. These initial stages mainly involve configuring the CMT CNC machine for the part production process. The operator must ensure an adequate supply of raw material for the machine to complete the building operation. However, the machine setup entails more than just material feeding; it also requires maintaining the oxygen content within safe limits in the chamber. Given the propensity for oxidation of the raw material or molten pool, creating an inert gas atmosphere becomes crucial. Helium, nitrogen, argon, or their combinations are typically employed to minimize oxidation effects. Consequently, it's imperative to monitor the pressure levels in the gas tanks before commencing the procedure.

✓ Build-Up Process:

The machinery used to make the component is basically an automated system that is capable of doing the critical task. As a result, it may operate without supervision for the vast majority of the time. However, a check of the material amount power supply is still required from time to time to ensure appropriate operating procedures.

✓ Component Separation and Post-Processing:

Once the formation process is completed, the component is removed from the base plate. However, before extraction, it undergoes cleaning either with a brush or a vacuum cleaner. The support structures are then removed using either hand tools or machinery. Consequently, the surface quality of the component face connected to the support structure is often compromised, necessitating post-processing. This post-processing involves refining, sandpapering, sealing, and other finishing procedures. Moreover, CMT components are manufactured to meet specific implementation requirements. Consequently, the part is often deemed unusable in its as-formed (straight off the machine) condition and requires additional processing, such as heat treatment.

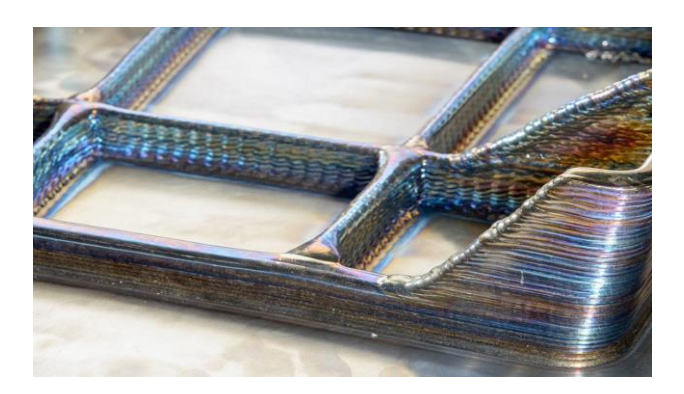


Figure I.2: A piece manufactured after the machine finishes it, and as is clear in the picture, it still needs to go through sanding, heat treatment, and even chemical treatments to obtain the perfect clean final shape [32].

I.1.3. CMT machine setup and working principle:

The schematic working principle of CMT-WAAM (Cold Metal Transfer - Wire Arc Additive Manufacturing) is illustrated in the provided figure. This process utilizes a consumable wire electrode and an inert gas to safeguard the weld pool from atmospheric contamination. Here's a concise overview of the operational principle and the setup.

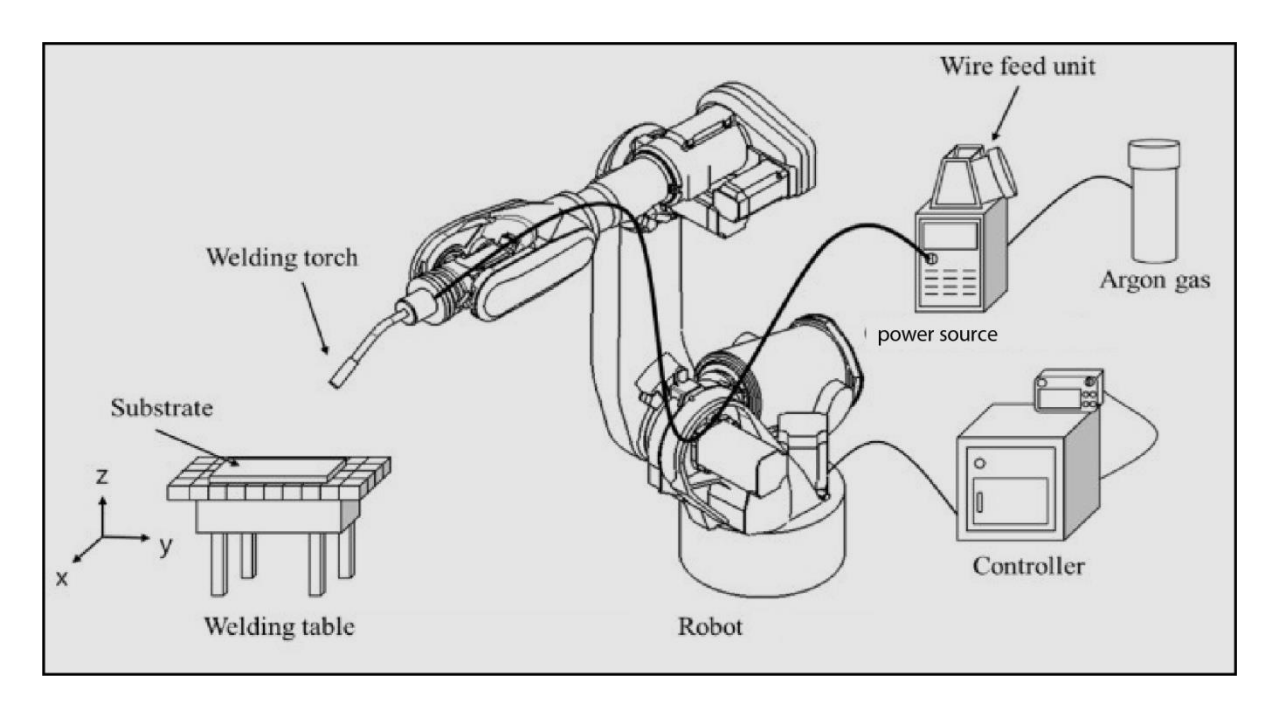


Figure I.3: CMT machine basic parts [30].

I.1.3.1. Setup:

As shown in the picture above the CMT machine can be divided into the following basic parts:

- <u>Power source:</u> It provides the electrical energy required to generate an arc between the wire electrode and the workpiece.
- The wire feeder: Is responsible for managing the welding wire. It involves mounting a spool of welding wire onto the feeder, which then pulls the wire electrode through a cable and delivers it to the welding gun.
- Welding gun: It is used to control the feed wire electrode and direct the welding current to the workpiece
- <u>The shielding gas supply system:</u> Provides inert gases like argon or helium through a nozzle attached to the welding gun. This inert gas shields the weld pool, preventing contamination from the surrounding environment.
- **Ground clamp:** This is connected to the workpiece and completes the electrical circuit required for welding.
- <u>Controller:</u> The software that controls the CMT-WAAM system dictates all process operation and ensure that the part is manufactured as intended .it includes
- <u>Tool path generation:</u> To convert designs into machine instructions and printing strategies.

- Robot kinematics: Control to transform all programming into physical motion.
- Sensors: For safe and efficient operation to ensure high quality prints.
- Robotic hardware: A multi axes robotic hand builded parts layer by layer by the deposition of metal wire into the desired near-net-shape precisely.

I.1.3.2. Working principle of CMT:

In the CMT process, the welding gun is positioned in close proximity to the workpiece, with the wire electrode fed through it. Upon pulling the trigger on the welding gun, the power source generates an arc between the workpiece and the wire electrode. This arc produces heat, softening and melting both the wire electrode and the workpiece, creating a weld pool. Concurrently, the inert gas flows through the nozzle on the welding gun, forming a protective shield around the weld pool, preventing atmospheric contamination.

When the electrode wire tip contacts the molten pool, the servomotor of the welding torch's "robacter drive" is reversed via digital process control. This action retracts the wire, facilitating droplet transfer, as depicted in Figure I.4. Throughout the metal transfer process, the current decreases to near-zero, effectively minimizing spatter generation. Once the metal transfer is complete, the arc reignites, and the wire is fed forward again, with the set welding current reflowing. As the weld pool cools, it solidifies, forming a sturdy welded joint [7].

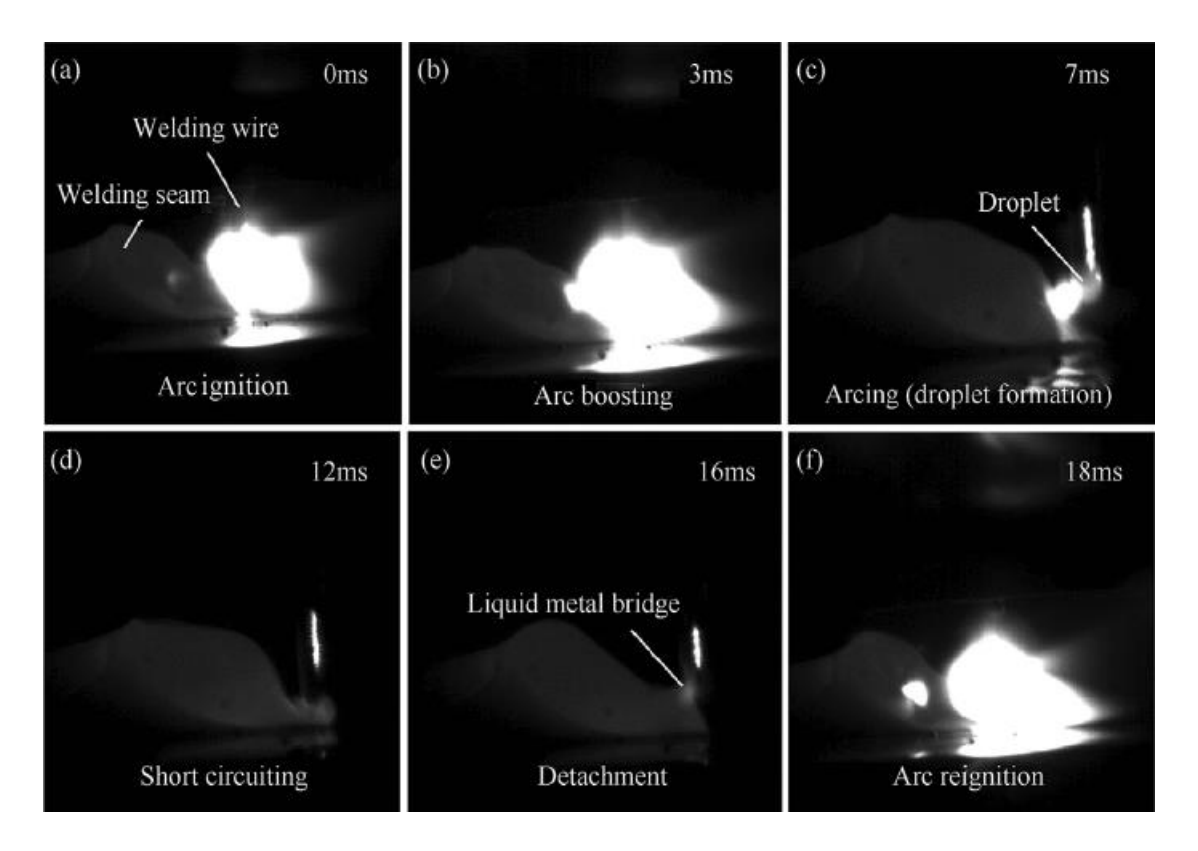


Figure I.4: High-speed images of droplet transfer [10].

A typical CMT welding electrical signal cycle is defined as the duration required to deposit a droplet of molten electrode into the weld pool. Some significant elements affecting the regulation of the size of the generated drop and its detachment are the magnitudes of the current and voltage, the wire-feed speed, the speed of travel, and the frequency. Analyzing the current and voltage waveform is crucial for understanding the energy distribution during different phases of the droplet transfer process [8]. This cycle is typically divided into three phases as follows proceed with description of the three phases.

- The peak current phase: This is a constant arc voltage corresponding to a high pulse of current causing the ignition of the welding arc easily and then heats the wire electrode to form droplet.
- <u>The background current phase:</u> The phase corresponds to a lower current. The current is decreased to prevent the globular transfer of the little liquid droplet formed on the wire tip. This phase continues until short circuiting occurs.
- The short-circuiting phase: In this phase, the arc voltage is brought to zero. At the same time, the return signal is provided to the wire feeder which gives the wire a back-drawing force. This phase assists in the liquid fracture and transfer of material into the welding pool [9].

The intricate waveform of the welding current in the CMT process, coupled with the "back feeding" mechanism of the filler wire that mechanically facilitates metal transfer, presents challenges in comprehending the correlation between welding parameters, metal transfer, and heat transfer [10], as illustrated in Figure 3.3.

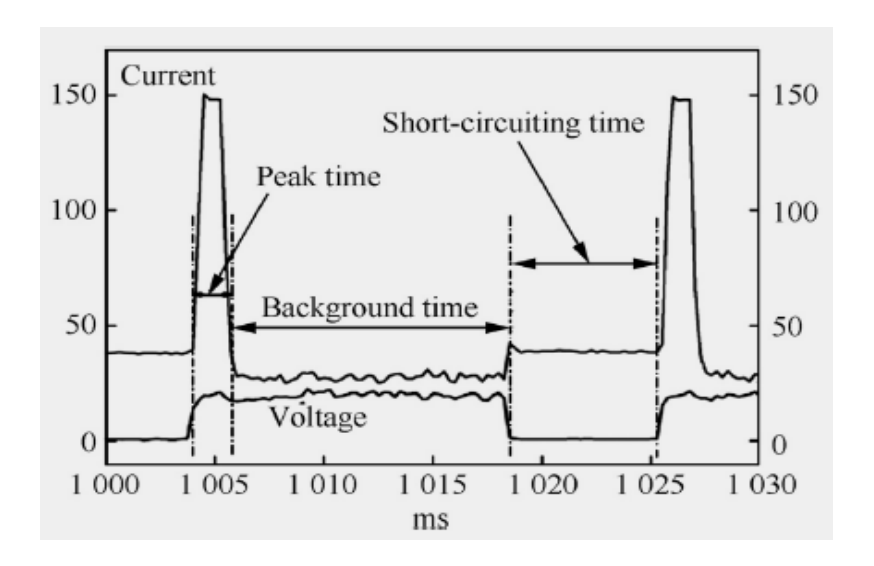


Figure I.5: Current and Voltage waveforms of CMT process [11].

I.1.4. Various Process Parameters and Their Influence during CMT process:

The CMT fabrication technique plays a pivotal role in determining the quality of the additively manufactured component. It involves complex multi-physical and interdisciplinary phenomena, necessitating extensive research to fully comprehend the physics and material science underlying this technology and achieve precise control over the production process. Various physical processes, such as heat transfer from the arc to the electrode wire, wire electrode melting, droplet formation, droplet deposition onto the substrate, cooling, and solidification of the beads, are involved and influence the overall process.

The performance and dimensional accuracy of the final product can be significantly affected by each of these procedures. Numerous technical factors govern these operations, and several studies have been conducted to investigate how these technological factors impact the geometry, surface morphology, and mechanical properties of additively fabricated products.

I.1.4.1. Electrode Polarity:

In CMT, the polarity of the welding electrode plays a significant role in weld quality and deposition rate. The two electrode polarities used in MIG welding are direct current electrode negative (DCEN) and direct current electrode positive (DCEP). DCEN polarity, also known as "straight polarity," involves the electrode being negative and the workpiece positive. This polarity is commonly preferred in the CMT process because it offers better penetration and control over heat input, resulting in stronger and more reliable welds. Conversely, DCEP polarity, also known as "reverse polarity," has the electrode positive and the workpiece negative. This polarity is generally avoided in the CMT process due to its tendency to yield lower deposition rates and lower-quality welds. Approximately two-thirds of the heat is generated at the wire electrode, with the remaining one-third produced at the substrate terminal, owing to fluctuations in voltage drop and current density at the cathode, anode, and plasma regions.

I.1.4.2. Wire Feed Speed (WFS) and Welding Speed:

In CMT process, the wire feed speed (WFS) and the attraction and retraction frequency of the wire tip along with their synchronization to the welding torch moving speed are crucial parameters affecting deposition quality and efficiency. Higher WFS increases deposition rate, shaping the bead, but excessive or insufficient WFS may lead to defects like porosity and

incomplete fusion due to altered heat input. Similarly, welding speed inversely affects deposition rate, bead shape, and heat input, thus influencing material properties and defect formation. Optimization of these parameters is essential to ensure desired deposition quality and efficiency.

I.1.4.3. Substrate and Interlayer Temperature:

The substrate and interlayer temperatures are critical parameters in the CMT process, influencing deposition quality and efficiency by impacting important properties like mechanical and microstructural characteristics of the fabricated component. The substrate temperature, representing the base material temperature before deposition, and the interlayer temperature, representing the previously deposited layer's temperature before the next layer, play vital roles. Here's a summary of their effects:

• Metallurgical bonding:

Proper substrate and interlayer temperatures are crucial for achieving metallurgical bonding between deposited layers and the base material. Too low temperatures can result in poor adhesion and weak mechanical properties due to inadequate bonding, while excessively high temperatures can cause over-tempering or material melting, weakening mechanical properties.

• Residual stress:

Substrate and interlayer temperatures impact residual stress in the deposited material. High temperatures can lead to increased residual stresses due to uneven cooling rates, while low temperatures can result in higher residual stresses due to differences in thermal expansion coefficients between the deposited material and the base material [33].

• Material properties:

Substrate and interlayer temperatures also influence material properties such as hardness, toughness, and ductility. Elevated temperatures may reduce material strength and toughness, while lower temperatures can increase material hardness, potentially leading to increased susceptibility to cracking and other defects.

I.1.4.4. Shielding Gas:

Shielding gas is an integral component of the CMT process, serving to protect the molten metal from atmospheric contaminants that can lead to oxidation and defects in the final product. It plays a crucial role in shielding the weld pool and stabilizing the arc, thereby

enhancing weld quality. Commonly used gases in the CMT process fall into two categories: active gases and inert gases. Carbon dioxide, an active gas, is frequently utilized due to its low cost and ready availability, although its use can lead to oxide production, spatter, and increased penetration due to the presence of oxygen. Argon, an inert gas, is often preferred for shielding non-ferrous metals like aluminum, copper, and titanium. It provides excellent arc stability, penetration, and prevents oxidation of the molten metal. Helium, another inert gas, is suitable for welding high-strength materials due to its ability to provide greater heat input and deeper penetration compared to argon. Carbon dioxide is a cost-effective option commonly used for welding mild steel, although it may result in more spatter and require higher voltage and amperage settings.

I.1.5. Applications of CMT

It is evident that the CMT process is highly suitable for manufacturing large-sized parts and components with numerous components, whether intricate or of large scale, having been already manufactured through this process. Some of the broad applications of CMT are as follows:

• Aerospace:

CMT is utilized in manufacturing aerospace components like turbine blades, landing gear, and engine parts. It enables the production of intricate geometries and facilitates the use of high-performance materials, contributing to enhanced performance and efficiency in aerospace applications.

• Automotive:

The automotive sector benefits from CMT in the production of engine blocks, transmission components, and suspension parts. The technology enables the fabrication of lightweight components with improved strength and durability, enhancing overall vehicle performance and fuel efficiency.

• Tooling:

CMT is employed in manufacturing tooling components such as molds, dies, and fixtures. It allows for the customization of tooling with reduced lead times and lower costs, enabling efficient production processes in various manufacturing industries.

• Architecture:

In architecture, CMT is used to manufacture components such as building facades and structural elements. The technology enables the creation of unique designs while minimizing

material waste, offering architects and designers greater flexibility and sustainability in construction projects.

I.1.6. Advantages and benefits of CMT

CMT welding offers numerous advantages, such as excellent weld joint quality, higher productivity, reduced operator fatigue and improved process control. It also reduces the burn-through risk due to its precise control over heat input and execution time. In addition, it provides good arc stability resulting in less spatter and improved weld bead shape. The following are the key advantages of CMT Welding:

• Precise Welding:

CMT welding is a highly precise technique that can produce high-quality welds. It uses a controlled and consistent wire feed that provides greater accuracy, even when welding thin metal sheets. This precision is essential when welding parts that require attention to detail, like aerospace, automotive, and medical devices.

• Reduced Heat Input:

Since CMT welding uses lower power and smaller welding arcs, it results in less heat input. This is advantageous as it reduces the risk of heat distortion, often when welding thicker parts. It also improves the weld's quality and reduces the required finishing.

• Less Spatter:

CMT welding produces less spatter compared to traditional welding techniques. This is a huge benefit, especially when welding parts that require a high degree of cosmetic finishing. It also reduces post-weld cleanup time, resulting in more efficient production [12].

From the early days of CMT, the technology has been evolved substantially. Advancement after advancement is announced almost daily. But why such enthusiasm exists in industry and academia to try to understand this process and work hard to address its challenges and adopt it to their products? There are several main factors for this motivation [6]:

• Rapid Prototyping:

CMT accelerates design cycles with cost-effective functional prototypes, reducing lead times.

• <u>Low-Volume Production:</u>

Simplifies supply chains and reduces investment barriers for niche production, enhancing flexibility.

• Lower Material Costs:

Initial costs are lower for CMT due to minimal tooling requirements, expediting breakeven points.

• Geometric Complexity:

Enables intricate designs without cost penalties, fostering "design for use" over "design for manufacture.

• Light weighting:

Linked with topology optimization, CMT produces high-strength, lightweight components, beneficial for resource efficiency.

• Parts Consolidation:

Reduces part count, assembly costs, and overall project risks while improving performance.

• Functionally Graded Materials:

Allows tailored material properties within components, particularly with DED processes.

• Conformal Cooling Channels:

Enhances productivity by optimizing cooling efficiency, especially in mold inserts.

• Parts Repair:

CMT offers safe, cost-effective solutions for tooling maintenance, prolonging tool life.

• Supply Shortage Solutions:

Provides resilience during crises by enabling local production of critical components.

• Localized Manufacturing:

Supports local economies and crisis response, shifting towards decentralized production.

• Health and Humanitarian Benefits:

Customized medical devices aid patient care, while AM explores solutions for humanitarian issues.

• Benefits for Developing Countries:

CMT facilitates industrialization pathways, particularly beneficial for less developed economies [13].

I.1.7. Common defects encountered in CMT

CMT is a relatively new technology for producing metal parts with high geometric complexity and accuracy. However, like any manufacturing process, it suffers from defects that can compromise the quality and functionality of the final product. Some common defects in the CMT process include porosity, lack of fusion, cracking, undercut, inclusions, and delamination.

I.1.7.1. Porosity

Porosity in the CMT process refers to voids within deposited material, compromising part properties. Factors contributing to porosity include improper welding parameters (e.g., speed, current, and voltage), inadequate shielding gas coverage, and workpiece surface cleanliness. Low-quality welding wire or improper wire feed speed can also contribute.

Optimizing welding parameters, ensuring high-quality welding wire and shielding gas, and proper surface cleaning are crucial for minimizing porosity. Post-processing techniques like hot isostatic pressing (HIP) or vacuum impregnation may be necessary to further reduce porosity and improve mechanical properties.

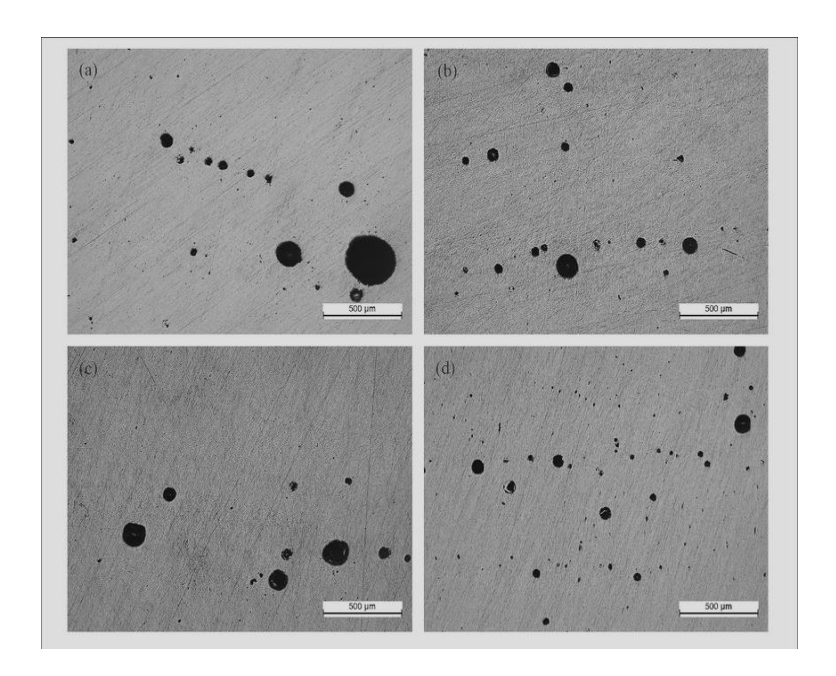


Figure I.6: Micrograph showing the holes formed during CMT process [29].

I.1.7.2. Lack of fusion

Lack of fusion, a common defect in the CMT process, occurs when deposited material fails to properly fuse with the underlying layer, weakening joints and reducing final part mechanical properties. Factors contributing to this defect include improper welding parameters (e.g., speed, current, and voltage), inadequate preheating or interpass temperature control, and use of low-quality welding wire or shielding gas.

Optimizing welding parameters to ensure sufficient heat input and fusion, along with proper preheating and interpass temperature control, is essential to mitigate lack of fusion. Using high-quality welding wire and ensuring adequate shielding gas coverage improves deposited material quality and reduces lack of fusion risk. Post-processing techniques like grinding, milling, or rewelding can address identified defects after inspecting the finished part for signs of lack of fusion and other welding defects.

I.1.7.3. Cracking

Cracking, a common defect in the CMT process, significantly compromises final part properties, especially mechanical ones. Several factors contribute to cracking:

• Residual stress:

Thermal stress buildup during CMT, particularly in large or complex geometries, can lead to cracking due to residual stress within the deposited material.

• **Inadequate interlayer bonding:**

Weak bonding between successive layers creates vulnerable points prone to cracking. Insufficient heat input or poor fusion between layers contributes to this issue.

• **Inadequate filler material:**

Mismatched filler material and base metal thermal properties create stress points within the deposited material, leading to cracking.

• Poor shielding gas coverage:

Inadequate shielding gas coverage results in oxidation and porosity, creating weak points susceptible to cracking within the deposited material.

It is important to optimize the welding parameters to minimize residual stress and ensure strong interlayer bonding to address cracking in CMT process. Proper filler material selection and shielding gas coverage can also help to reduce the risk of cracking. Additionally, heat treatment or stress relief annealing can be used to minimize residual stress and enhance the mechanical

properties of the final part. It is also important to inspect the finished part for signs of cracking and address any issues that are identified through appropriate repairs or re-welding as needed.

I.1.7.4. Undercut

Undercut, a common welding defect in the CMT process refers to a groove or depression at the base of the weld, compromising final part mechanical properties. Several factors contribute to its occurrence:

• Improper welding parameters:

Excessive heat input due to high current or voltage or low welding speed can lead to undercut formation.

• Inadequate cleaning:

Contaminants on the work-piece surface, resulting from inadequate cleaning before welding, contribute to undercut formation.

• Inadequate filler material:

Mismatched filler material and base metal thermal properties create stress points within the deposited material, leading to undercut.

• Poor joint preparation:

Improperly prepared joints create weak points susceptible to undercut.

Optimizing welding parameters for adequate heat input and fusion, proper workpiece surface cleaning, and joint preparation are crucial to mitigate undercut in the CMT process. Using high-quality filler material matching the base metal minimizes undercut risk. Inspecting finished parts for undercut signs and addressing issues through repairs or re-welding as needed ensures defect-free final parts.

I.1.7.5. Inclusion:

Inclusions, common in the CMT process, are non-metallic materials trapped within the deposited material. Several factors contribute to their occurrence:

• Improper welding wire selection:

High non-metallic material content in welding wire leads to inclusion formation.

• **Inadequate cleaning:**

Contaminants on the work-piece surface, due to insufficient cleaning before welding, contribute to inclusion formation.

• Poor shielding gas coverage:

Inadequate shielding gas coverage results in oxidation and inclusion formation within deposited material.

• <u>Improper welding parameters:</u>

Excessive heat input from high welding current or voltage or slow welding speed leads to inclusion formation.

I.2. Thermal phenomena in CMT process

The weld pool created during CMT process (possibly supplied by an external supply of matter) is the seat of very complex thermo-physical processes involving interdependent thermal, convective, chemical and electromagnetic phenomena (Figure I.7). The morphology of the bath (molten volume, geometry, etc.) is conditioned by numerous parameters [14] that we can group into two categories:

I.2.1. Parameters linked to incident energy

- Spatial distribution of energy in the arc.
- Arc pressure.
- Arc efficiency.

I.2.2. Parameters linked to the convection of liquid metal

The convection movements of the liquid metal significantly influence the shape of the cord [15, 16, 17]. The bath is in balance under the action of forces of different origin, which are:

- 1- The forces of gravity (buoyancy).
- 2- Surface tensions (Marangoni forces).
- 3- The viscosity of the liquid metal.
- 4- Aerodynamic shear.
- 5- Electromagnetic forces (Lorentz forces).

Each of these forces will act differently on the geometry of the bath. So, for example, Lorentz forces and surface tension currents (Marangoni force in the case where the tension gradient is

positive) increase penetration, opposite to buoyancy forces and aerodynamic shear forces of the shielding gas [18].

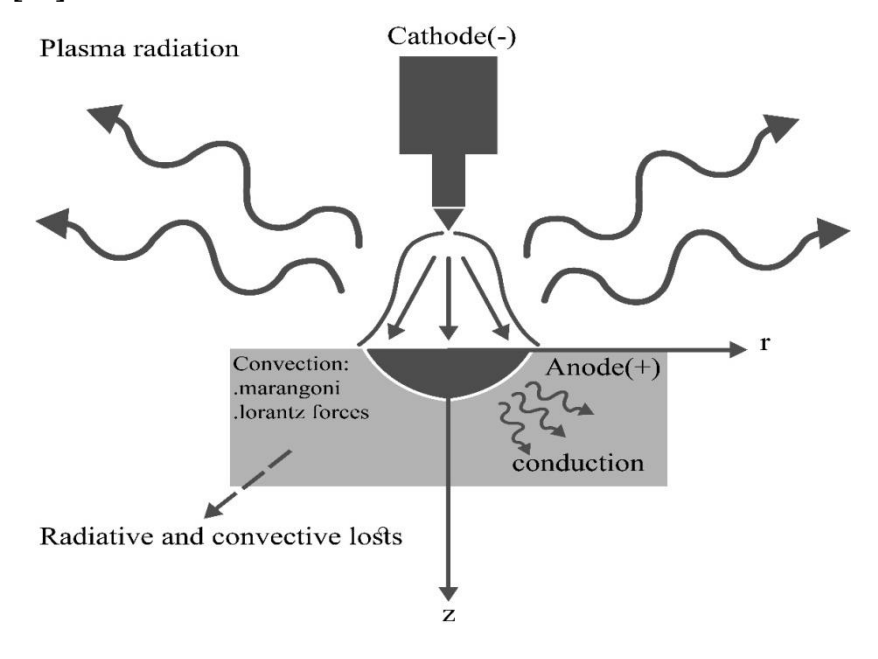


Figure I.7: Energy transfer in CMT process

I.3. State of the art on the simulation and analysis of the thermal aspect of CMT

I.3.1. Consequences and interaction of different physical phenomena

When discussing the consequences and interactions of these different phenomena in CMT welding, several aspects may be considered:

• Thermal Dynamics:

Understanding the heat transfer mechanisms and thermal gradients involved in the CMT process is crucial. This includes heat input, heat affected zones, and the formation of weld pools.

• Material Interaction:

Consideration of how different metals interact during welding is important. This involves metallurgical transformations, such as phase changes, solidification behavior, and potential formation of intermetallic compounds.

• Weld Pool Dynamics:

The behavior of the molten weld pool influences the final weld characteristics. Factors such as surface tension, fluid flow dynamics, and solidification rate affect weld pool geometry and microstructure.

• Electrical and Magnetic Effects:

CMT welding often involves the use of electrical currents and magnetic fields. Understanding their influence on arc stability, metal transfer modes (e.g., droplet detachment), and arc shape is essential.

• Gas Shielding and Atmosphere:

The choice of shielding gas and its flow rate influence weld quality and properties. Interaction between the shielding gas and the arc, as well as gas flow dynamics around the weld pool, affect gas coverage and protection from atmospheric contamination.

• Mechanical Properties:

The consequences of various welding parameters and phenomena on the mechanical properties of the welded joint, including strength, ductility, and toughness, must be assessed.

• Defect Formation:

Consideration of potential defects, such as porosity, lack of fusion, or solidification cracks, and their underlying causes is important for process optimization and defect prevention.

• Process Stability and Control:

Interaction between different phenomena can affect process stability and repeatability. Control strategies, such as arc voltage regulation or wire feed rate modulation, may be employed to mitigate variations and ensure consistent weld quality.

By understanding and analyzing these aspects, researchers and practitioners can optimize the CMT welding process, predict the consequences of different parameters, and improve the quality and reliability of welded joints. And generally, the interactions between these different phenomena can be defined in six steps:

- 1- Temperature field causes phase changes and micro-structural modifications.
- 2- The absorption and release of latent heat causes the temperature field to vary.
- 3- The temperature field causes thermal deformations and affects the properties mechanics which are a function of temperature.
- 4- Mechanical deformations, which are accompanied by heat release (dissipation intrinsic), vary the thermal conditions at the boundaries (but very small effect).
- 5- The elastic and plastic properties of the material vary with the modification of the metallurgical composition. To thermal deformations are therefore added plasticity deformations of the transformation [19, 20].

6- The mechanical effect on the metallurgical state is weak and is represented by the fact that the stress states, in the material, vary the kinetics of microstructural modifications and the temperatures at which these modifications occur.

I.3.2. Mathematical models of heat sources

In the context of Cold Metal Transfer (CMT) welding, a heat source model refers to a mathematical representation or computational framework used to simulate the distribution and behavior of heat generated during the welding process. CMT welding is characterized by its precise control and reduced heat input, making accurate heat source modeling crucial for understanding and optimizing the process.

Heat source models in CMT welding typically take into account factors such as the welding current, voltage, torch angle, retracting cycle of filler, and material properties to approximate the heat input from the welding arc. These models may vary in complexity, ranging from simple analytical equations to more sophisticated numerical simulations using finite element methods or computational fluid dynamics.

By simulating the heat input, these models enable engineers and researchers to predict temperature distribution, thermal cycles, and metallurgical transformations in the welded material. This insight helps in optimizing welding parameters, minimizing distortion, and ensuring high-quality welds in CMT welding applications.

The construction and relevance of the thermal model is mainly based on the type of heat source. To model the heat input of a CMT or mostly any welding process, two methods are possible [21]:

• Imposing the temperature on the weld pool:

This approach is simple to use (knowledge of the shape of the melted zone is sufficient) and makes it possible to obtain a fairly realistic correlation between the experiment and the model. However, it underestimates the quantity of energy provided by the process as well as the thermal field induced in the assembly. The use of this technique is generally discouraged [22, 21].

• Imposition of a heat flow:

Which can be a surface heat flow or a volume heat flow. This flow is determined by the welding power brought to the assembly, and that means the nominal power multiplied by the efficiency of the process that must be adjusted. The shape of the distribution of this flux is substantially linked to the welding process considered and dependent on it. For welding processes involving high energy densities, such as Electron Beam welding or Laser welding, the energy is deposited deep in a capillary considered as a volume heat source while, simultaneously, the vaporization of part of the metal and the plasma act as a surface heat source. In this case, the heat source is often modeled as the superposition of a volume source and a surface source [23].

In the case of CMT procedure, the energy coming from the arc is deposited mainly on the surface. The heat input results from electro-magneto thermo fluid interactions coupled with a cover of plasma. This plasma can be modeled as a point heat source, in line segments heat source or a surface heat source. However, a volumetric heat sources suitable when we want to include in the formulation of the heat input the energetic contribution of the phenomena which take place in the weld pool according to an adequate form [24].

The heat input therefore also depends on the presence or absence of filler metal as well as the type of single or multi-pass process [26].

One thing should be putting in account beside choosing the right heat source model to simulate the thermal, mechanical or metallurgical phenomena occurring during the cold metal transfer process, is the retracting mechanism of the welding filler. This mechanism happens each time a short circuit is detected, to give cooling time before every placed drop, so the heat source here becomes periodic, and a pulse function must be integrated in the heat flux governing equation.

In the following, we present some adapted models of heat sources, where the mathematical expressions are written in a reference linked to the source.

I.3.2.1. Surface heat sources

There are two predominant surface heat source design types: circular and bi-elliptical, with different forms of flux distribution allowing the study of the influence operational and geometric parameters on the morphology of the drop-by-drop welded deposition path. They are especially used for thin sheets [25].

1) Circular:

The way of representing this surface flow at constant or variable density, on a disk of constant radius Rd or infinite, is summarized in Table I.1.

Table II.1 :surface heat sources examples.

Constant flow on a disk of radius R_d	Gaussian flow with infinite reparation	Gaussian flow with finite distribution on a disk of radius R_s
Qm Rd y x=X-vt	Qm X x=X-vt	$q(r)$ Q_m R_s $x=X-vt$
$q(x,y) = q(r) = \begin{cases} Q_m & r \le R_d \\ 0 & r > R_d \end{cases}$ $Q_m = \frac{Q_0}{A} = \frac{Q_0}{\pi R_d^2}$ $Q_0 = UI\eta$ $r^2 = x^2 + y^2$	$q(x,y) = q(r) = Q_m e^{-Kr^2}$ $Q_m = \frac{Q_0}{2\pi\sigma^2}$ $K = 1/(2\sigma^2)$	$q(x,y) = q(r) = Q_m e^{\frac{-3r^2}{Rs^2}}$ $si \ r \le R_s$ $q(x,y) = 0$ $si \ r > R_s$ $Q_m = \frac{3Q_0}{\pi R_s^2}$
(I.3)	(I.2)	(I.3)
$f(x,y) = \begin{cases} 1 & r \le R_d \\ 0 & r > R_d \end{cases}$ $A = \pi R_d^2$	$f(x,y) = e^{-Kr^2}$ $A = \frac{\pi}{K}$	$f(x,y) = e^{\frac{-3r^2}{Rs^2}}$ $A = \frac{\pi R_s^2}{3}$

Where σ is the standard deviation of the Gaussian (in m) and r is the radial distance (Figure I.4). K is sometimes called the source distribution coefficient, when it tends towards zero, we find the case of the point source [24]. In the literature, other forms of distribution can be considered. But all are following the general equation form bellow.

$$q(x,y) = Q_m \frac{f(x,y)}{A} \tag{I.4}$$

Where f(x, y) is the surface distribution function and Q_m is the maximum of the power density expressed in (W/m^2) .

2) <u>double-ellipsoid:</u>

Its formulation is based on the consideration of a surface distribution at different radius from the heat source onto the welded joint. This heat source is similar to the form of the molten pool which moves under the electrode, considering that it is two half-ellipses (Figure I.8) [24,27]. The mathematical expression of this model written in a reference linked to the part is:

$$q_s = q(r_i, t) = q(x, y, t) = Q_m e^{f(x, y, t)}$$
 (I.5)

With

$$Q_m = \frac{3Q_0}{\pi r_x (r_{yr} + r_{yf})/2} \quad \text{were} \quad Q_0 = U I \eta$$

And

$$f(x, y, t) = -3\left(\frac{x^2}{r_x^2} + \frac{(y - vt)^2}{r_y^2}\right)$$

Where $r_y = r_{yf}$ or $r_y = r_{yr}$ Depends on whether the point considered (x, y) is respectively in front or the rear of the center of the bi-elliptical molten pool (Figure I.8). These radiuses are fixed in such a way that the flux $q(r_i)$ is equal to 5% of the maximum flux Qm, on the contour of this geometry.

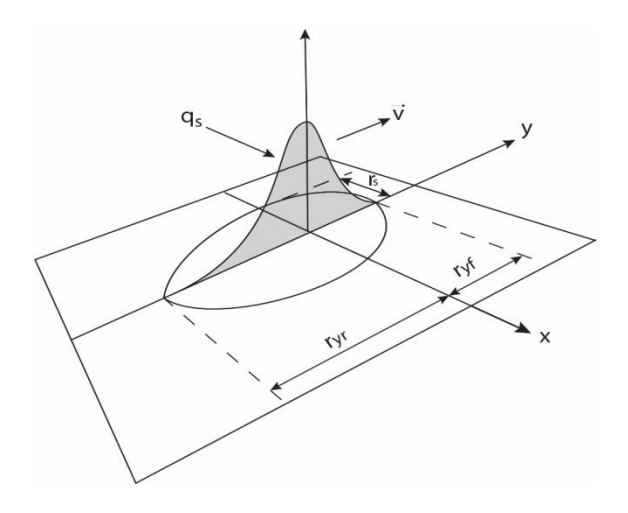


Figure I.8:: Illustration of double-ellipsoid heat source shape

I.3.2.2. Volume heat sources:

In the case where the welding power is distributed in volume, we model the contribution of heat as being an internal source of heat, that is to say a volume density of heat flux applied within the material. This last type of modeling is more suitable when we want to include the energy contribution in the formulation of the heat input phenomena that take place in the weld pool and the participation of the filler metal. The volume flow of heat, expressed in W/m3, is then written (in a reference linked to the source [14]:

$$q_v(x, y, z) = Q_0(x, y, z) \text{ with } \int_{V} q_v(x, y, z) . dv = Q_0 = UI\eta$$
 (I.6)

The most commonly used form of the distribution function g(x, y, z) can be a half-sphere or an ellipsoid having radii a, b and c (Table I.3). The mathematical expression that describes the ellipsoid in the case of a Cartesian coordinate system [28, 24] is as follows.

$$q_v(x, y, z) = \frac{6\sqrt{3}.Q_0}{abc\pi\sqrt{\pi}}e^{\left(-3\left[\frac{x^2}{a^2} + \frac{y^2}{b^2} + \frac{z^2}{c^2}\right]\right)}$$
(I.7)

Radiuses a, b and c correspond to rays for which the energy is equal to 5% of the peak.

a) Case of a constant distribution of the volume flow

This is the case of a constant energy density on a half-sphere of radius R (TableI.2.a). From equation (I.6) we arrive at:

$$q_v(x, y, z) = Q_m. 1 = cte \ and \ q_v = \frac{Q_0}{V_{half-sphere}} = \frac{2Q_0}{\left(\frac{4}{3}\pi R^3\right)}$$
 (I.8)

Table I.2: some models adapted for the simple volume heat source.

Volume heat source: $q_v(x, y, z) = Q_0 g(x, y, z)$	
Constant in a half-sphere with radius R	3D Gaussian with a finite distribution of
	radius a b c
$q_v(x, y, z) = \begin{cases} Q_m = cte & if \ r \le R_d \\ 0 & if \ r > R_d \end{cases}$	$q_{v}(x, y, z) = \frac{6\sqrt{3}. Q_{0}}{abc\pi\sqrt{\pi}} e^{\left(-3\left[\frac{x^{2}}{a^{2}} + \frac{y^{2}}{b^{2}} + \frac{z^{2}}{c^{2}}\right]\right)}$
(a) Z Q_{m} R_{α} $X=X-vt$	Q_m R_d Q_m R_d $X=X-vt$

b) Arc case:

widely used in CMT process simulation and arc welding with material addition (TIG, MIG/MAG), Goldak [24] suggests a volume source in the shape of two half-ellipsoids (Figure I.9); these allow to take into account the difference in heat input between the front and back of the electrode. This source is described by the following relationships:

$$q_{v}(x, y, z) = \frac{6\sqrt{3} \cdot Q_{0} f_{i}}{a_{i} b c \pi \sqrt{\pi}} e^{\left(-3\left[\frac{x^{2}}{a_{i}^{2}} + \frac{y^{2}}{b^{2}} + \frac{z^{2}}{c^{2}}\right]\right)}$$

$$f_{f} + f_{r} = 2$$
(I. 9)

With
$$\begin{cases} i = f \text{ if } x \ge 0 \\ i = r \text{ if } x < 0 \end{cases}$$

and to ensure continuity in x=0 we have:

$$f_f = \frac{2a_f}{a_f + a_r}$$
 and $f_r = \frac{2a_v}{a_f + a_r}$

Were $(f_f = 0.6 \text{ and } f_r = 1.4)$ [24].

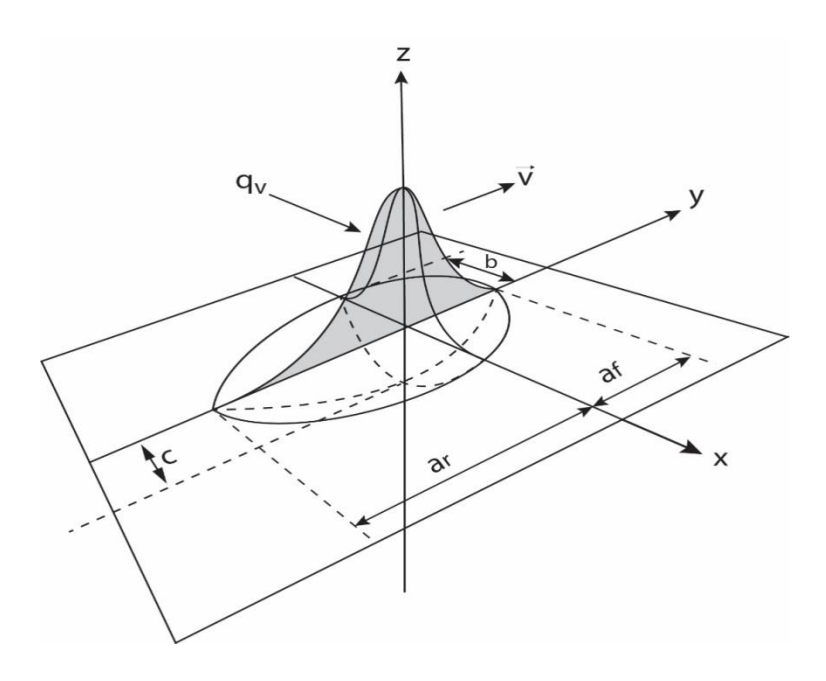


Figure I.9: 3D double-ellipsoid heat sources.

CHAPTER II numerical modeling

II. Chapter II: numerical modulization

II.1.welding of metal plate

II.1.1. Thermal modeling

The complete modeling of thermal processes involving electric arcs and molten pools is highly complex, requiring consideration of various factors like thermo-fluid heat transfers and electromagnetic phenomena. While extensive literature exists on modeling these aspects, our study simplifies by focusing solely on heat conduction. We replace the intricate details of the arc and molten pool with a simplified heat source. While this approach provides insights, it's important to acknowledge its limitations in accurately representing the system.

II.1.2. Thermal problem: equation

II.1.2.1. Hypotheses

To study and model heat transfers during a welding (figure II.1), hypotheses are required:

- 1-The 3D axisymmetric heat transfer problem (ABFE plane of symmetry),
- 2-Throughout the study, it is assumed that the heat source is moving. Although complex paths of the source can be considered, we place ourselves in the case of a rectilinear translation at constant speed along an axis in Cartesian coordinates (case of plate welding).
- 3-The regime is considered Transitional,
- 4- The X axis coincides with the welding direction
- 5- The physical properties of the material are considered constant.
- 6-The flow in the weld pool and the electromagnetic phenomena (the forces of gravity (buoyancy), surface tensions (Marangoni forces), viscosity of the liquid metal, aerodynamic shear, electromagnetic forces (Lorentz forces)) are considered negligible.
- 7-Heat losses by convection and radiation through free surfaces and the boundaries of the room are taken into account

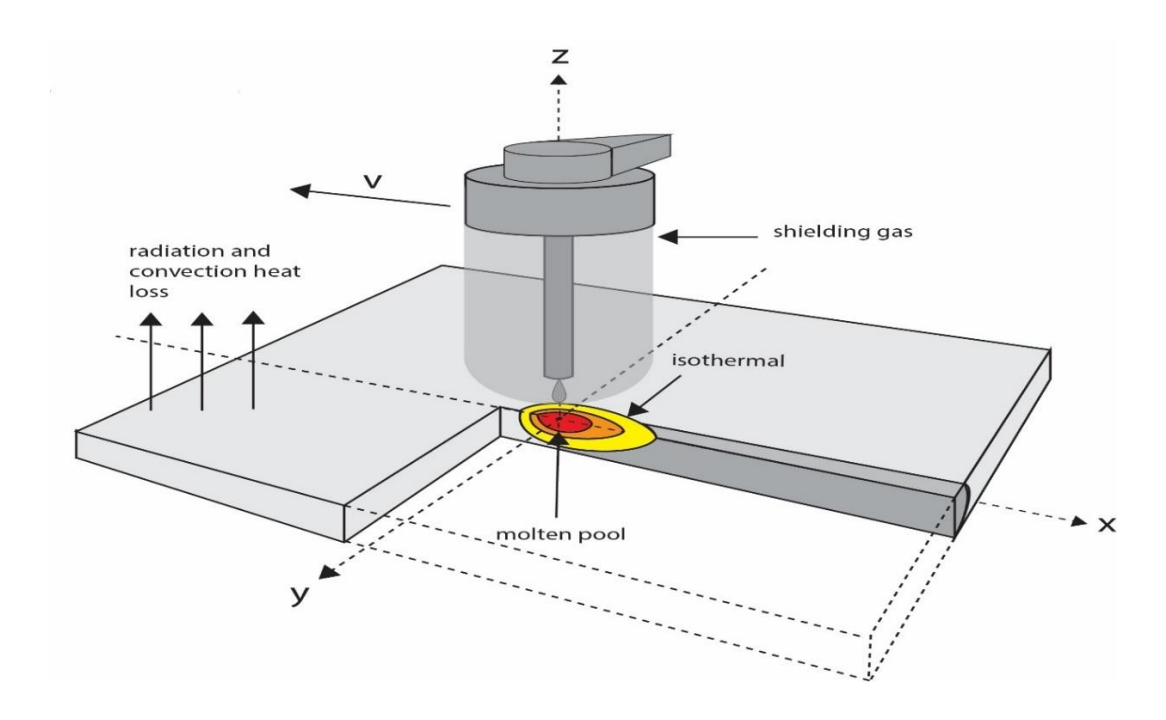


Figure II.1: the welding process of two thin sheets

II.1.2.2. Heat governing equation

The heat conduction equation in the domain Ω (domain defined by the two metal plates to weld) (figure: II.1) is written for the three-dimensional case.

$$\rho c_p \frac{\partial(T)}{\partial t} = \frac{\partial}{\partial x} \left(K \frac{\partial T}{\partial x} \right) + \frac{\partial}{\partial y} \left(K \frac{\partial T}{\partial y} \right) + \frac{\partial}{\partial z} \left(K \frac{\partial T}{\partial z} \right) + S \tag{II. 1}$$

Where T is the temperature, t the time, ρ the density of the material to be welded, Cp the specific heat, K the thermal conductivity and S the heat generated or absorbed per unit of time

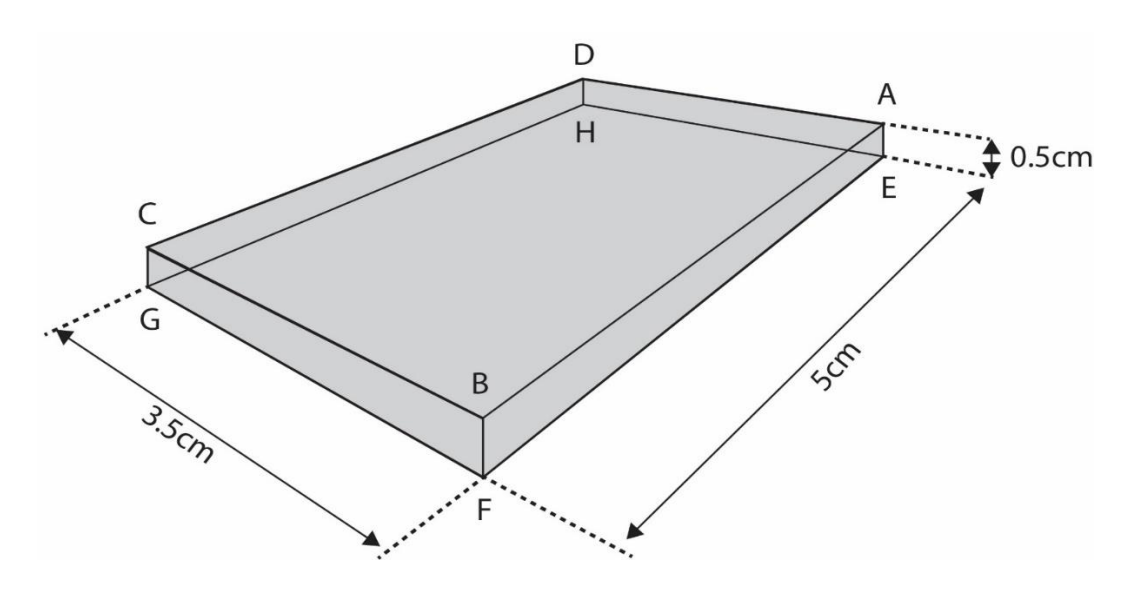


Figure II.2: Ω domain and boundaries

The general form of the equation above is

$$\rho c_p \frac{\partial T}{\partial t} = -div(-K \overrightarrow{grad} \overrightarrow{T}) + S \tag{II. 2}$$

The solution of this equation gives the temperature distribution in the domain Ω , that means the change in temperature with relative to the change in position and time.

II.1.2.3. Boundary and initial conditions

The boundary conditions are determined from the equations of the heat flow exchanged with the surrounding environment by convection and radiation.

1) The energy given by the electric arc is modeled by a heat source S which is moves with a speed v along the x axis, this heat flux is q is transmitted to the plate through the upper face (ABCD).

$$q_n = S - [h_{\infty}(T - T_{\infty}) + \sigma \varepsilon (T^4 - T_{\infty}^4)]$$
 (II. 3)

2) At the borders (ADHE), (DCGH), (BCGF) and (EFGH) (Figures 2.II), the flow *qn* is equal to:

$$q_n = h_{\infty}(T - T_{\infty}) + \sigma \varepsilon (T^4 - T_{\infty}^4) \tag{II.4}$$

Were

 h_{∞} : convection coefficient.

T: temperature at the edge of the assembly (*K*).

 T_{∞} : ambient temperature (K).

 ε : thermal emissivity.

 σ : Boltzmann constant equal to 5.67. 10^{-8} w/ m^2K^4 .

3)In the symmetry plan (ABFE), the heat flow is zero:

$$q_n = -K\frac{\partial T}{\partial x} = 0 (II.5)$$

4)-The initial temperature of the material is assumed equal to the ambient temperature

II.1.2.4. Final equations system

We have the three following equations

$$\rho c_{p} \frac{\partial(T)}{\partial t} = \frac{\partial}{\partial x} \left(K \frac{\partial T}{\partial x} \right) + \frac{\partial}{\partial y} \left(K \frac{\partial T}{\partial y} \right) + \frac{\partial}{\partial z} \left(K \frac{\partial T}{\partial z} \right) + S$$

$$q_{n} = S - \left[h_{\infty} (T - T_{\infty}) + \sigma \varepsilon (T^{4} - T_{\infty}^{4}) \right] in (ADHE), (DCGH), (BCGF) and (EFGH)$$

$$q_{n} = 0 in (ABFE) \tag{II. 6}$$

The source term S will be modeled subsequently to close the system of equations. The equation the final differential is therefore a nonlinear partial differential equation.

II.1.2.5. Heat source models

In our study, the heat source model used is The Goldak Double-Ellipsoid Heat Source. Were The center point of the weld arc moves along the x axis, at a velocity v. Its current position is thus given by $x_0 = v.t$. The heat source by Goldak is defined by two regions that join at x_0 , and whose shapes are ellipsoidal. The widths a and depths b of these regions are equal, but the front and rear lengths, c_f and c_r , may differ, see Figure 4. The heat source is given by:

$$q_{v} = \begin{cases} Q_{m} \cdot e^{\left(-3\left[\frac{(x-x_{0})^{2}}{c_{f}^{2}} + \frac{y^{2}}{a^{2}} + \frac{z^{2}}{b^{2}}\right]\right)}(x \ge x_{0}) \\ Q_{m} \cdot e^{\left(-3\left[\frac{(x-x_{0})^{2}}{c_{f}^{2}} + \frac{y^{2}}{a^{2}} + \frac{z^{2}}{b^{2}}\right]\right)}(x < x_{0}) \end{cases}$$
(II. 7)

where Q_m as mentioned in chapter one is the power density of the weld, given by:

$$Q_{m} = \frac{6\sqrt{3}. Q_{0} f_{r}}{c_{r} b c \pi \sqrt{\pi}} = \frac{6\sqrt{3}. Q_{0} f_{f}}{c_{f} b c \pi \sqrt{\pi}}$$
(II. 8)

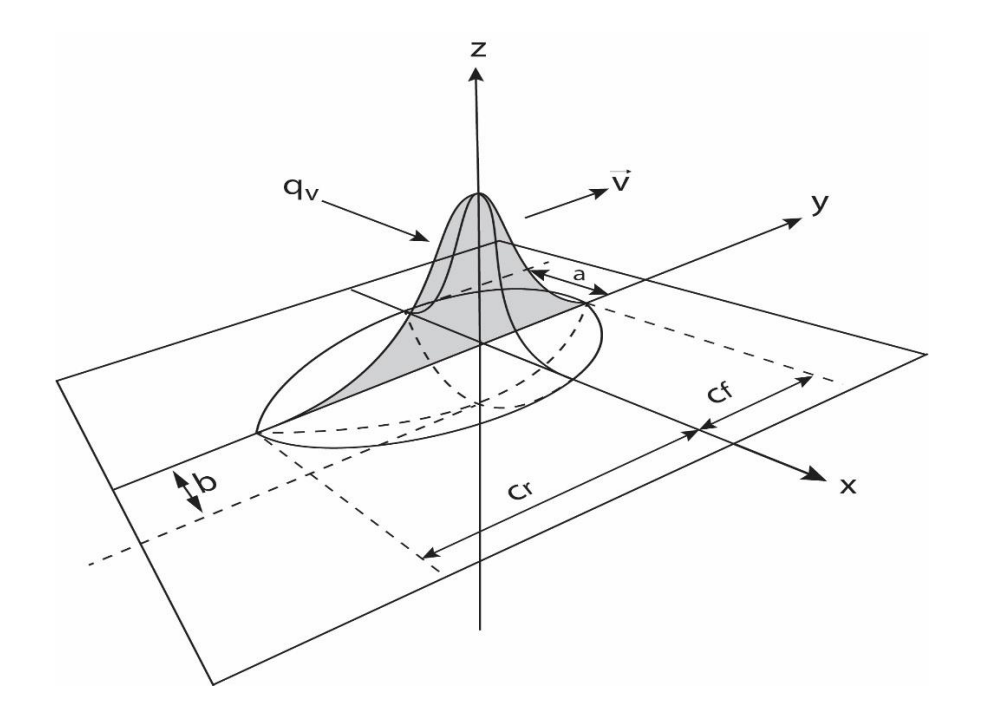


Figure II.3 : 3D double-ellipsoid heat sources.

II.1.2.6. Pulsing effect

The pulsing effect as mentioned in chapter one is the result of the automatic current cut each time a drop of melting feeding wire is in touch with the molten pool causing a short circuit, the

modeling of this effect required the integration of a periodic function β into the moving heat source heat flux equation.

$$q(n)_{pulsed} = q(n).\beta \tag{II.9}$$

Were

$$\beta = rect1\left(mod\left(t[s], \frac{1}{f}\right)\right) \tag{II. 10}$$

Were f is the frequency of the pulsing, rect1 is the COMSOL rectangular pulse function module and mod is the COMSOL command that create the repetition of the pulse every (1/f) step in time t.

II.1.3. Materials

The materials used in this simulation are the titanium grade one alloy, aluminum 1050 alloy and the ARMCO iron alloy. The thermal properties such as thermal conductivity, heat capacity, and materials density will be taken from the COMSOL material library.

II.1.4. properties

All the properties needed are gathered in the table below.

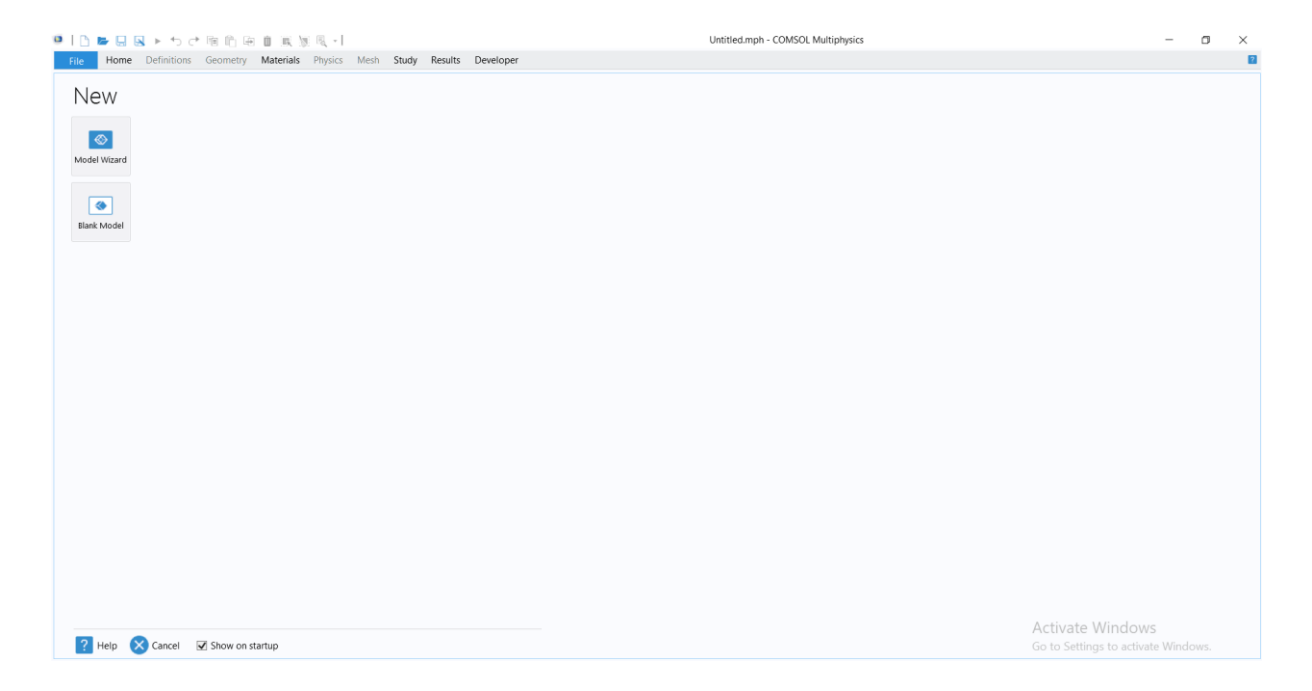
Table II.1: simulation properties.

Name	value	description
L_{x}	0.05m	Plate length
L_{y}	0.035m	Plate width
L_z	0.005m/0.002m/0.008m	Plate thickness
Q_0	800W /850W /900W	Weld power
v	0.001m/s	Welding speed
\boldsymbol{A}	0.004m	Goldak ellipsoid measurement
В	0.004m	Goldak ellipsoid depth
C_r	0.008m	Goldak ellipsoid length, rear
C_f	0.004m	Goldak ellipsoid, front
f_r	1.3333	Goldak parameter
f_f	0.66667	Goldak parameter
F	50Hz	Pulse frequency
ε	0.4	emissivity
h	$10W/m^2.K$	Convective heat transfer coefficient

II.1.5. COMSOL modeling Instructions

1) Choosing physical model

- Run COMSOL Multiphysics program

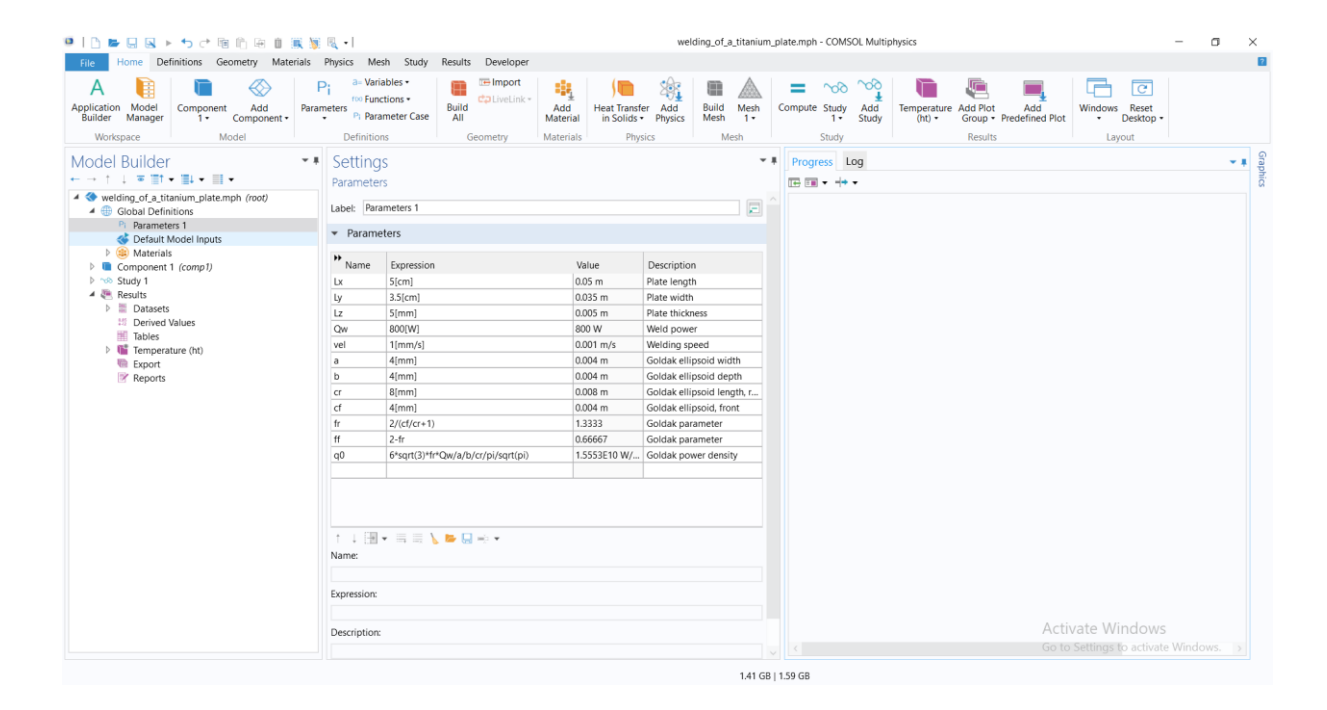


- From the File menu, choose New.
- In the New window, click Model Wizard.
- In the Model Wizard window, click 3D.
- In the Select Physics tree, select Heat Transfer>Heat Transfer in Solids (ht)
- Click Add.
- Click Study.
- In the Select Study tree, select General Studies>Time Dependent.
- Click ☑ Done.

By clicking done you will enter the COMSOL Multiphysics main work section, where you can start defining your simulation step by step

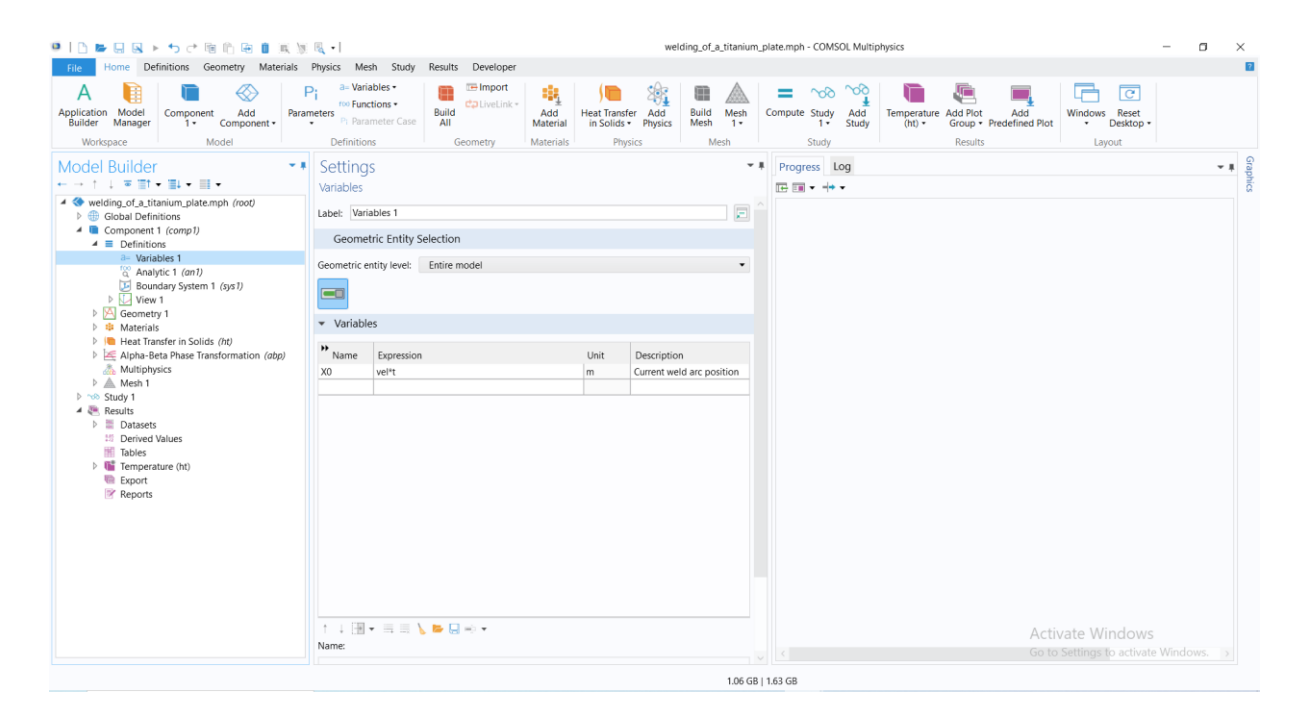
2) Properties

- In the Model Builder window, under Global Definitions click Parameters 1.
- In the Settings window for Parameters, locate the Parameters section.
- In the table, enter the settings provided in table II.1.



3) Variables

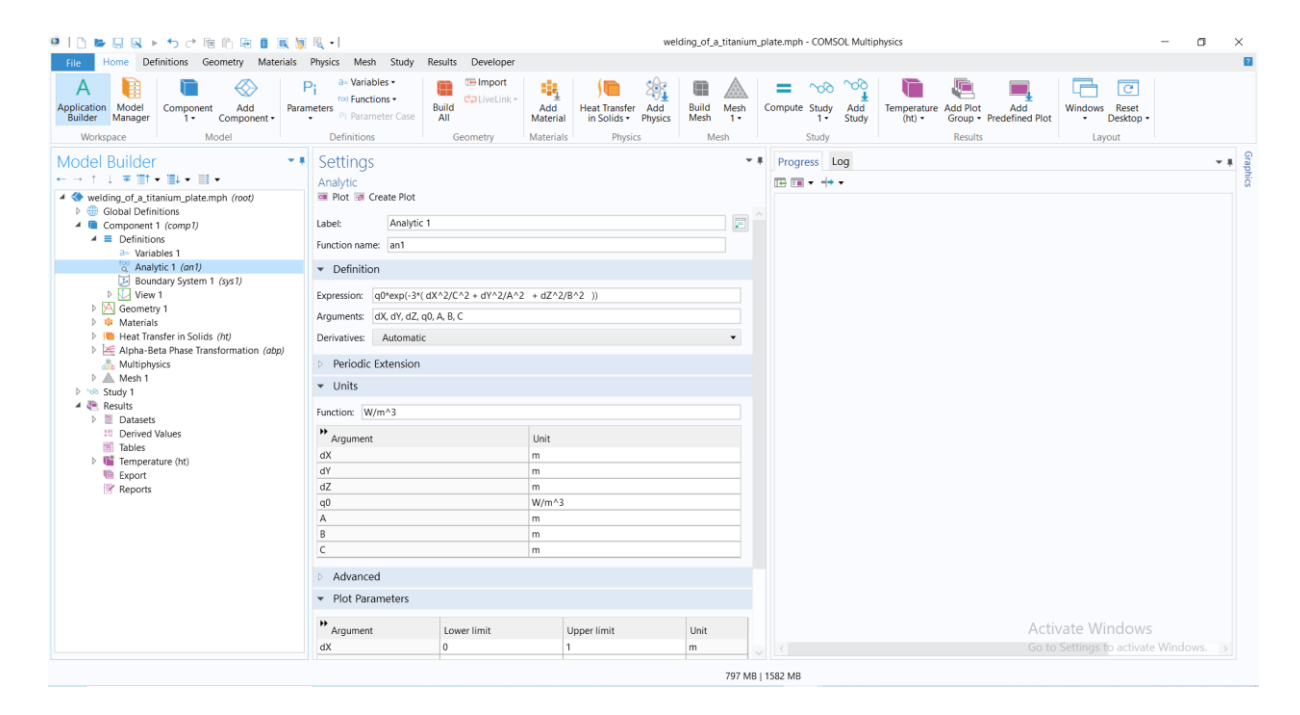
- In the Model Builder window, expand the Component 1 (comp1).
- Right-click Definitions and choose Variables.
- In the Settings window for Variables, locate the Variables section.
- In the table, enter the settings for x_0 .



4) Heat flux analytical function

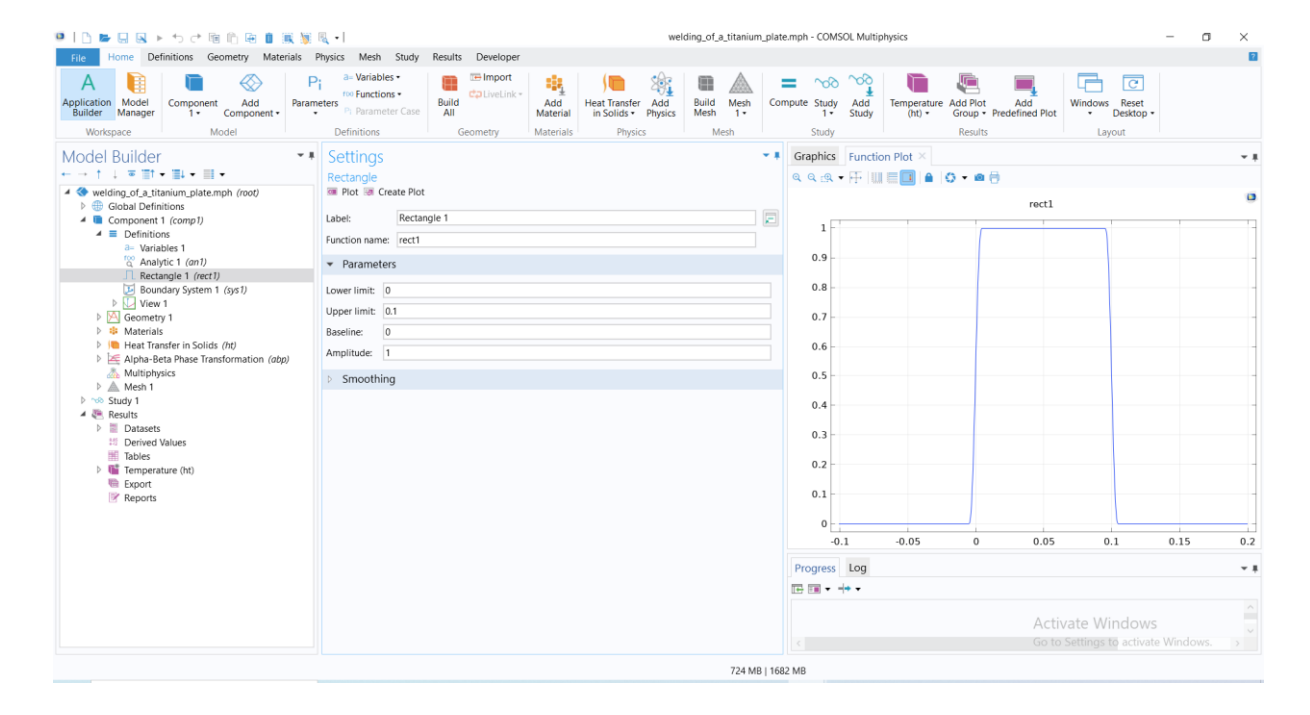
- In the Home toolbar, click Functions and choose Local>Analytic.
- In the Settings window for Analytic, locate the Definition section.

- In the Expression text field, type
- In the Arguments text field, type dX, dY, dZ, q0, A, B, C.
- Locate the Units section. In the Function text field, type W/m^3.
- In the table, enter the units of arguments



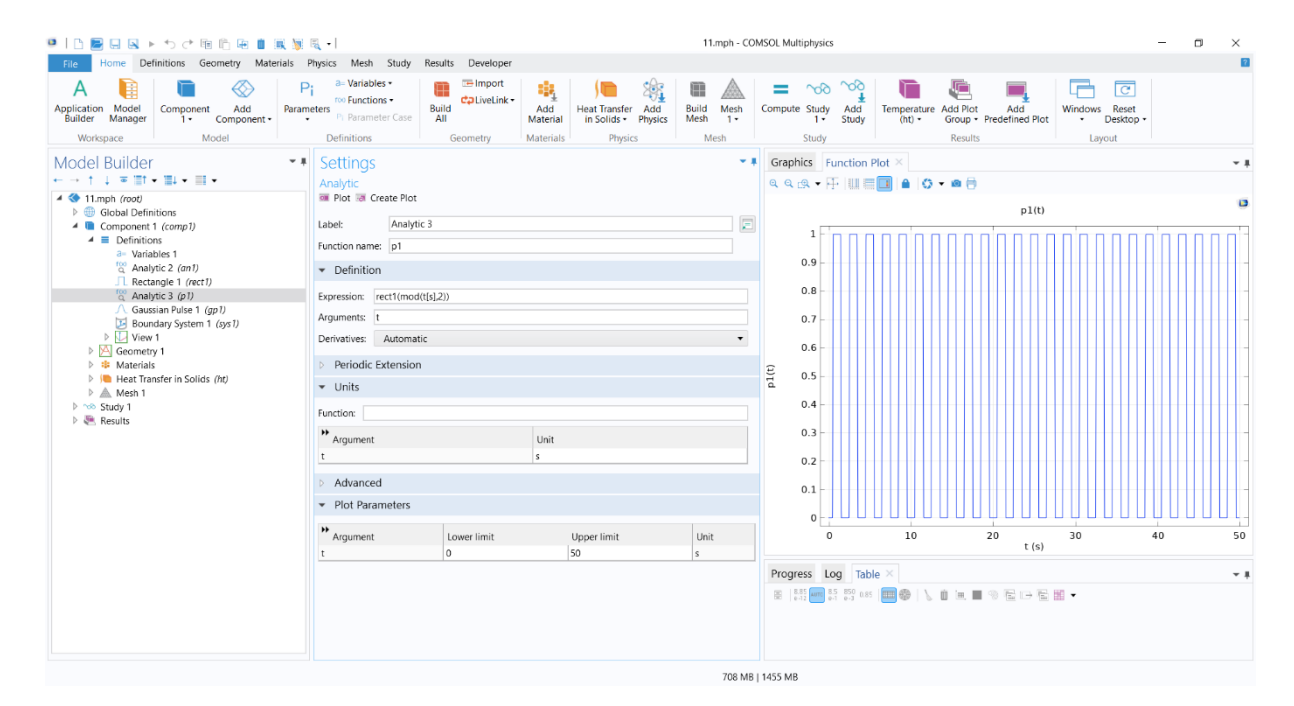
5) Rectangular function

- In the Home toolbar, click Functions and choose Local>Rectangle.
- inter the parameters for the rectangular pulse in the parameter section.



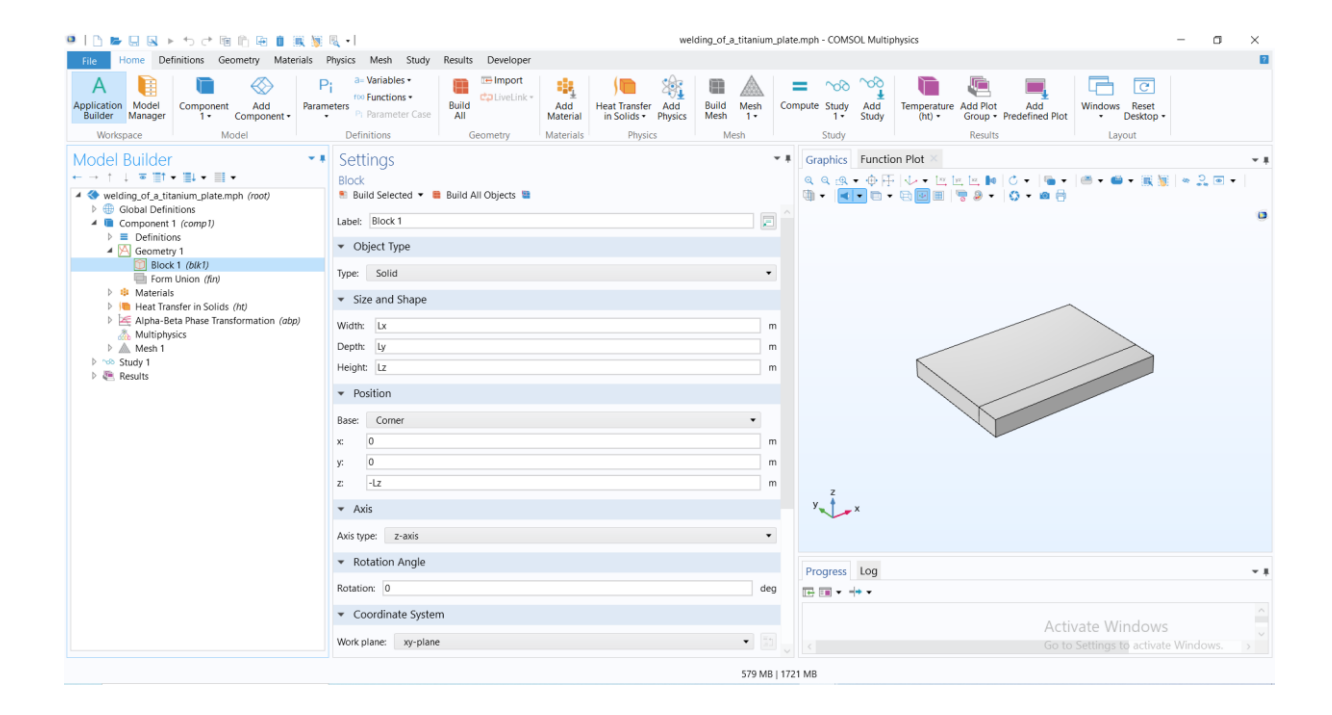
6) Modeling of pulse function

- In the Home toolbar, click Functions and choose Local>Analytic.
- in the Function name write (Pulse1).
- in the Expression section write the pulse function expression.
- in the Argument section write t.
- in the Units section set the t unit to second.
- in the Plot Parameters section set the lower and upper limits of the function as the beginning and ending time of the welding process.



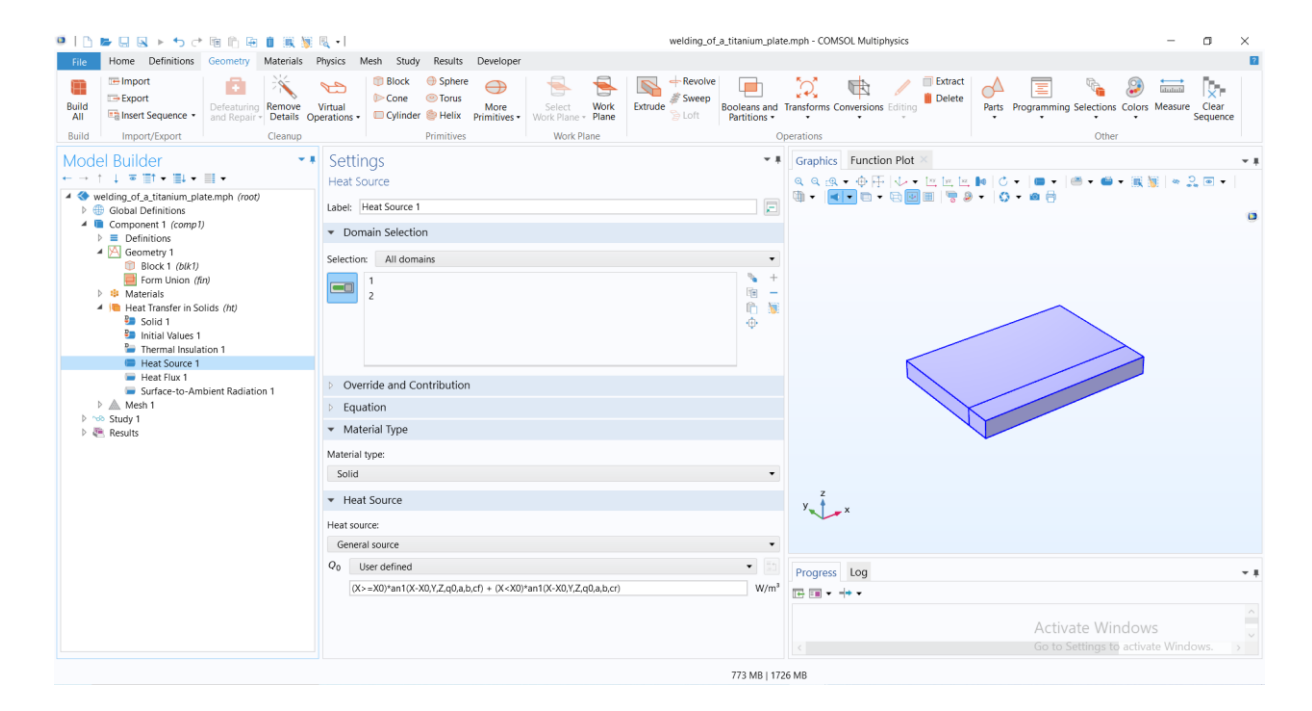
7) Creating the geometry

- in the Model Builder window, expand the Component 1 (comp1)>Geometry 1 node.
- right-click Geometry 1 and choose Block.
- in the Settings window for Block, locate the Size and Shape section.
- in the Width text field, type Lx.
- in the Depth text field, type Ly.
- in the Height text field, type Lz.
- locate the Position section. In the z text field, type -Lz.
- lick to expand the Layers section. Find the Layer position subsection. Select the Front check box.
- clear the Bottom check box, and in the table, enter the layer 1 thickness.
- click Build All.



8) Heat source

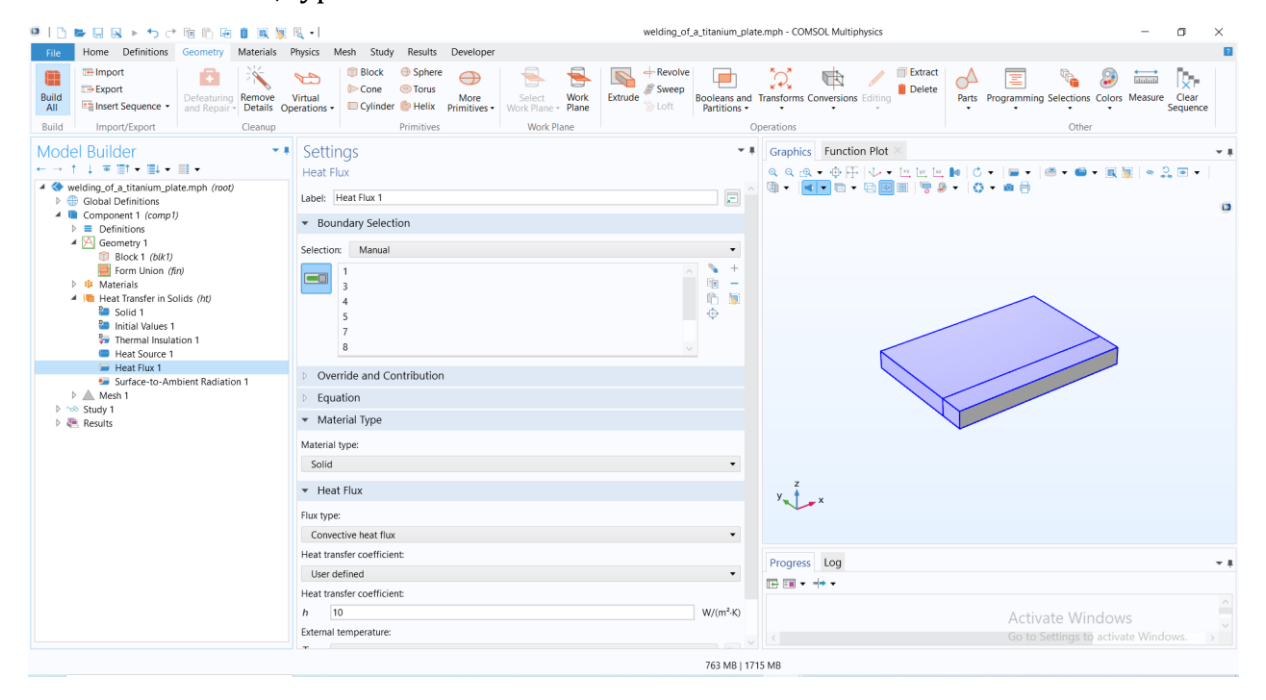
- In the Model Builder window, under Component 1 (comp1) right-click Heat Transfer in Solids (ht) and choose Heat Source.
- In the Settings window for Heat Source, locate the Domain Selection section.
- From the Selection list, choose All domains.
- Locate the Heat Source section. In the Q0 text field



9) Convective flux

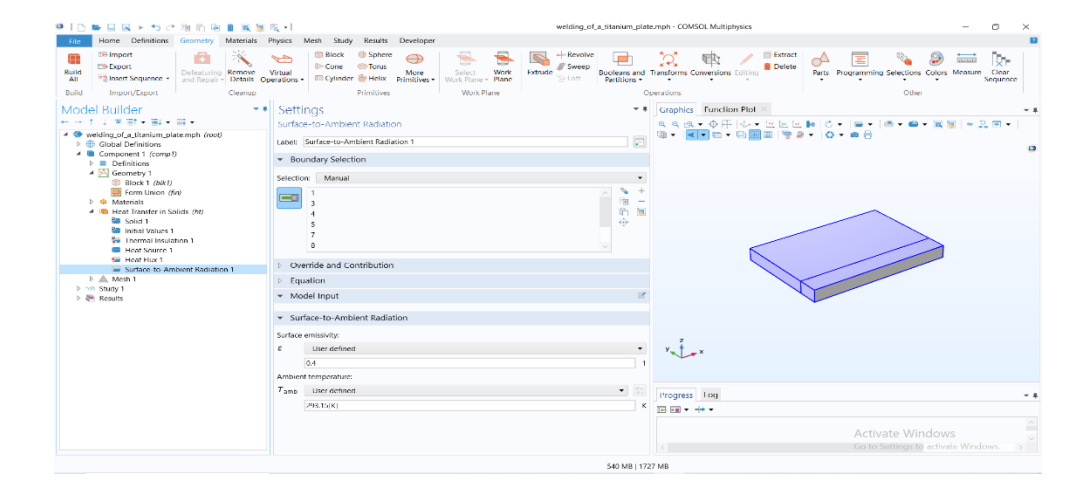
- in the Physics toolbar, click Boundaries and choose Heat Flux.

- select Boundaries 1, 3–5, and 7–11 only.
- in the Settings window for Heat Flux, locate the Material Type section.
- from the Material type list, choose Solid.
- Locate the Heat Flux section. From the Flux type list, choose Convective heat flux.
- In the *h* text field, type 10.



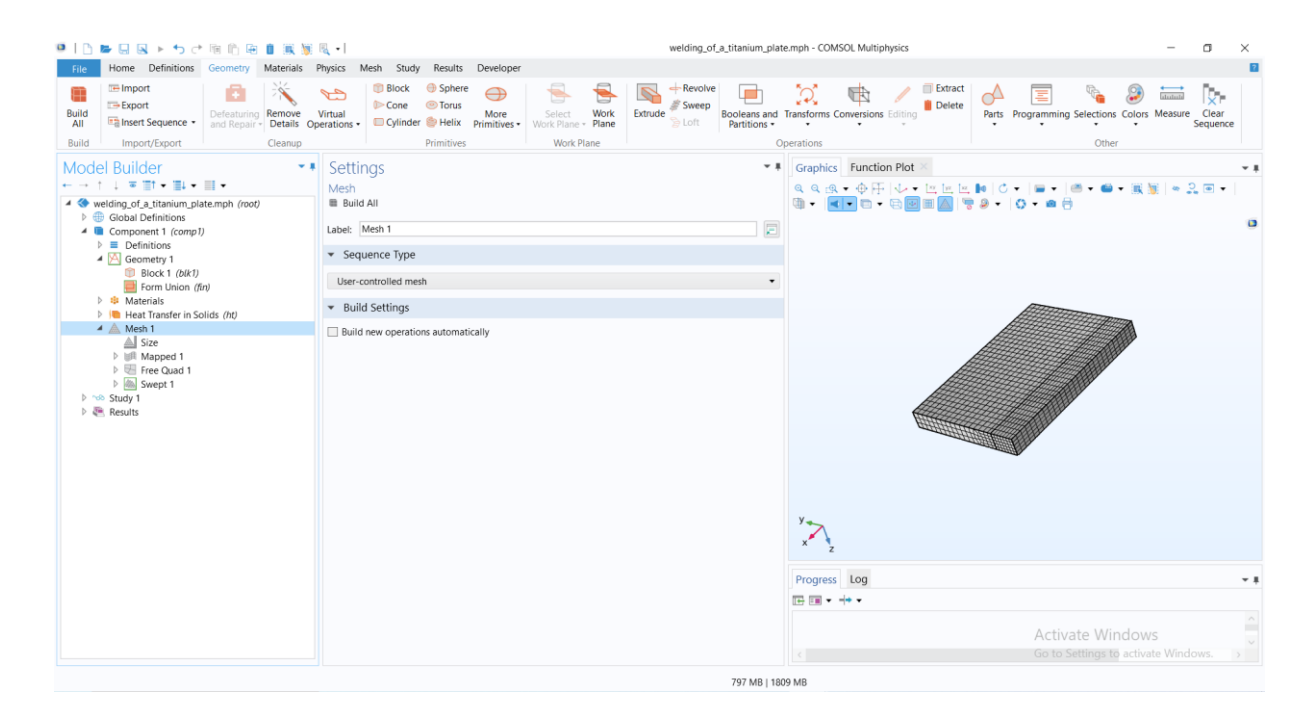
10) Radiative flux

- in the Physics toolbar, click Doundaries and choose Surface-to-Ambient Radiation.
- Select Boundaries 1, 3–5, and 7–11 only.
- In the Settings window for Surface-to-Ambient Radiation, locate the Surface-to-Ambient Radiation section.
- From the ε list, choose User defined. In the associated text field, type 0.4.



11) Mesh creation

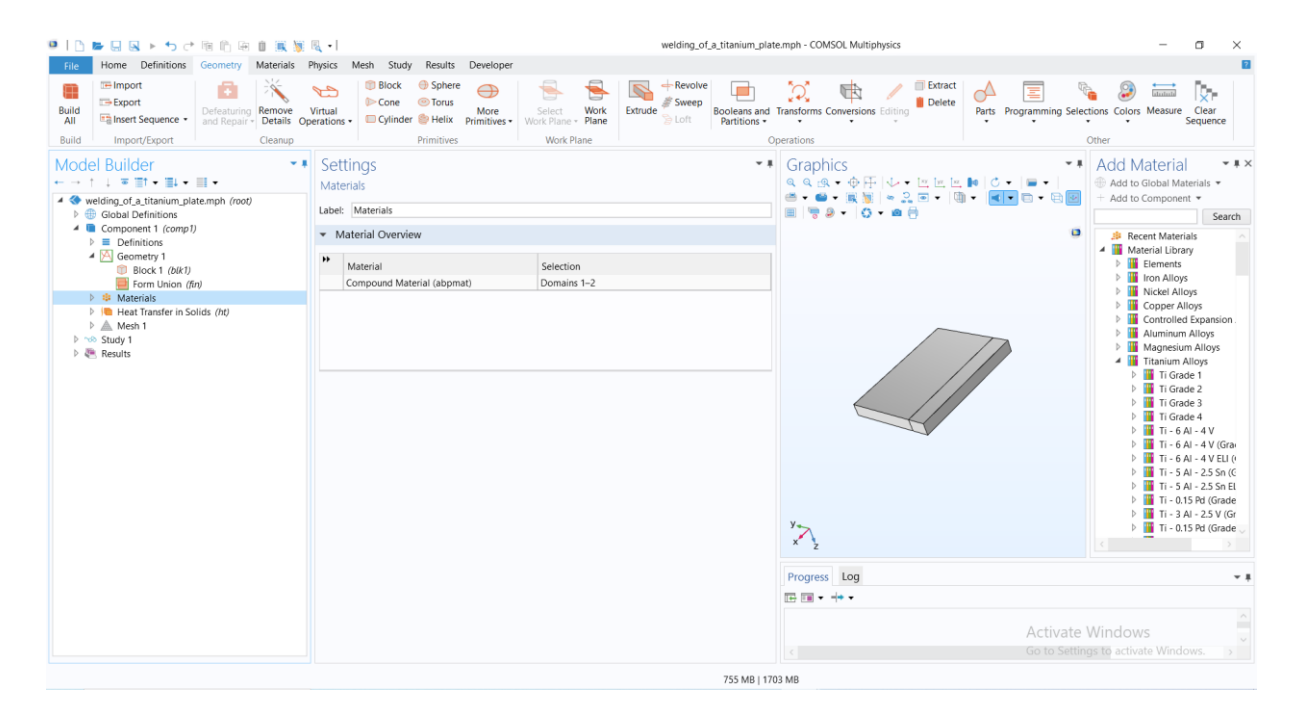
- in the Mesh toolbar, click \(\triangle \) Boundary and choose Mapped.
- Select Boundary 1 only.
- right-click Mapped 1 and choose Size.
- in the Settings window for Size, locate the Element Size section.
- from the Predefined list, choose Extremely fine.
- in the Mesh toolbar, click \(\triangle \) Boundary and choose Free Quad.
- select Boundary 5 only.
- right-click Free Quad 1 and choose Size.
- in the Settings window for Size, locate the Element Size section.
- from the Predefined list, choose Extra fine.
- in the Mesh toolbar, click Swept.
- right-click Swept 1 and choose Size.
- in the Settings window for Size, locate the Element Size section.
- From the Predefined list, choose Extra fine.
- click Build All.



12) Material

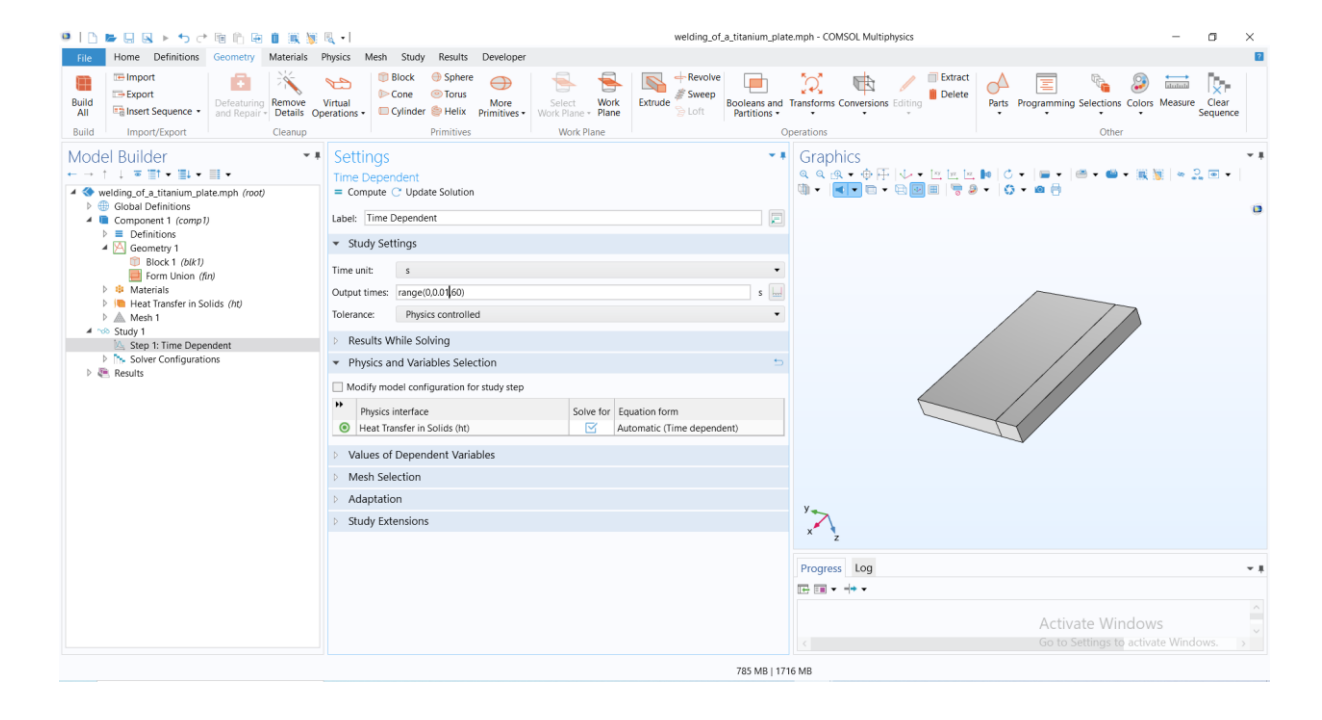
- in the Model Builder window, expand the Material.
- choose add materiel from library.
- choose the desired material.

- add material to component.



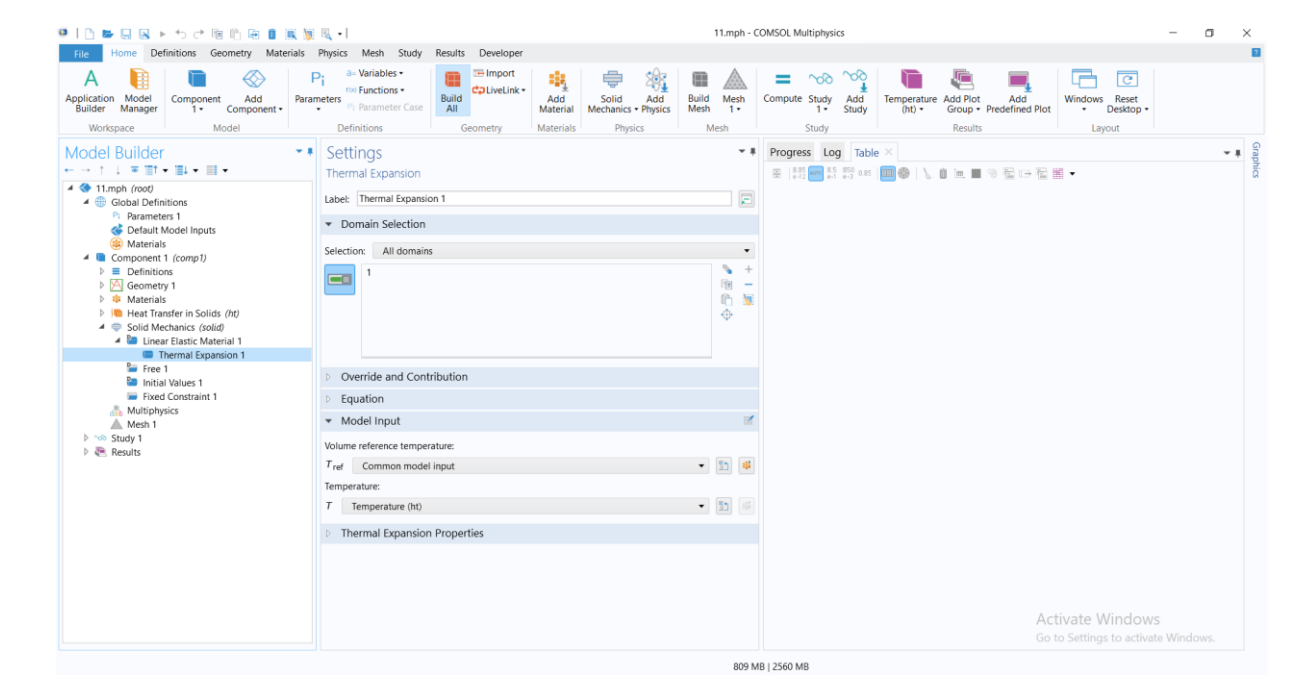
13) Study

- in the Model Builder window, under Study 1 click Step 1: Time Dependent.
- in the Settings window for Time Dependent, locate the Study Settings section.
- in the Output times text field, add the time range and steps.
- in the Home toolbar, click = Compute.



To simulate the thermal displacement a coupling between heat transfer in solids and solid mechanics is necessary.

- click on [®] add physics and choose [●] solid mechanics
- in the Model Builder window, under solid mechanics choose thermal expansion.
- in temperature set temperature (ht).
- click Build All.
- click = Compute.



III. Chapter III: results and discussion

III.1. welding of metal plate results

this simulation aimed to study the results of changing different parameters such as plate thickness, welding power and plate material on the temperature distribution and how its behave during CMT welding.

III.1.1-meshing effect

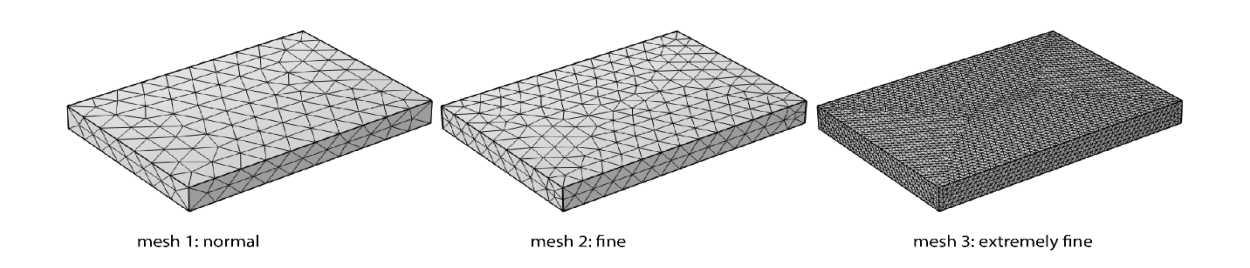


Figure III.1: different mesh types.

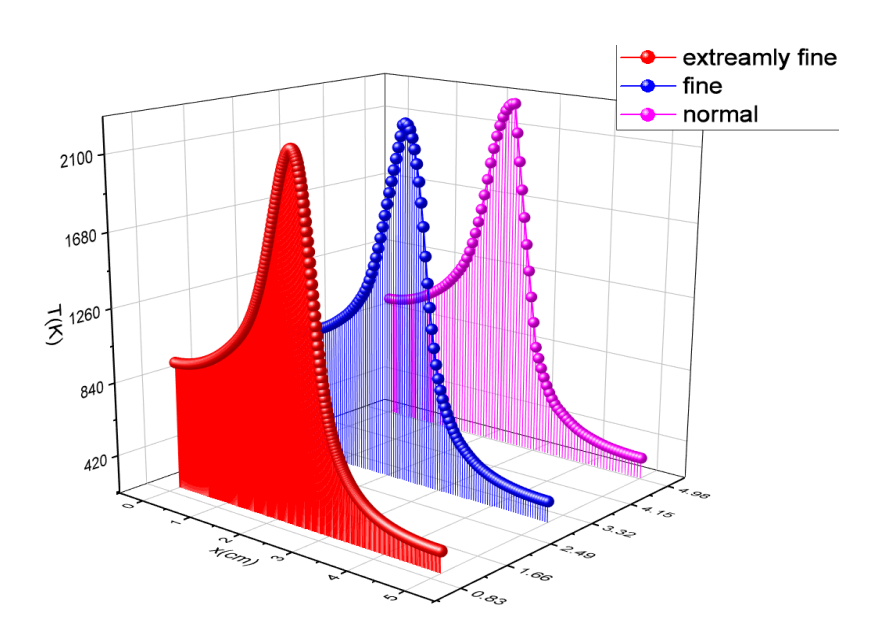


Figure III.2: temperature destribution for three mesh types.

The more refined the mesh the more accurate the results with a smooth gaussian curve transition of temperature value from a point to the next one indicating a mush realistic change in the temperature gradient. Based on that the extremely fine mesh is chosen with a 142669 tetrahedral element, 10312 triangular face and 360 edge elements.

III.1.2-The influence of plate thickness on temperature distribution.

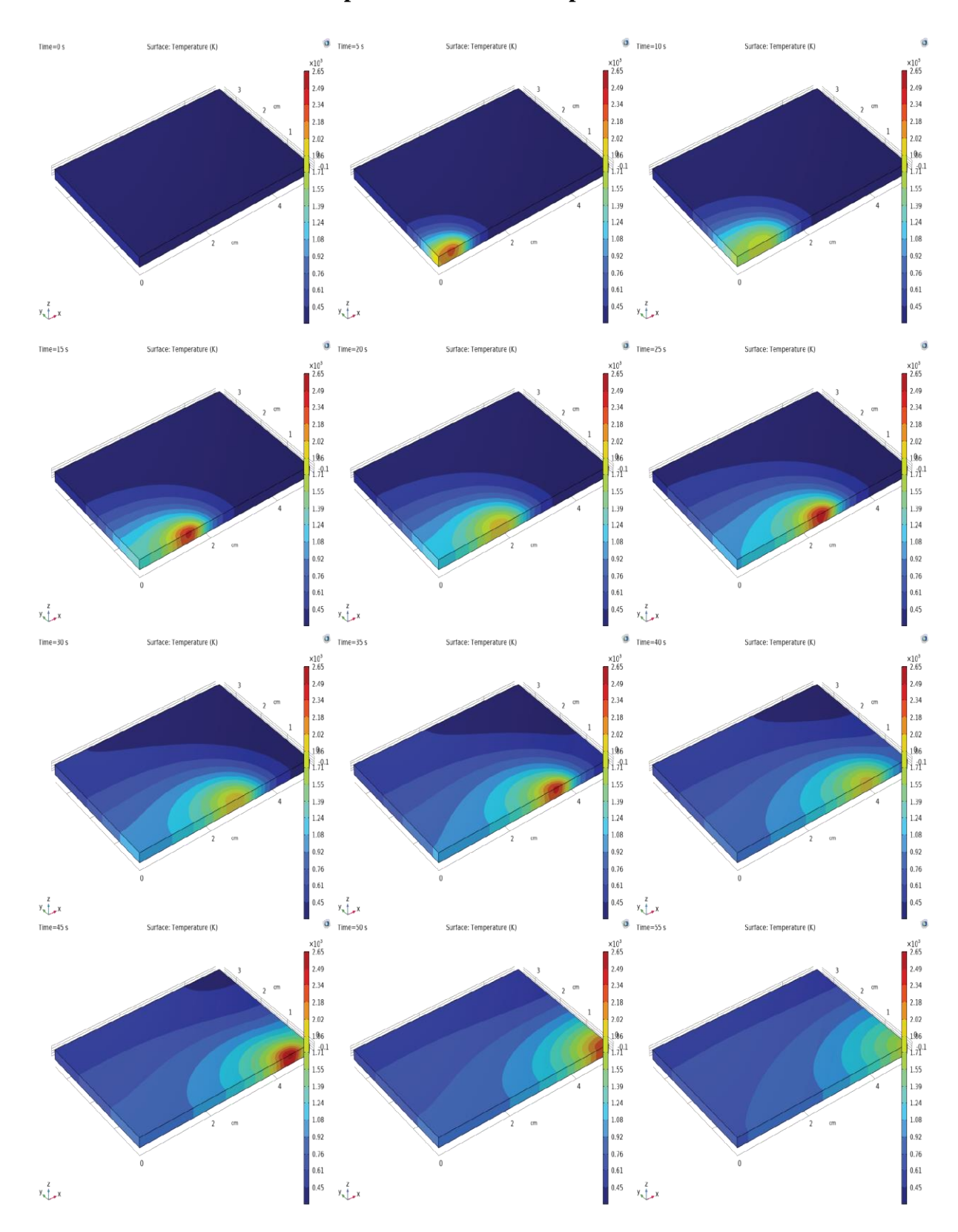


Figure III.3: temperature distribution in a 2mm height titanium plate in different time steps with 800W welding power.

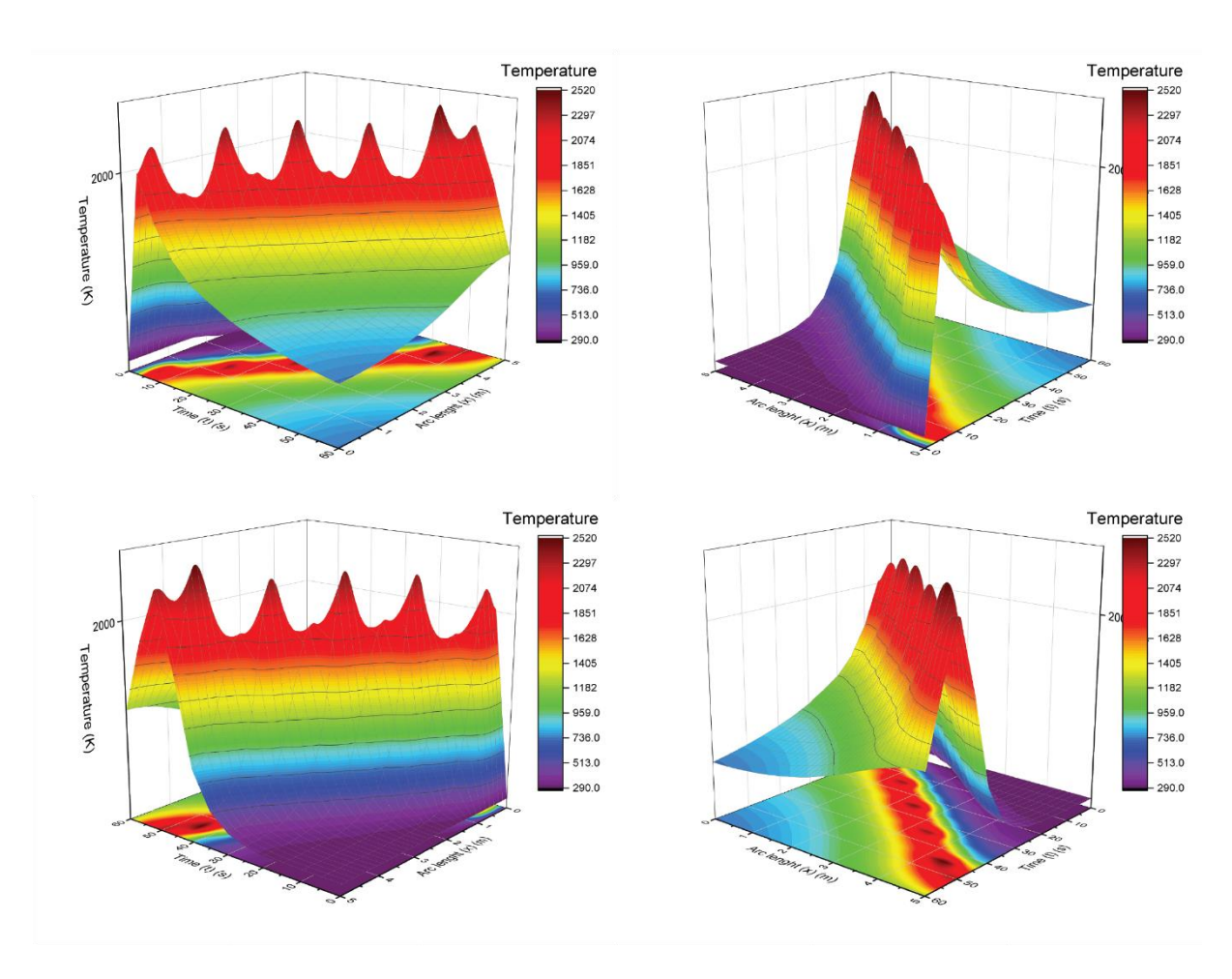


Figure III.4: 3D graphic representation temperature evolution along the welding path at different time steps in a 2mm height titanium plate with 800W welding power.

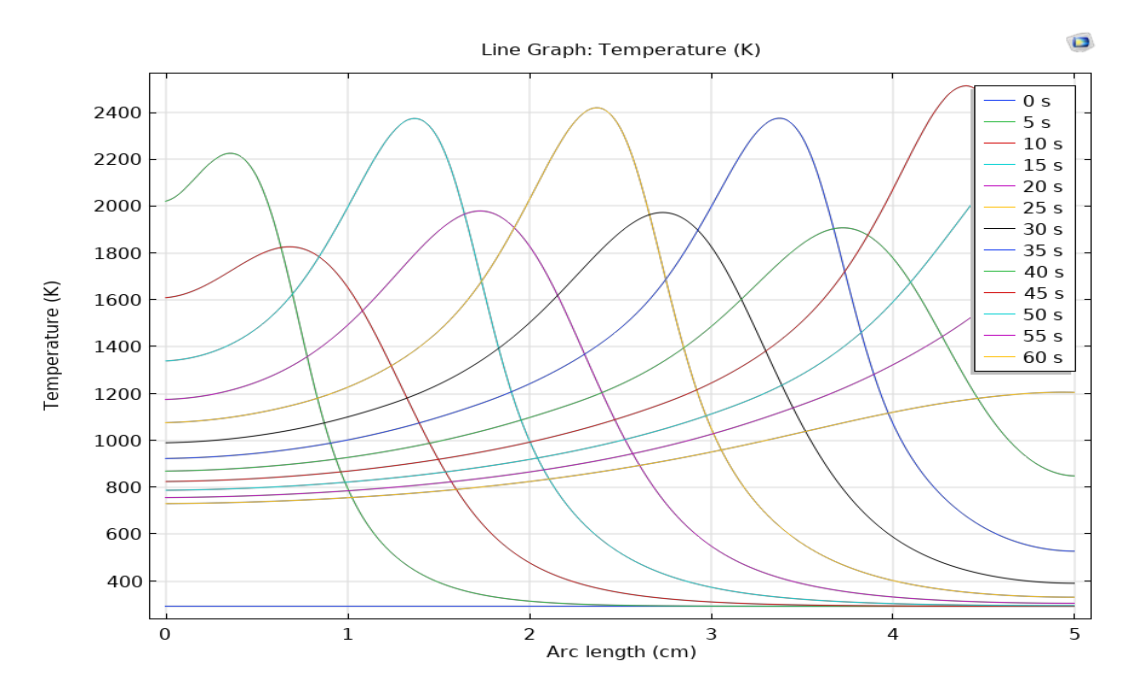


Figure III.5: 2D graphic representation temperature evolution along the welding path at different time steps in a 2mm height titanium plate with 800W welding power.

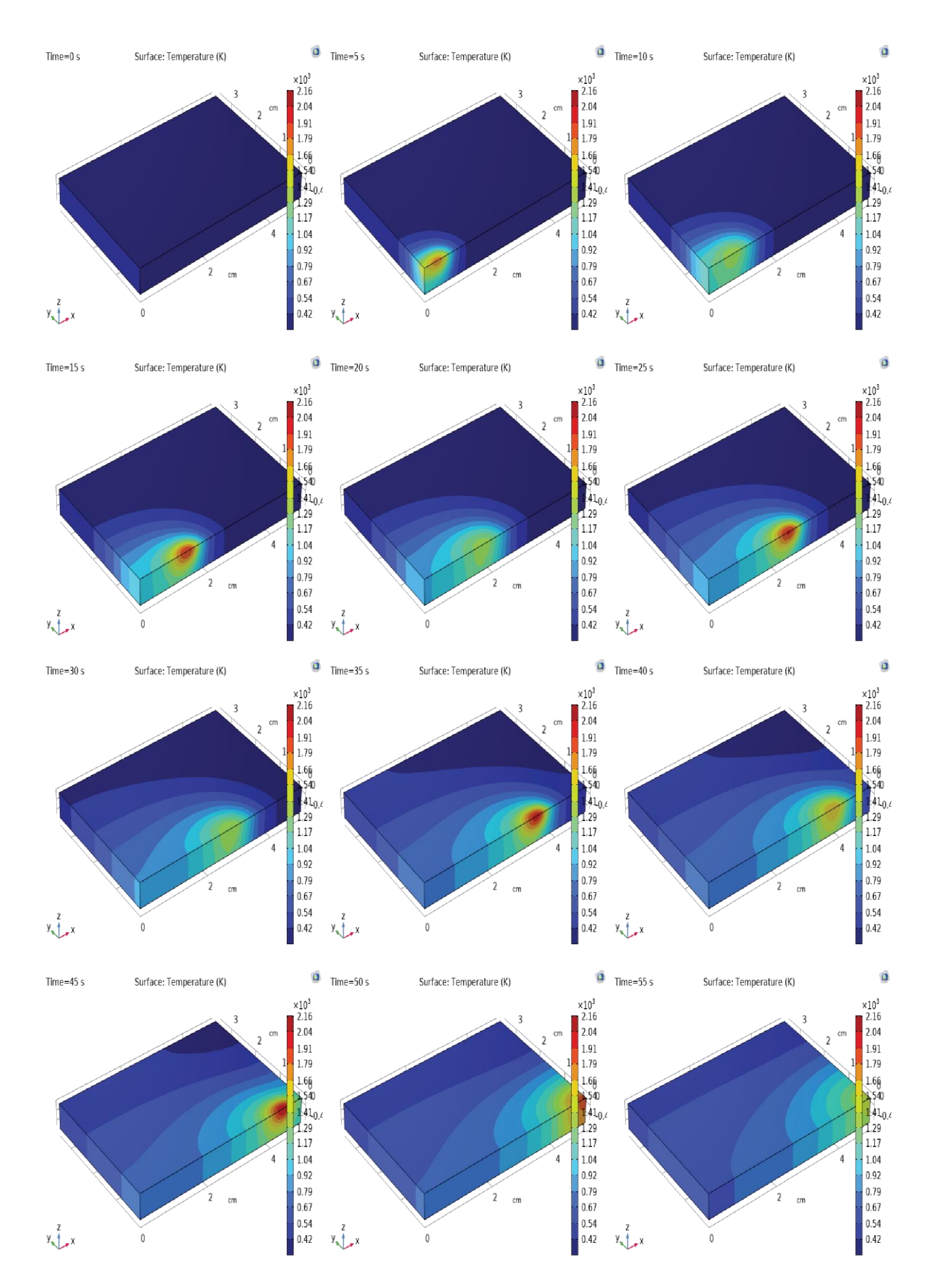


Figure III.6: temperature distribution in a 5mm height titanium plate in different time steps with 800W welding power.

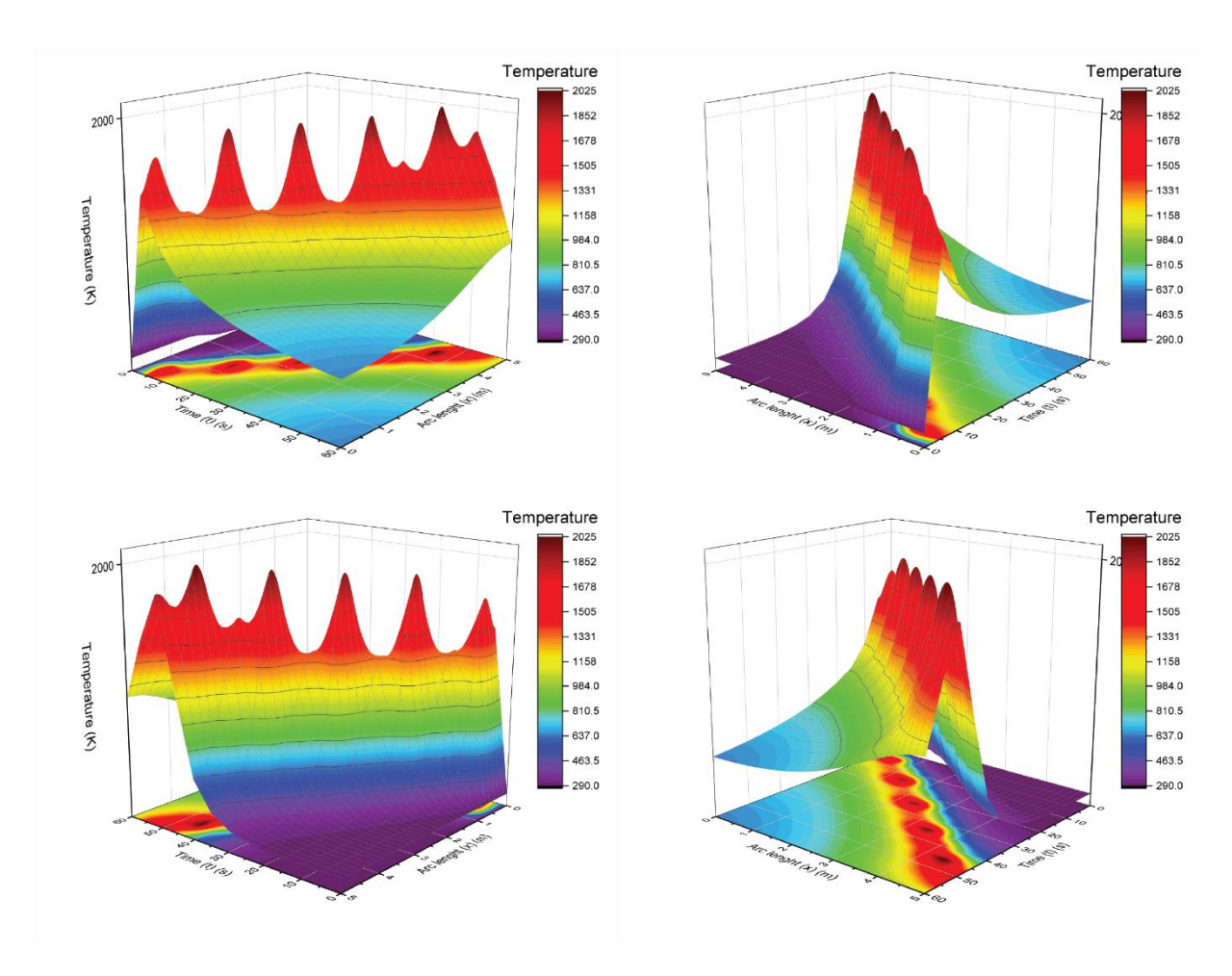


Figure III.7: 3D graphic representation temperature evolution along the welding path at different time steps in a 5mm height titanium plate with 800W welding power.

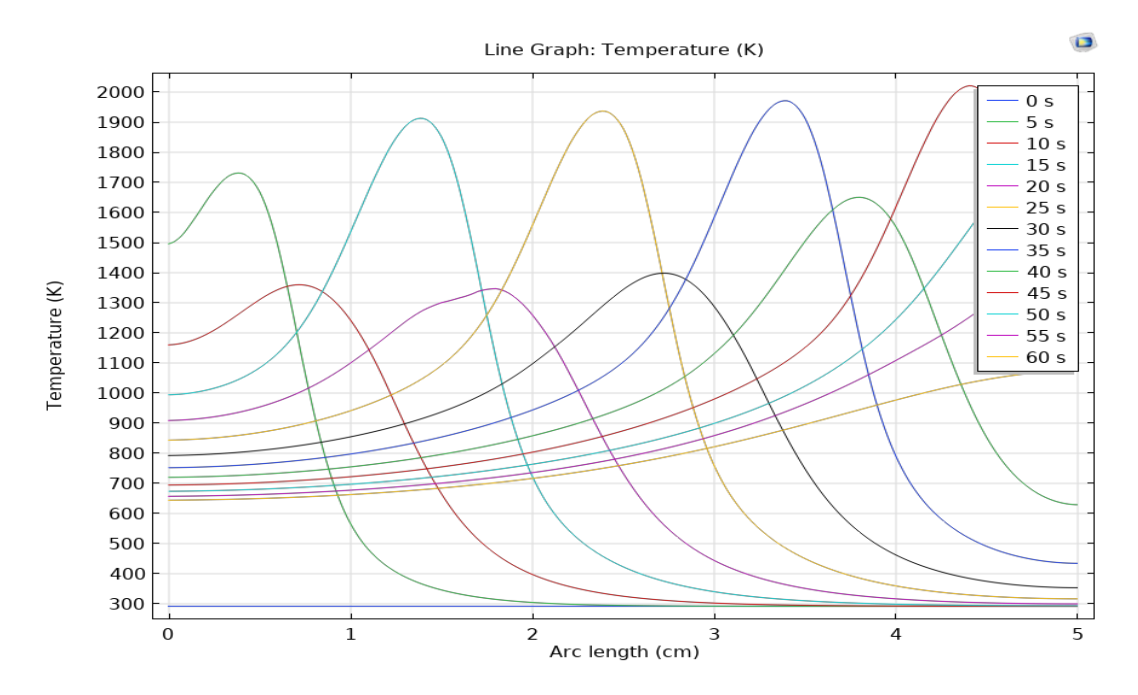


Figure III.8: 2D graphic representation temperature evolution along the welding path at different time steps in a 5mm height titanium plate with 800W welding power.

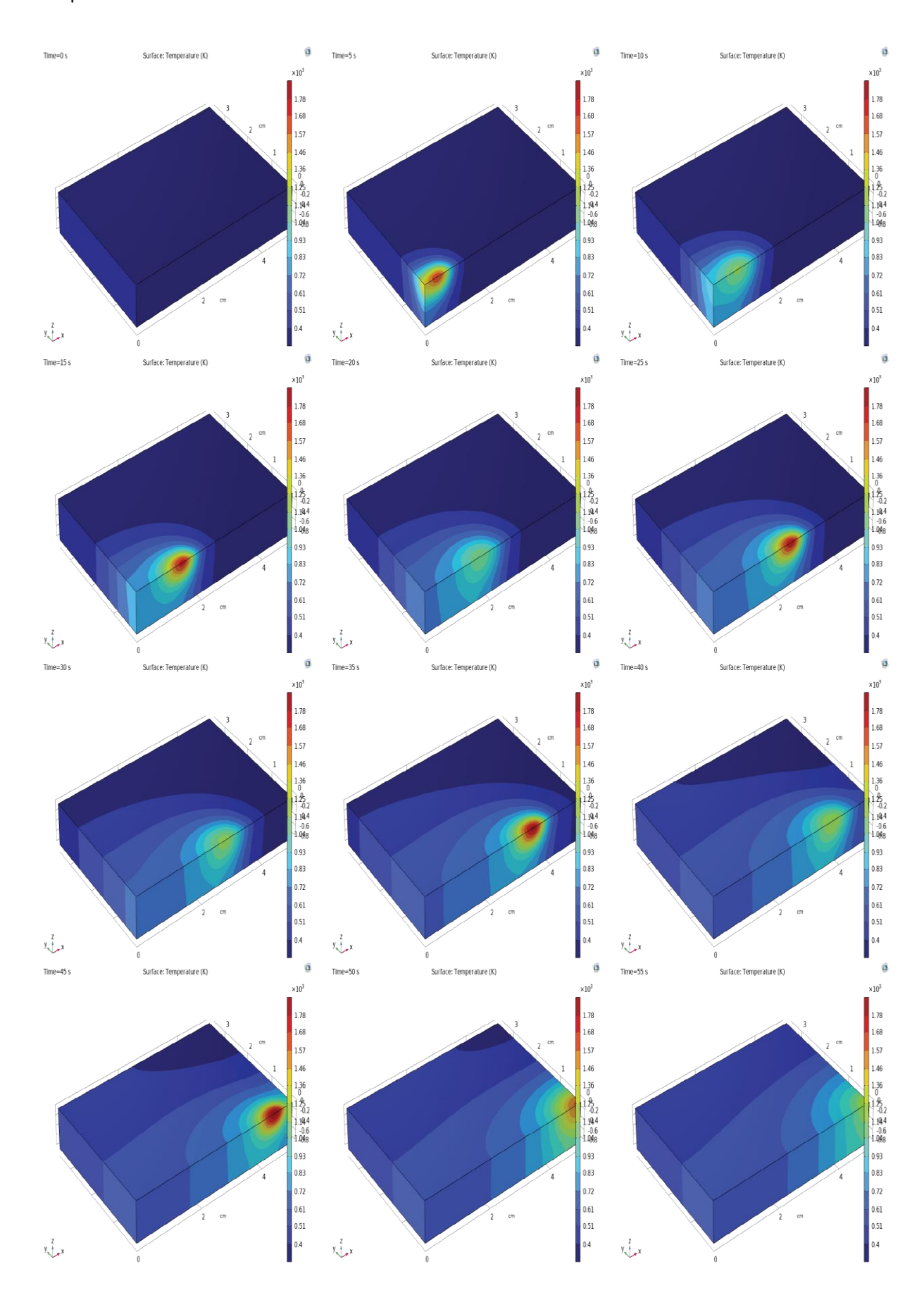


Figure III.9: temperature distribution in a 8mm height titanium plate in different time steps with 800W welding power

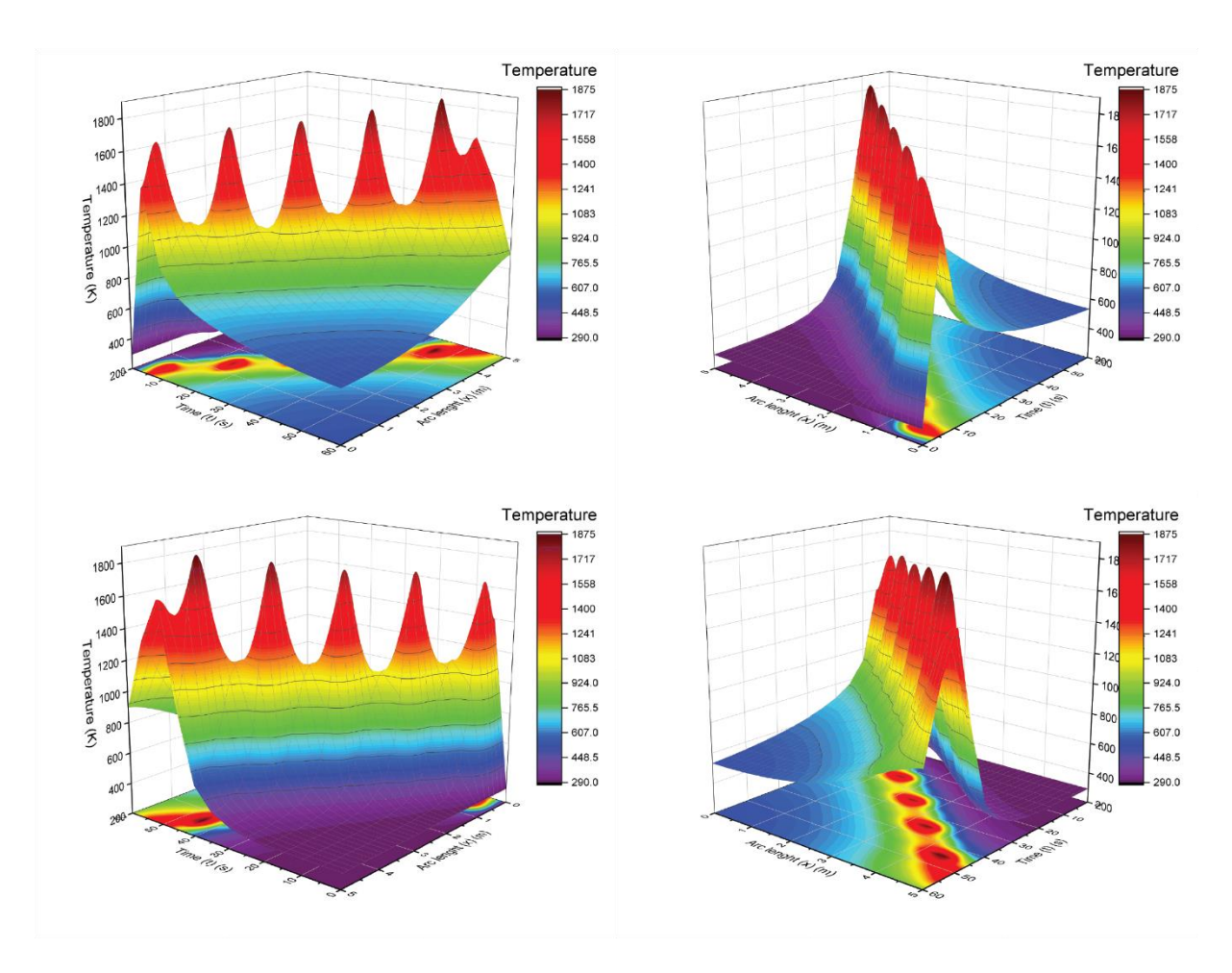


Figure III.10: 3D graphic representation temperature evolution along the welding path at different time steps in a 8mm height titanium plate with 800W welding power.

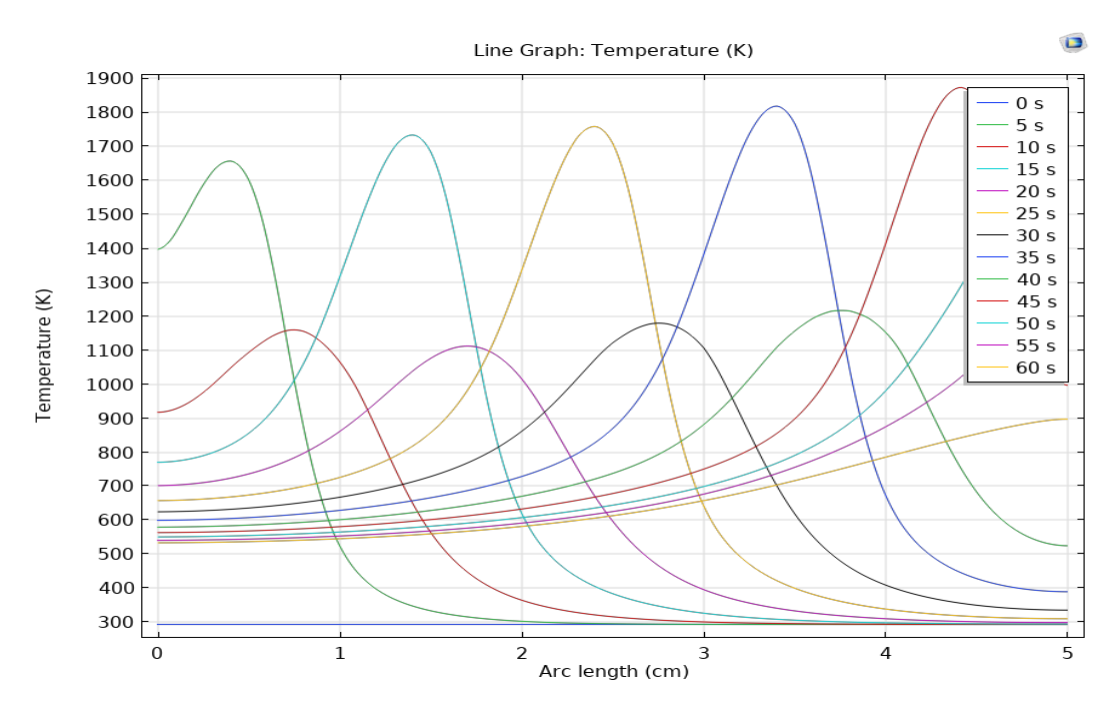


Figure III.11: 2D graphic representation temperature evolution along the welding path at different time steps in a 8mm height titanium plate with 800W welding power.

As it observed under the condition of same material, thicker plates have higher thermal mass and therefore, they absorb more heat during welding. As a result, they exhibit slower heating rates and require more energy input to reach the desired welding temperature which is better be above the welded metal melting point. On the contrary, thinner plate heat up more quickly and reach higher temperature degree due to it lower thermal mass. The more the thicker is the plates, the more it tends to exhibit larger temperature gradients across their thickness compared to thinner plates. This is because heat dissipates more slowly through thicker materials, leading to greater temperature differentials between the weld zone and the surrounding material.

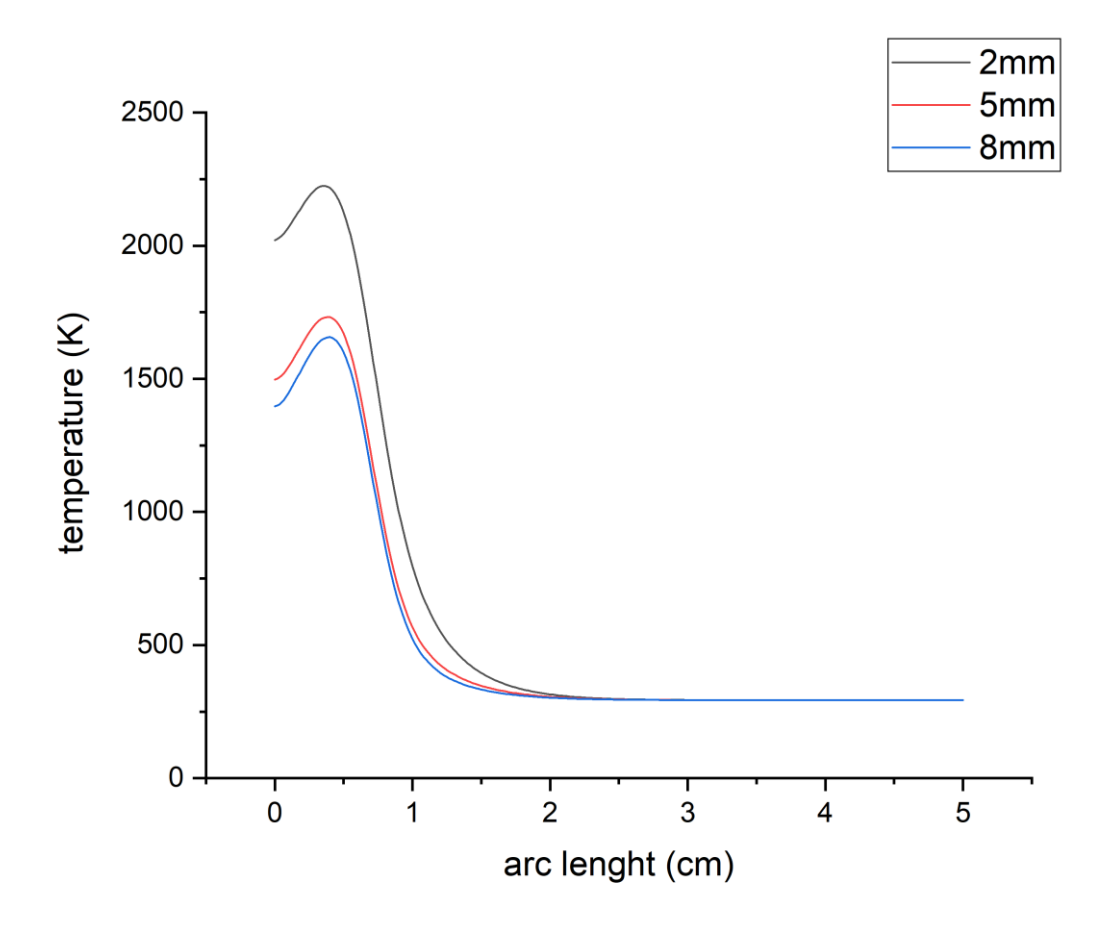


Figure III.12: 2D graphic representation temperature evolution along the welding path at t=5s in the different thickness plates.

III.1.3-The influence of welding power on temperature distribution

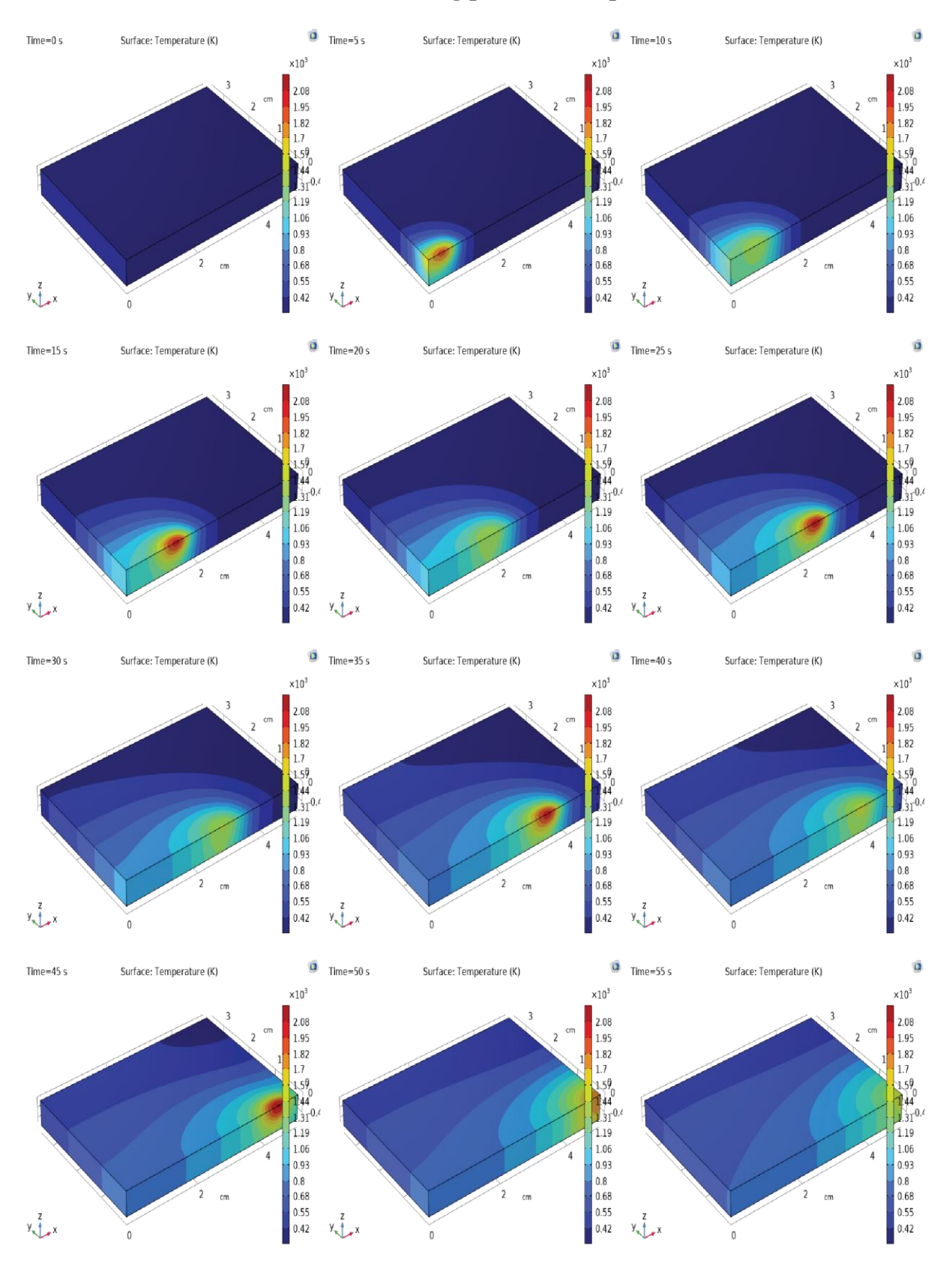


Figure III.13: temperature distribution in a 5mm height titanium plate in different time steps with 850W.

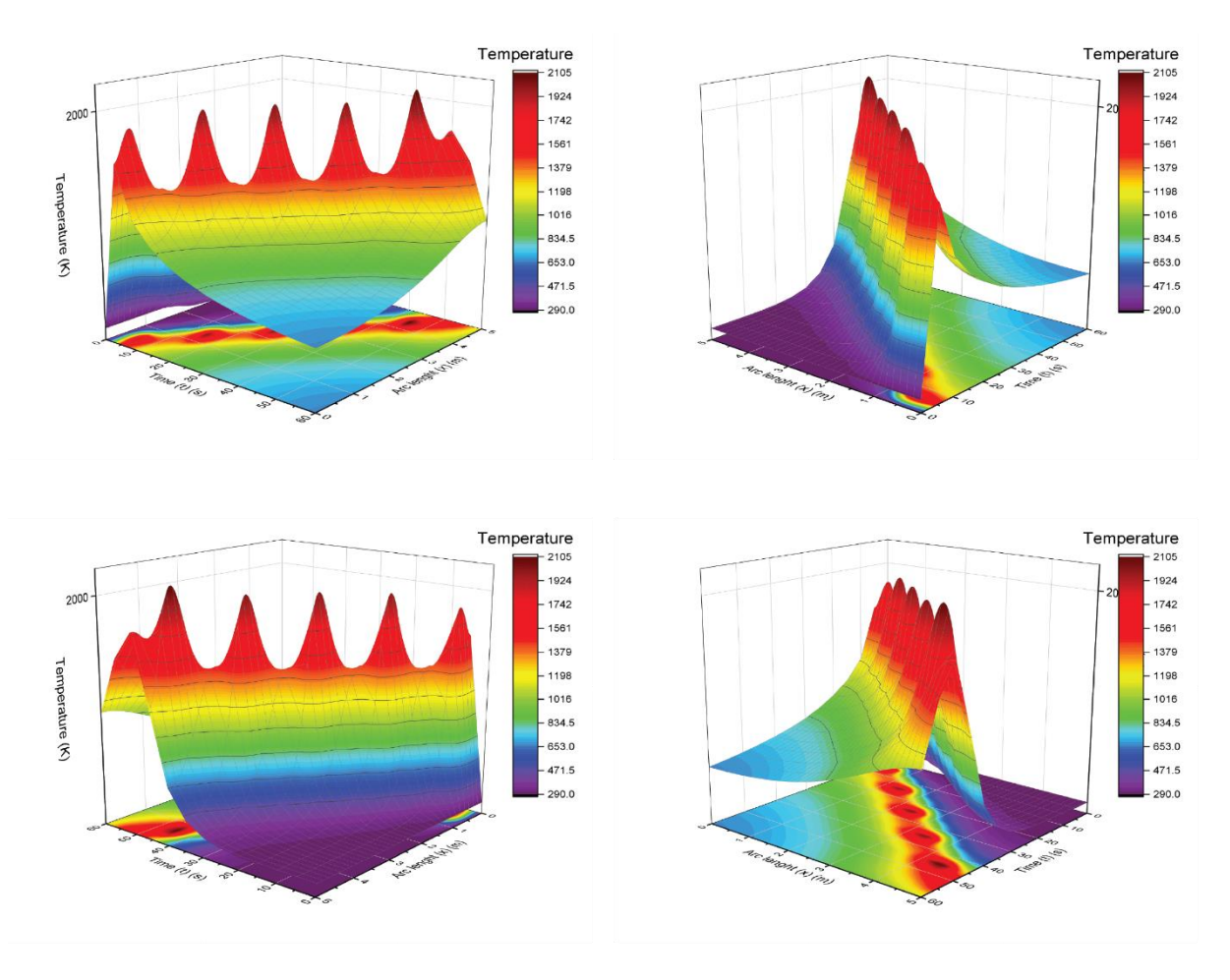


Figure III.14: 3D graphic representation temperature evolution along the welding path at different time steps in a 5mm height titanium plate with 850W welding power

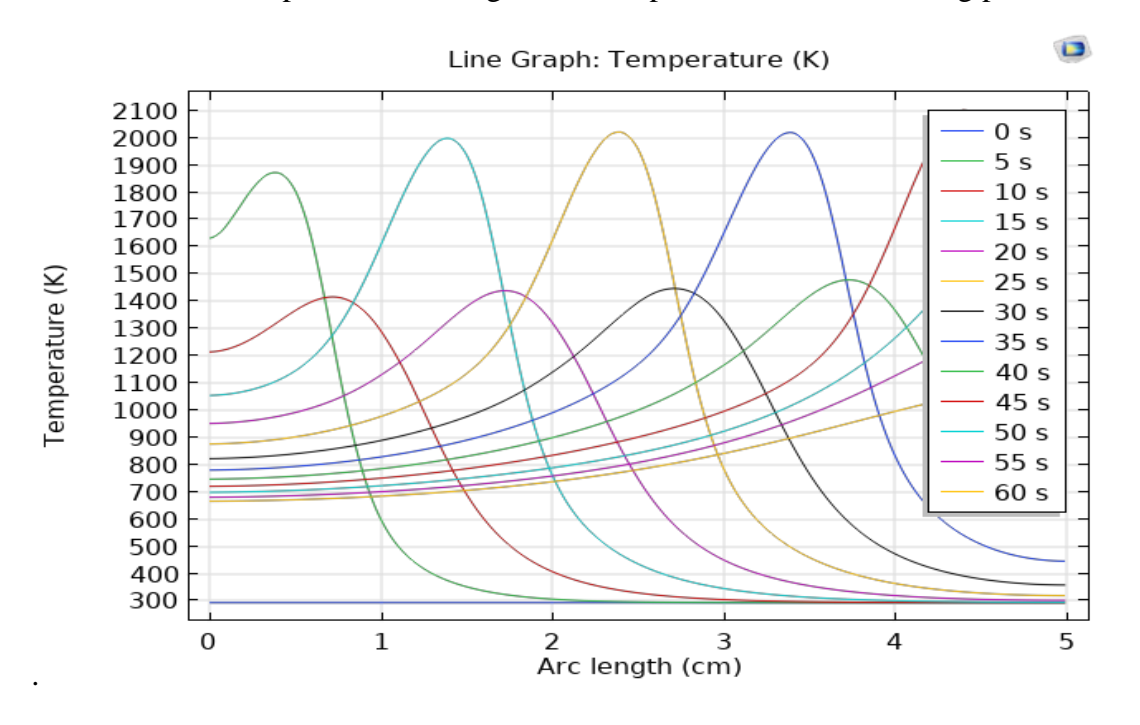


Figure III.15: 2D graphic representation temperature evolution along the welding path at different time steps in a 5mm height titanium plate with 850W welding power.

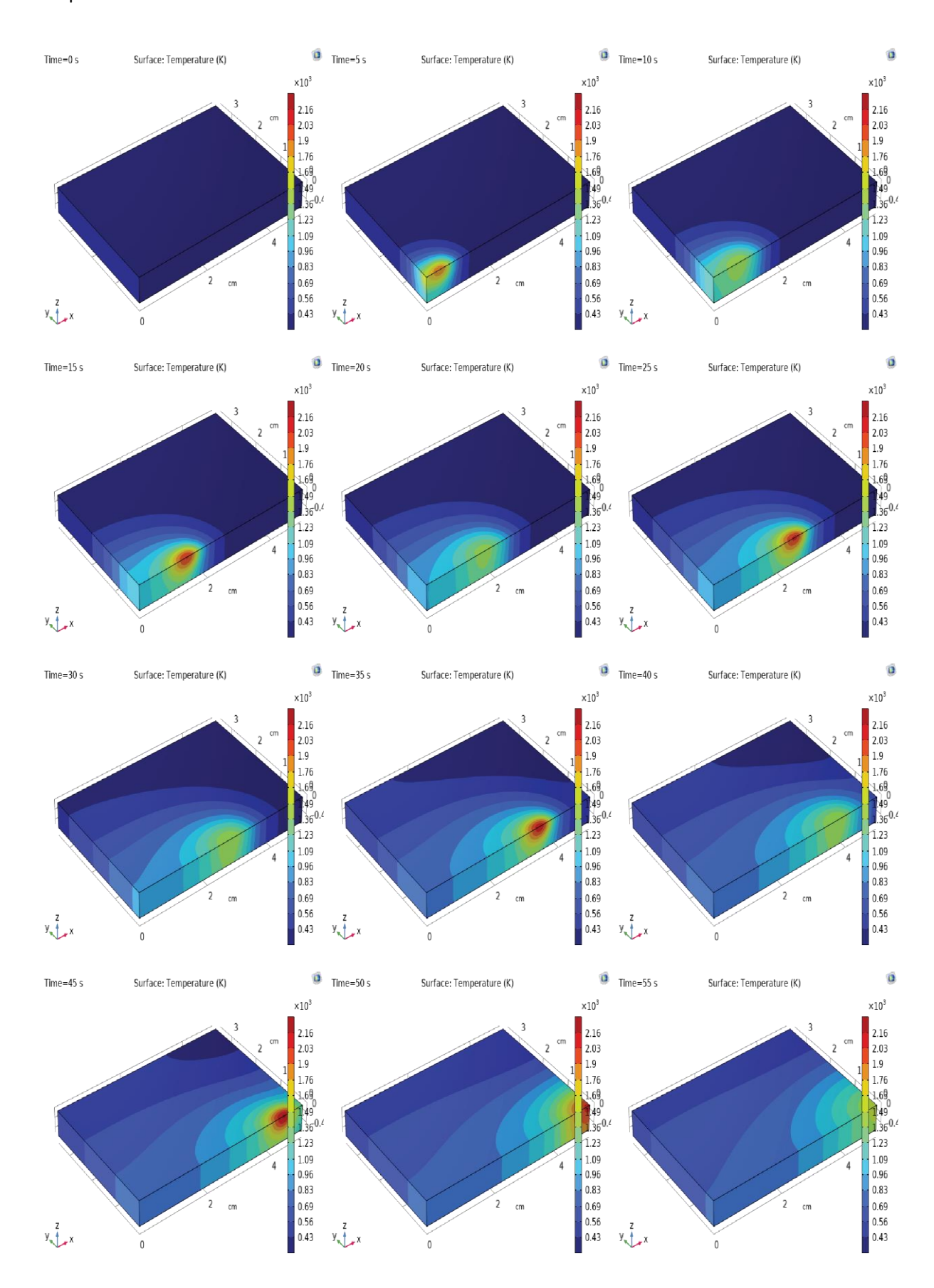


Figure III.16: temperature distribution in a 5mm height titanium plate in different time steps with 900W welding power.

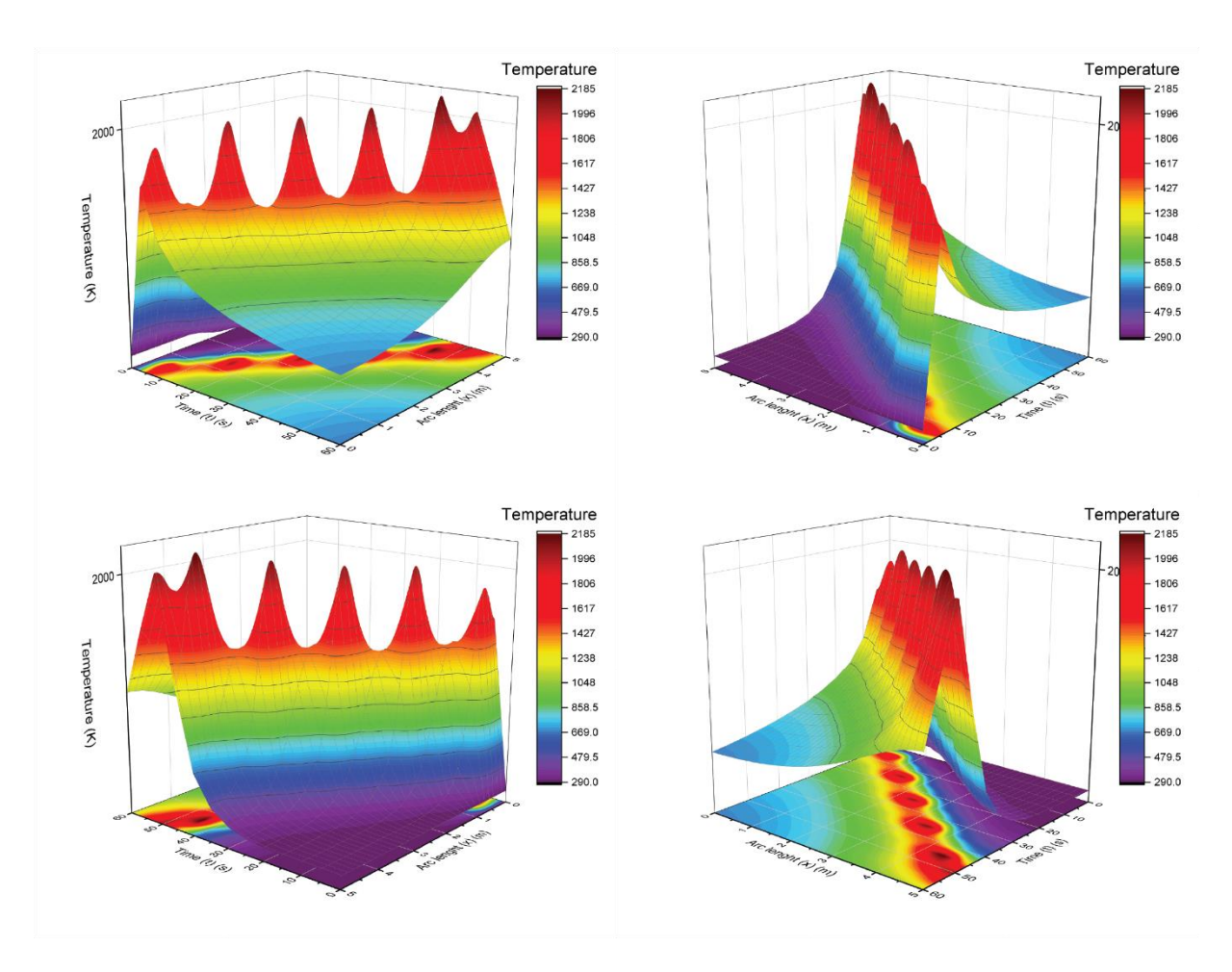


Figure III.17: 3D graphic representation temperature evolution along the welding path at different time steps in a 5mm height titanium plate with 900W welding power

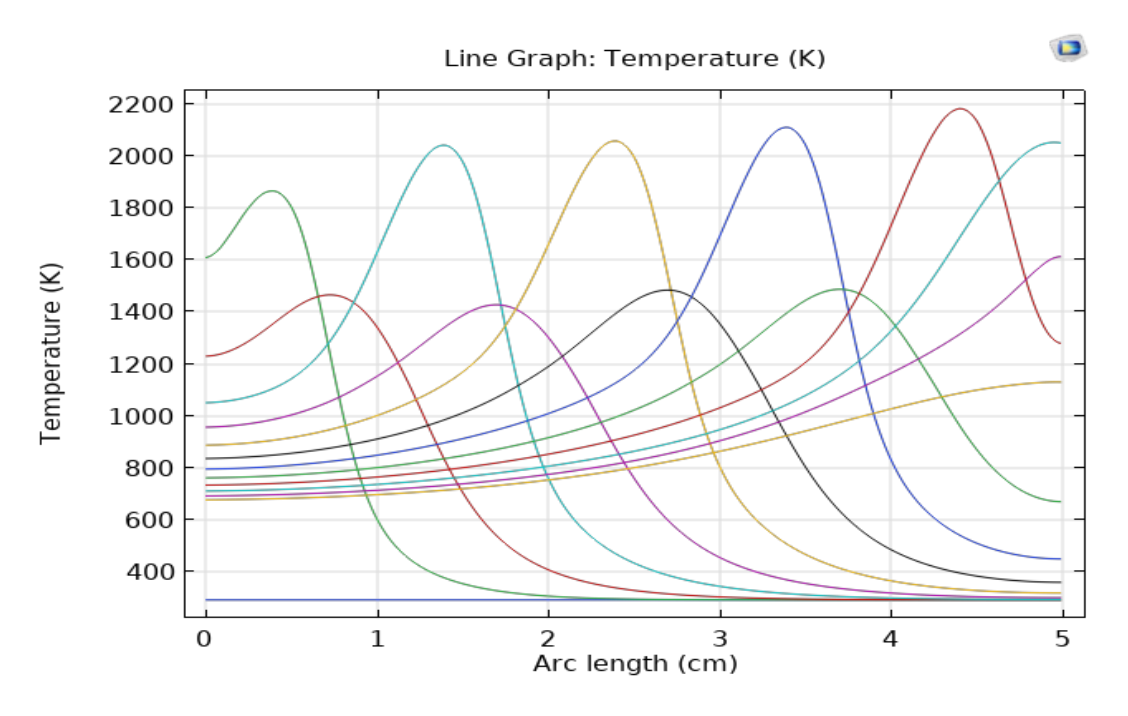


Figure III.18: 2D graphic representation temperature evolution along the welding path at different time steps in a 5mm height titanium plate with 900W welding power

The simulations of temperature distribution show distinct differences at welding powers of 800 watts, 850 watts, and 900 watts. In the 800 watts case, the heat distribution exhibits a pronounced temperature increase around the source, but with the smallest high-temperature region and the least extensive temperature gradient compared to the other cases. The 850 watts simulation shows a moderate high-temperature region and a more extensive temperature gradient than the 800 watts case, but still less so than the 900 watts case. The 900 watts simulation reveals the largest heat-affected zone (HAZ), the highest peak temperatures, and the most extensive temperature gradient. This indicates that higher welding power causes a larger area to reach higher temperatures more quickly. Increasing the power from 800 watts to 900 watts results in progressively higher peak temperatures, larger HAZ, and steeper temperature gradients, which can influence the microstructure and mechanical properties of the weld, potentially introducing more thermal stresses and distortions.

III.1.4-The influence of welded material on temperature distribution

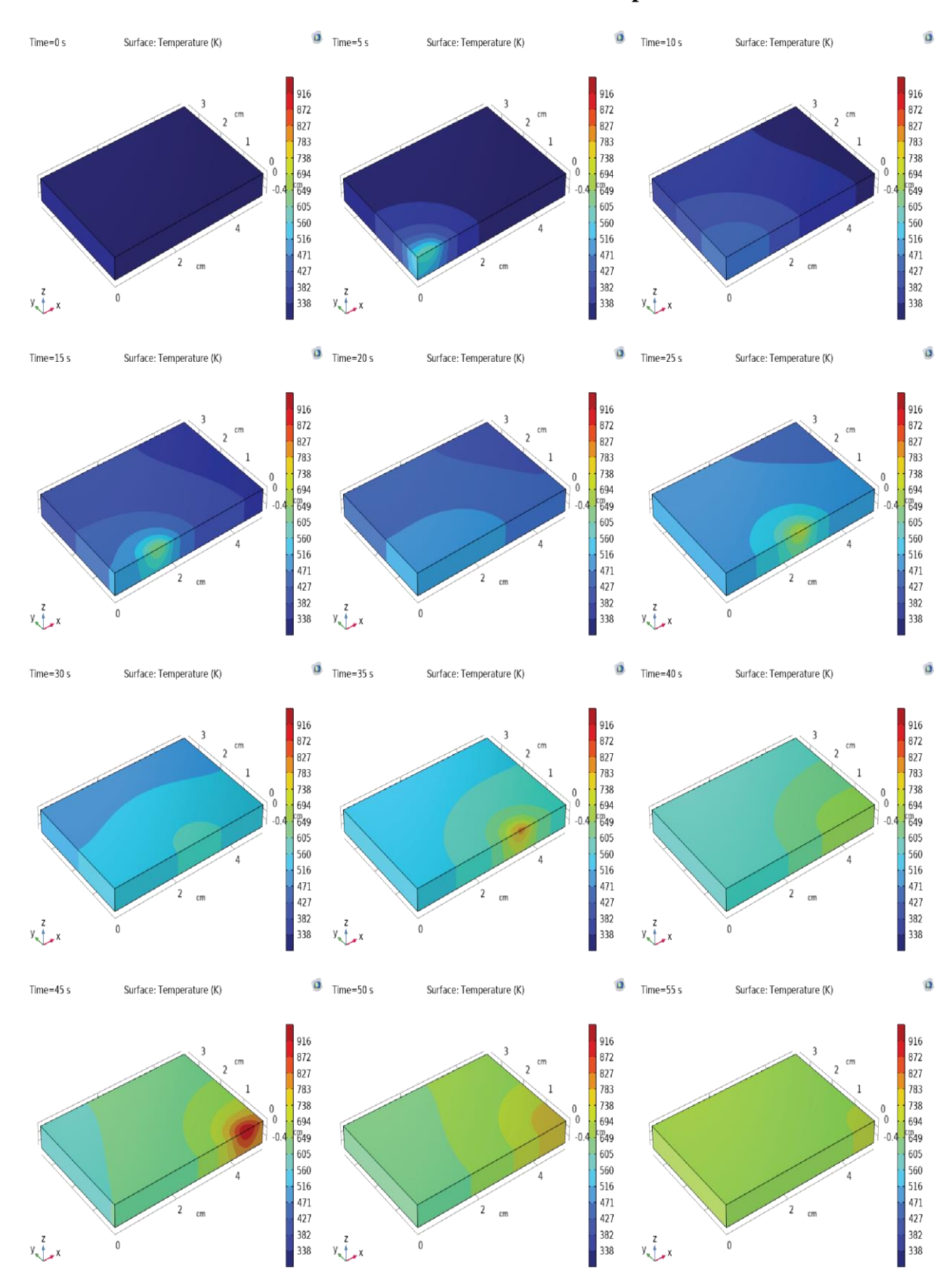


Figure III.19: temperature distribution in a 5mm height aluminum plate in different time steps with 800W welding power

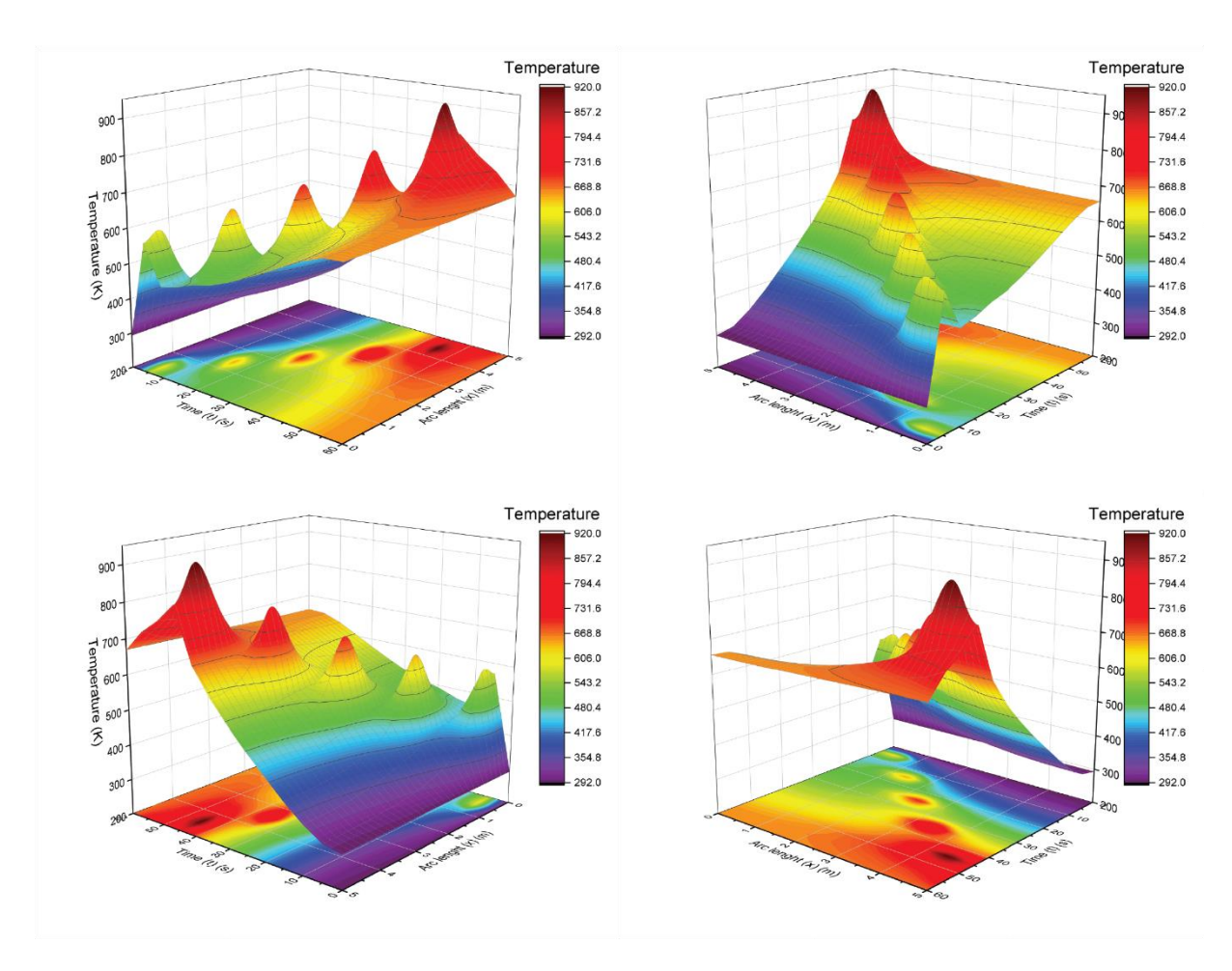


Figure III.20: 3D graphic representation temperature evolution along the welding path at different time steps in a 5mm height aluminum plate with 800W welding power

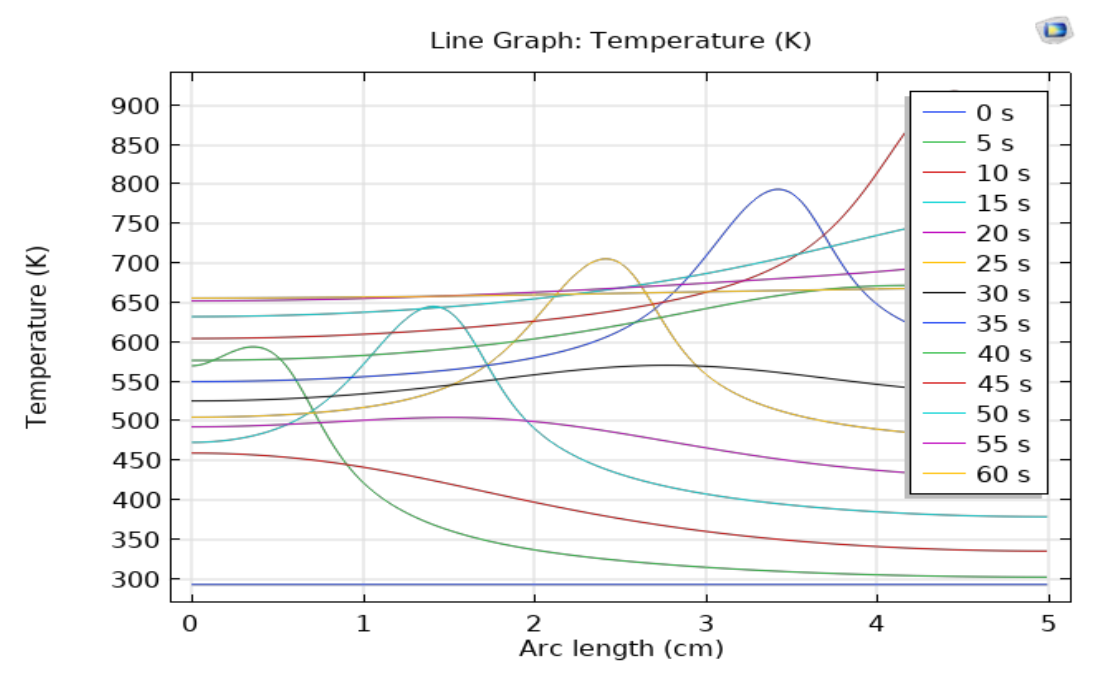


Figure III.21: 2D graphic representation temperature evolution along the welding path at different time steps in a 5mm height aluminum plate with 800W welding power

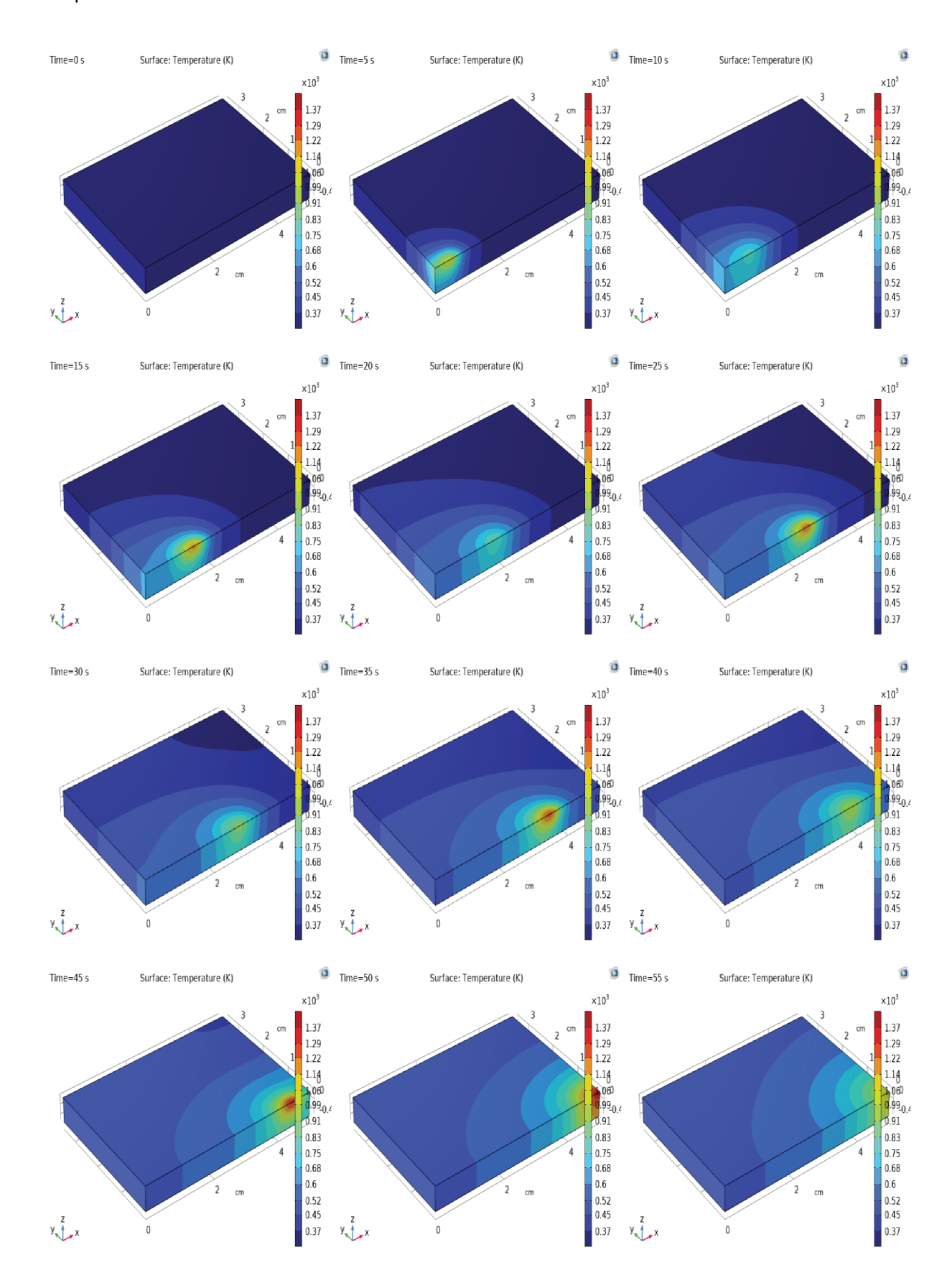


Figure III.22: temperature distribution in a 5mm height iron plate in different time steps with 800W welding power

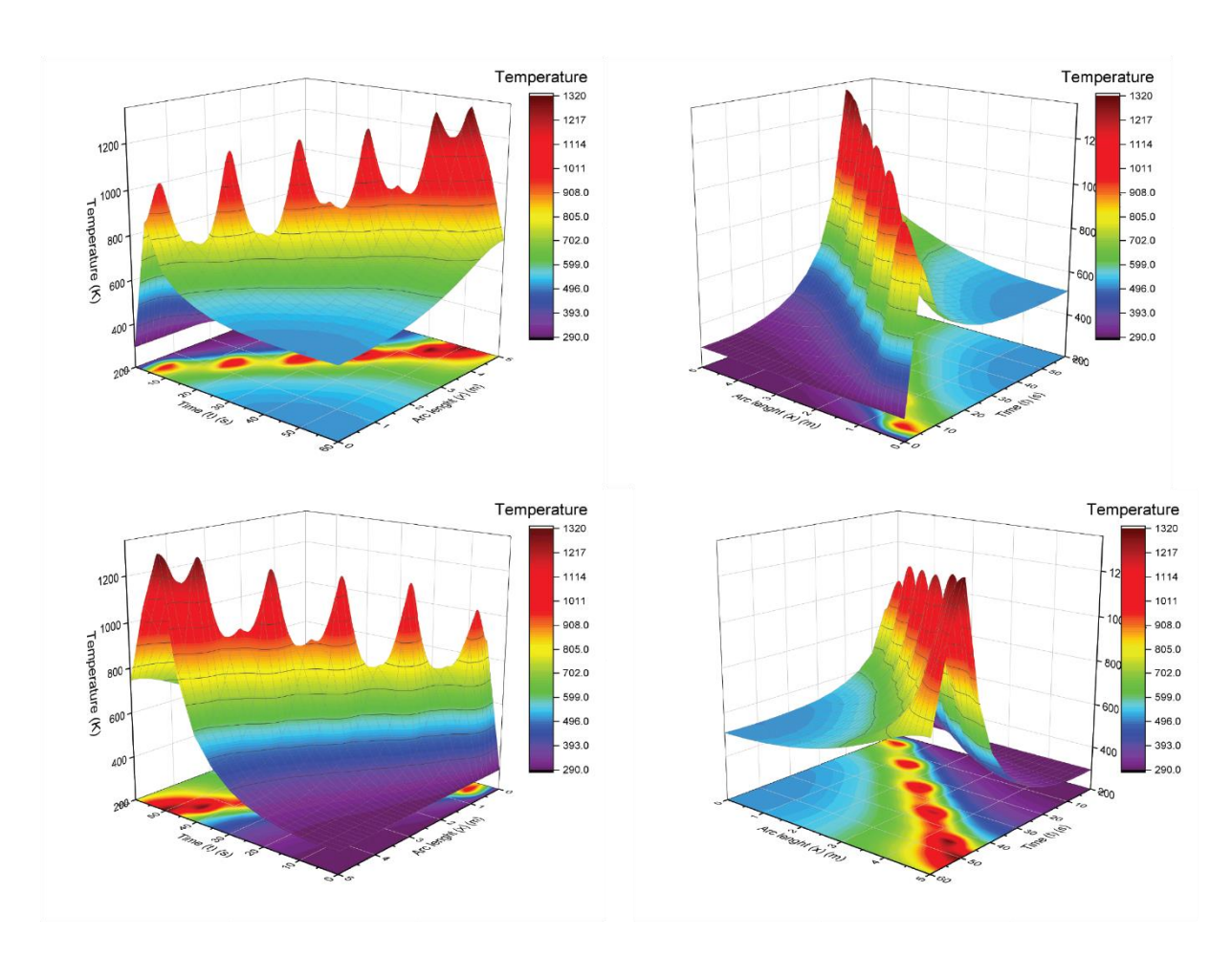


Figure III.23: 3D graphic representation temperature evolution along the welding path at different time steps in a 5mm height iron plate with 800W welding power

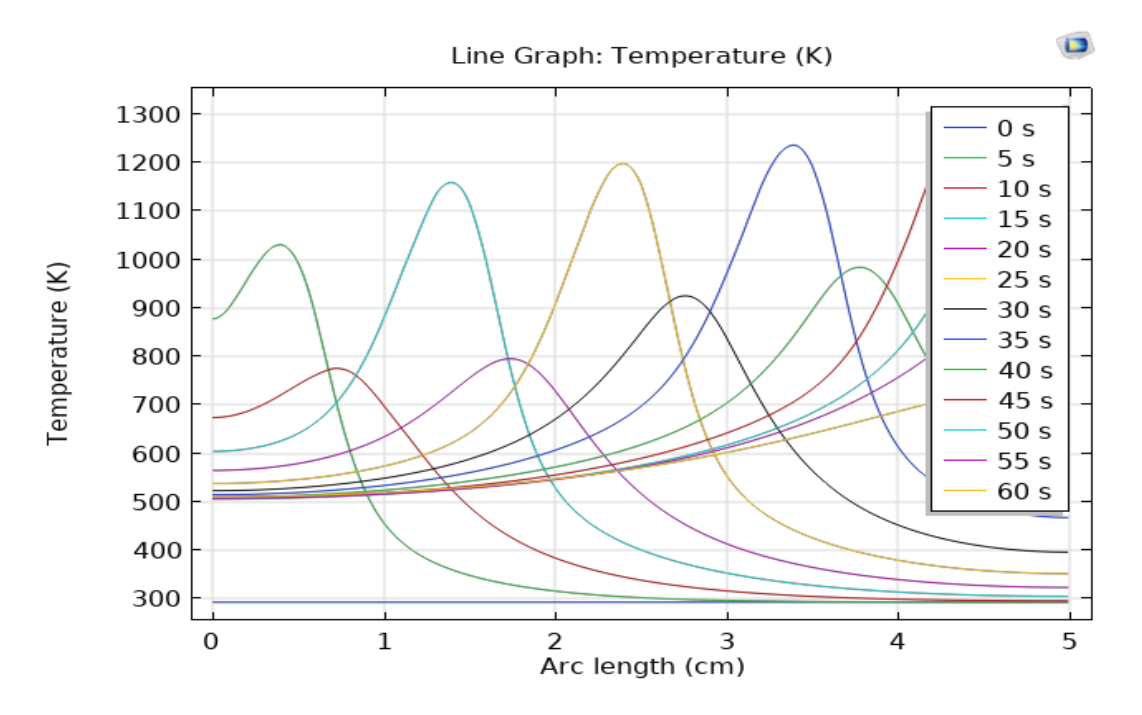


Figure III.24: 3D graphic representation temperature evolution along the welding path at different time steps in a 5mm height iron plate with 800W welding power

From what we could observe, Titanium exhibits a relatively lower thermal conductivity compared to aluminum and iron. This results in the heat being more localized near the welding point, with the temperature gradient diminishing quickly as the distance from the weld increases. Consequently, the heat-affected zone (HAZ) is relatively small, and the temperature rise is more confined to the area immediately around the weld. Aluminum has a high thermal conductivity, causing the heat to spread more quickly and evenly across the plate. This leads to a wider heat-affected zone as compared to titanium. Despite the high-power input, the temperature distribution is more uniform, and the peak temperature is lower than in titanium, due to the rapid dissipation of heat. Iron has thermal properties that fall between those of titanium and aluminum. The temperature distribution shows a moderate spread of heat, larger than that of titanium but less extensive than aluminum. The heat-affected zone is more pronounced than in titanium but not as extensive as in aluminum, indicating moderate thermal conductivity and heat dissipation.

Due to the exposer of the tree plates to the same surrounding temperature, at the moment zero All three plates start at a uniform baseline temperature. Ten seconds after, Initial heat concentration is highest in titanium, moderate in iron, and lowest in aluminum due to rapid heat dissipation. And then Over time, the differences become more pronounced. Titanium maintains a high peak temperature close to the weld. Aluminum shows a broadening and relatively even distribution of temperature, indicating effective heat spreading. Iron shows an intermediate behavior, with a noticeable but not as broad temperature spread as aluminum.

So, it is clearly that we could say that the change in material significantly affects the temperature distribution due to differences in thermal conductivity. Titanium, with its low thermal conductivity, confines heat close to the weld. Aluminum, with high thermal conductivity, spreads the heat more effectively, resulting in a lower peak temperature but a wider affected area. Iron shows intermediate characteristics, balancing between localized heating and heat spreading. This understanding is crucial for optimizing welding parameters and predicting material behavior during welding processes.

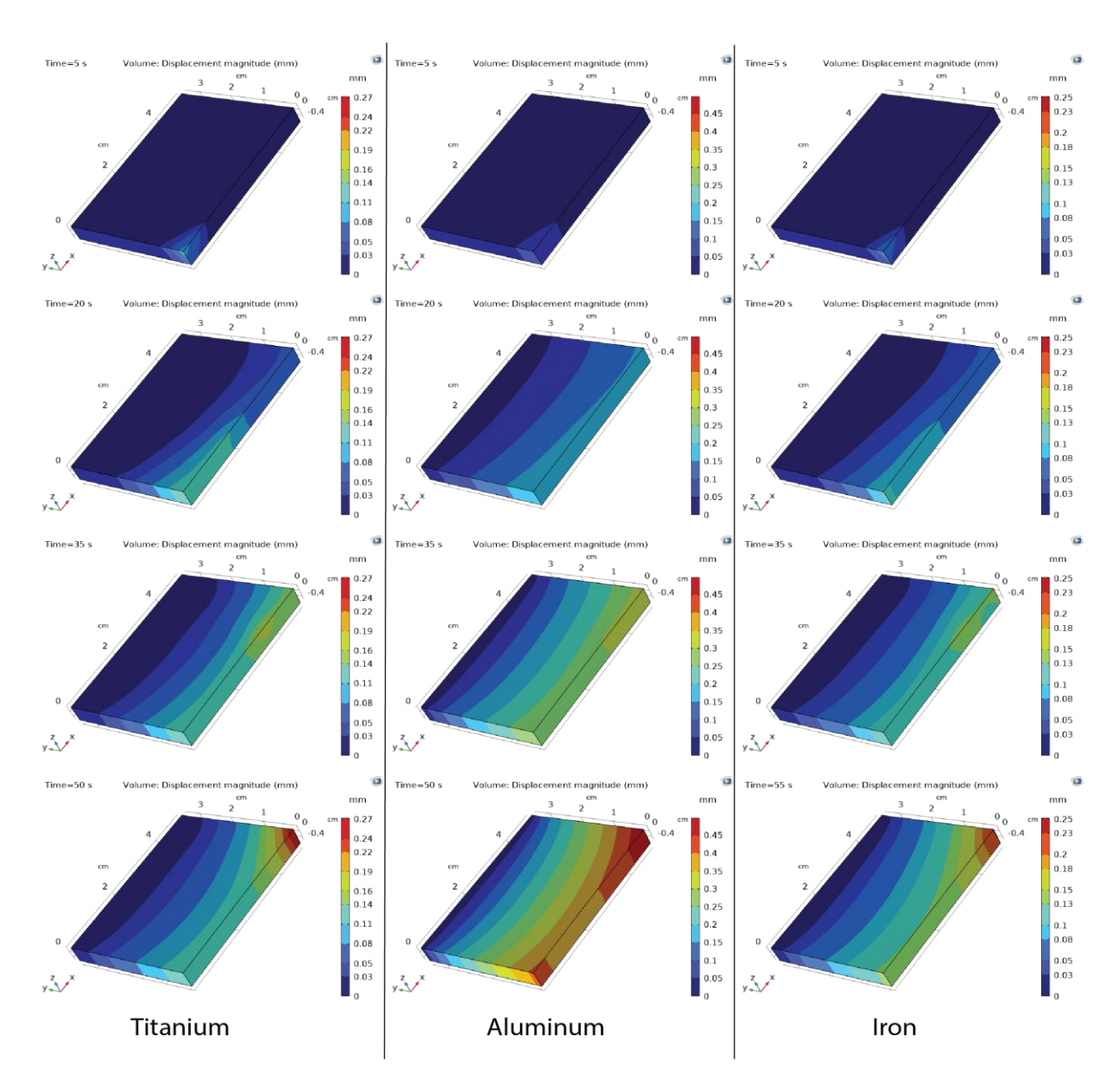


Figure III.25: volume displacement magnitude distribution in a 5mm height titanium, aluminum and iron plates in different time steps with 800W welding power

As it observed, Titanium Grade 1 exhibits significant but localized deformation, with displacement reaching up to 0.26 mm peak due to its lower thermal conductivity, which confines heat near the welding area, resulting in concentrated thermal expansion. Aluminum 1050 shows the highest displacement peak at 0.46 mm, reflecting its high thermal conductivity that allows heat to spread quickly and uniformly, leading to extensive thermal expansion and more uniform deformation across the plate. In contrast, Armco Iron displays a maximum reached displacement of 0.25 mm, which, while close to titanium's, indicates that iron's moderate thermal conductivity allows for a broader distribution of heat compared to titanium but still results in significant localized deformation. Over time, displacement increases for all materials, with titanium showing significant localized deformation, aluminum exhibiting

extensive and uniform deformation, and iron displaying notable localized displacement. These differences underscore the critical role of thermal properties in material behavior during welding, informing material selection and process parameters to manage thermal stresses and achieve desired outcomes. Further details contours on how displacement varies along the welding path during time for the three materials are shown in figure II.26.

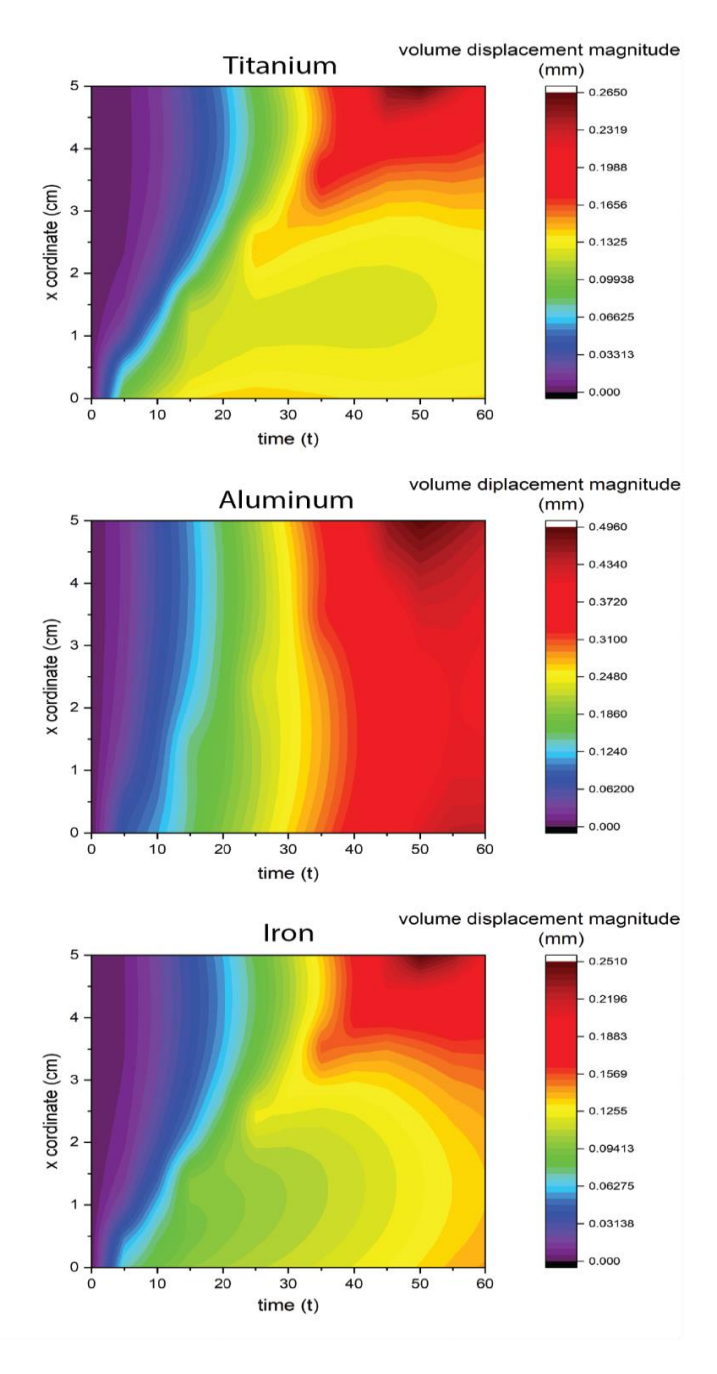


Figure III.26: volume displacement magnitude distribution in a 5mm height titanium, aluminum and iron plate, along the welding path in different time steps with 800W welding power

GENERAL CONCLUSION

In this study, we investigated the thermal behavior of Cold Metal Transfer (CMT) welding using numerical simulations with COMSOL Multiphysics. focusing on key parameters such as plate thickness, welding power, and material type. we found that thicker plates (5mm and 8mm) absorbed more heat and had slower heating rates compared to thinner plates (2mm), which reached peak temperatures more quickly due to their lower thermal mass. When I increased the welding power from 800W to 900W, the peak temperatures and heat-affected zones grew larger, particularly noticeable in the 5mm thick titanium plate. This highlighted the importance of precise control over welding parameters to maintain weld quality. My analysis of different materials revealed that titanium, with its lower thermal conductivity, showed localized deformation, while aluminum, with higher conductivity, exhibited extensive deformation. Iron displayed moderate deformation, illustrating the critical role of material properties in thermal management during welding. These insights enable engineers to optimize welding parameters for various materials and thicknesses, improving weld quality by mitigating thermal stresses and distortions. The findings underscore the industrial value of CMT welding, especially in the automotive and aerospace sectors, due to its ability to join dissimilar metals with minimal distortion and spatter. For future research, I recommend experimental validation of the numerical results and exploring additional materials and conditions to enhance the applicability of my findings. This detailed understanding of thermal behavior in CMT welding, supported by numerical data and simulations, emphasizes the importance of optimizing parameters and selecting the right materials for achieving high-quality welds, thereby advancing industrial welding practices.

REFRENCES

- [1] S. Pattanayak, S.K. Sahoo, Gas metal arc welding based additive manufacturing— A review, *CIRP J. Manuf. Sci. Technol.* 33 (2021) 398–442. https://doi.org/10.1016/j.cirpj.2021.04.010
- [2] https://words.englishbix.com/define/electric-arc
- [3] https://theweldings.com/electrodes/
- [4] The Characteristic of Cold Metal Transfer (CMT) and its application For Cladding
- [5] O. Panchenko, D. Kurushkin, I. Mushnikov, A. Khismatullin, A. Popovich, A high-performance WAAM process for Al–Mg–Mn using controlled short-circuiting metal transfer at increased wire feed rate and increased travel speed, *Mater. Des.* 195 (2020) 109040. https://doi.org/10.1016/j.matdes.2020.109040
- [6] Wire Arc Additive Manufacturing: Fundamental Sciences and Advance, Sandeep Rathee, Manu Srivastava
- [7] Furukawa K. New CMT arc welding process e welding of steel to aluminium dissimilar metals and welding of super-thin aluminium sheets. Weld Int 2006; 20(6):440e5.
- [8] Sun Zhe, LvYaohui, Xu Binshi, Liu Yuxin, Lin Jianjun, Wang Kaibo. Investigation of droplet transfer behaviours in cold metal transfer process on welding Ti-6Al-4V alloy. Int J Adv Manufacturing Technol 2015; 80(9): 2007e14.
- [9] Feng Jicai, Zhang Hongtao, He Peng. The CMT short-circuiting metal transfer process and its use in thin aluminium sheets welding. Mater Design 2009; 30: 1850e2.
- [10] Cold metal transfer (CMT) technology An overview
- [11] Mezrag B, Deschaux-Beaume F, Benachour M. Control of mass and heat transfer forsteel, aluminium joining using cold metal transfer process. SciTechnol Weld Join 2015; 20:189e98.
- [12] Advantages and Disadvantages Cold Metal Transfer (CMT) Welding https://blog.thepipingmart.com/other/cold-metal-transfer-cmt-welding-advantages-and-disadvantages/
- [13] A. Gadzala, 3D printing: Shaping Africa's future. Atlantic Council, 2018.
- [14] Analyse et étude numérique des échanges thermiques en cours d'une opération de soudage TIG sous logiciel COMSOL Multiphysics
- [15] Hong, K., Weckman, D. C., & Strong, A. B. (1998). "The influence of thermo-fluids phenomena in gas tungsten arc welds in high and low thermal conductivity metals". *Canadian Metallurgical Quarterly, Vol. 37*, (n. 3-4), pp. 293-303.
- [16] Blondeau, R. (2001b). "Procédés et applications industrielles du soudage". Paris- 238 pg.
- [17] Perry, N. (2000)." Etude et développement des flux solides en vue d'application en soudage ATIG appliqué au titane et ses alliages ainsi qu'aux aciers inoxydables", thèse Ecole Centrales de Nantes
- [18] Robert, Y. (2007). Simulation numérique du soudage du TA6V par laser YAG impulsionnel : caractérisation expérimentale et modélisation des aspects thermomécanique associées à ce procédé", thèse Ecole des Mines de Paris.
- [19] Hamide, M. (juillet 2008). "Modélisation numérique du soudage à l'arc des aciers". Thèse de l'Ecole supérieure des mines de Paris, France.
- [20] Kerrouault, N. (2001). "Fissuration à chaud en soudage d'un acier inoxydable austénitique" .Thèse de doctorat, Ecole centrale de Paris France.
- [21] Lindgren, L. E. (March 2001). "Finite element modeling and simulation of welding, Part2: Improved material modeling». Journal of Thermal Stresses, Vol. 24 (n.3), pp. 195-231.

- [22] Du, H, L. Hu, J. Liu & X. Hu (2004). A study on the metal flow in full penetration laser beam welding for titanium alloy, Computational Materials Science, Vol.29, pp.419-427.
- [23] Goldak, J., Chakravarti, A., &Bibby, M. (1984). "A new finite element model for welding heat sources". Metallurgical Transactions B, V.15B, pp. 299-305.
- [24] Etude du comportement thermique et mécanique des matériaux aéronautiques par des méthodes numériques : application au soudage de structures métalliques
- [25] Sur la modélisation du comportement thermomécanique et métallurgique des aciers. Application au procédé de soudage et de traitements thermiques, Ngoc Thuy Trinh
- [26] Aissani M., Maza, H., Belkessa, B., Maamache, B. (2005b). "Contribution à la modélisation du soudage TIG des tôles minces d'acier austénitique 304L par un modèle source bi-elliptique avec confrontation expérimentale". J. Phys. IV, Vol.124, pp 213-220
- [27] Depradeux, L. (2004). «Simulation numérique du soudage Acier 316L, Validation sur cas testes de complexité croissante», thèse de Doctorat INSA Lyon.
- [28] Wire and Arc Additive Manufacturing of High-Strength Al-Zn-Mg Aluminum Alloy
- [29] Repair of damaged parts using wire arc additive manufacturing in machine tools
- [30] https://www.3dnatives.com/format-fichier-3d-fabrication-additive-09052024/
- [31] https://metalblog.ctif.com/2020/04/27/la-fabrication-additive-waam/
- [32] Ballistic Evaluation of Aluminum Alloy (AA) 7075 Plate Repaired by Additive Friction Stir Deposition Using AA7075 Feedstock
- [33] Sethian, J. (1996): level Set Methods: Evolving Interfaces in Geometry, Fluid Mechanics, Computer Vision and Material Sciences. Cambridge University Press, Cambridge.
- [34] Hogea, C.S.; Murray, B.T.; Sethian, J.A. (2005): Implementation of the level set method for continuum mechanics based tumor growth models, FDMP: FDMP: Fluid Dynamics and Materials Processing, vol. 1, no. 2, pp. 109-130.
- [35] Lowengrub, J.S.; Xu, J-J.; Voigt, A. (2007): Surface Phase Separation and Flow in a Simple Model of Multicomponent Drops and Vesicles. FDMP: Fluid Dynamics and Materials Processing, vol. 3, no. 1, pp. 1-20.
- [36] El Ganaoui, M.; Bontoux, P. (1998): An homogenisation method for solid-liquid phase change during directional solidification, ASME, H.T.D., Numerical and Experimental Methods in Heat Transfer, éd. R.A. Nelson, T. Chopin, S.T. Thynell, vol. 361, no. 5, pp. 453-469.
- [37] El Ganaoui, M.; Bontoux, P.; Morvan, D. (1999): Localisation d'un front de solidification en interaction avec un bain fondu instationnaire. C. R. Acad. Sci. Paris, série IIb, t., vol. 327, pp. 41-48.
- [38] El Ganaoui, M.; Lamazouade, A.; Bontoux, P.; Morvan, D. (2002): Computational solution for fluid flow under solid/liquid phase change conditions, Int. J. Computers and Fluids, vol. 31, nos. 4-7, pp. 539-556.
- [39] Celentano, D.; Cruchaga, M.; Romero, J.; El Ganaoui, M. (2011) Numerical simulation of natural convection and phase-change in a horizontal Bridgman apparatus, International Journal of Numerical Methods for Heat & Fluid Flow, vol. 21, no. 4, pp. 366-376.
- [40] Voller, V. R.; Markatos, N. and Cross, M. (1985): Techniques for accounting for the moving interface in convection /diffusion phase change. Numerical Methods in Thermal Problems, vol. 1, pp. 595–609.
- [41] Mundo, C.; Sommerfeld, M.; Tropea, C.. (1995): Droplet-wall collisions. Experimental studies of the deformation and breakup process. International Journal of Multiphase Flow, vol. 21, no. 2, pp.151–173.
- [42] Ivosevic, M.; Richard, A.; Cairncross, B.; Knight, R. (2006): 3D predictions of thermally sprayed polymer splats: Modeling particle acceleration, heating and deformation

on impact with a flat substrate, Intern Journal of Heat and Mass Transfer, vol. 49, pp. 3285-3297.